CHARACTERIZATION OF THE EFFECT OF CRITICAL DESIGN PARAMETERS ON THE ELECTROCHEMICAL PERFORMANCE OF A LITHIUM-SULFUR BATTERY

by

Hatice Merve Bilal

B.S., Chemical Engineering, Izmir Institute of Technology, 2013

M.S., Fuel and Energy Technologies, Boğaziçi University, 2015

M.S., Chemical Engineering, Boğaziçi University, 2016

Submitted to the Institute for Graduate Studies in
Science and Engineering in partial fulfillment of
the requirements for the degree of
Doctor of Philosophy

Graduate Program in Chemical Engineering

Boğaziçi University

2022

to my daughter

ACKNOWLEDGEMENTS

I would like to express my gratitude to my thesis supervisor Assoc. Prof. Damla Eroğlu Pala for her endless support, priceless guidance and encouragement not just throughout my studies but especially during my pregnancy. Her success and attitude in academic life have been an aspiration for me and I feel so lucky to work with a scientist who always supports women empowerment in academic environment.

I thank to Prof. Ramazan Yıldırım, Assoc. Prof. Uğur Ünal, Assist. Prof. Betül Uralcan and Assoc. Prof. Burak Ülgüt for their valuable time and comments on my thesis as committee members.

I also appreciate Kardelen Kaya Özkiper, Ayşegül Karakuş, Özgü Özer for their support during my Ph.D. studies. Furthermore, I would like to express my gratitude to my esteemed colleague Kağan Yüksel for his collaborative behavior and support.

Cordial thanks are for Yakup Bal and Dilek Kirkoç for their friendly attitude and support.

Finally, I would like to thank my family; Ali Can, Aydan Can and Mehmet Can for their encouragement and never giving up trusting me in my endeavors. My dear husband, Rıza Bilal deserves special thanks for his encouraging attitude and endless love, without whom it would not be possible to complete this work successfully. Last but not least, I thank my beloved daughter Azra Bilal for giving me the best time of my life. This work is especially dedicated to her, hoping that it would be an inspiration for her life.

The financial support provided by Boğaziçi University Research Fund through Project BAP-14443SUP and BAP-20A05D5 is thankfully acknowledged.

ABSTRACT

CHARACTERIZATION OF THE EFFECT OF CRITICAL DESIGN PARAMETERS ON THE ELECTROCHEMICAL PERFORMANCE OF A LITHIUM-SULFUR BATTERY

Lithium-sulfur (Li-S) batteries provides high theoretical specific energy and energy density and their performance is greatly sensitive to cell design as a result of the highly complex reaction and polysulfide shuttle mechanisms within the cathode. Electrolyte-to-sulfur (E/S) ratio, carbon-to-sulfur (C/S) ratio, sulfur loading and carbon type are vital design parameters with a critical influence on the battery performance. Here, an integrated research methodology coupling experimental characterization and electrochemical modeling was applied to forecast the relation between the key design parameters and the discharge capacity, cycling performance and cell- and system-level specific energy and energy density of the Li-S battery. Firstly, the effect of the E/S ratio was examined; the highest initial discharge capacity was achieved with an E/S ratio of 20 µl mg^{-1}, whereas, the best capacity retention was observed for 13 µl mg^{-1}. Consequently, an E/S ratio of 13 µl mg^{-1} presented the best performance as the impact of the E/S ratio not only on the peak discharge capacity and capacity retention but also on cell- and system-level performance were considered. Secondly, the influence of the C/S ratio was investigated; the Li-S cell having a C/S ratio of 2 and an E/S ratio of 13 µl mg^{-1} has provided the highest initial capacity in addition to the best capacity retention. Model predictions suggested that increasing the C/S ratio worsens the battery metrics at the pack level at low E/S ratios. Finally, Li-S cells with different carbon type and sulfur loading were studied. The capacity retention of Li-S cells with AB (Acetylene Black) was unaffected by the S loading, but Li-S cells with Super C65 retain capacity at higher S loadings. Li-S cells with KB (Ketjen Black) were unable to attain good performance at higher S loadings, which was surprising given their significantly larger surface area. Super C65 was projected to have the best pack performance. At medium S loadings, when discharge capacities are maximized, Li-S cells with both AB and Super C65 cathodes attain the greatest system-level metrics.

ÖZET

KRİTİK TASARIM PARAMETRELERİNİN LİTYUM-KÜKÜRT PİLİN ELEKTROKİMYASAL PERFORMANSI ÜZERİNDEKİ ETKİSİNİN KARAKTERİZASYONU

Lityum-Kükürt (Li-S) piller yüksek teorik özgül enerjisi ve enerji yoğunluğuna sahiptir ve katot içindeki oldukça karmaşık reaksiyon ve polisülfid mekik mekanizmalarının bir sonucu olarak hücre tasarımına duyarlıdır. Elektrolit-kükürt (E/S) oranı, karbon-kükürt (C/S) oranı, kükürt yüklemesi ve karbon tipi, pil performansı üzerinde kritik bir etkiye sahip olan tasarım parametreleridir. Bu çalışmada bu parametrelerin, Li-S pilinin deşarj kapasitesi, döngü performansı ve hücre ve sistem düzeyinde spesifik enerji ve enerji yoğunluğu arasındaki ilişkiyi belirlemek için deneysel karakterizasyon ve elektrokimyasal modellemeyi birleştiren entegre bir araştırma metodu uygulanmıştır. İlk olarak, E/S oranının etkisi incelenmiştir; en yüksek başlangıç deşarj kapasitesi 20 µl mg^{-1} E/S oranı ile elde edilirken, en iyi kapasite korunumu 13 µl mg^{-1} için gözlenmiştir. Sonuç olarak, 13 µl mg^{-1}'lik bir E/S oranı, E/S oranının sadece en yüksek deşarj kapasitesi ve kapasite korunumu üzerindeki etkisi olarak değil, aynı zamanda hücre ve sistem seviyesi performansı üzerindeki etkisi olarak en iyi performansı sunmuştur. İkinci olarak, C/S oranının etkisi araştırılmıştır; C/S oranı 2 ve E/S oranı 13 µl mg^{-1} olan Li-S hücresi, en iyi kapasite korunumuna ek olarak en yüksek başlangıç kapasitesini sağlamıştır. Model tahminleri, artan C/S oranının, özellikle düşük E/S oranlarında, sistem düzeyinde pil ölçümlerini kötüleştirdiğini göstermektedir. Son olarak, farklı karbon tipi ve kükürt yüklemesine sahip Li-S hücreleri incelenmiştir. AB içeren Li-S hücrelerinin kapasite tutmasının S yüklemesinden etkilenmediği, ancak Super C65'li Li-S hücrelerinin kapasite korunumunun daha yüksek S yüklemelerinde yüksek olduğu görülmüştür. (KB) ile hazırlanmış Li-S hücreleri büyük yüzey alanları olmasına rağmen yüksek S yüklemelerinde iyi performans elde edememiştir. Super C65'in en iyi sistem performansına sahip olduğu öngörülmüştür. Orta seviyedeki S yüklemelerinde, deşarj kapasiteleri maksimum olduğundan hem AB hem de Super C65 katotlu Li-S hücreleri, sistem düzeyinde en yüksek değerleri elde etmiştir.

TABLE OF CONTENTS

ACKNOWLEDGEMENTS iv
ABSTRACT v
ÖZET vi
LIST OF FIGURES x
LIST OF TABLES xiv
LIST OF SYMBOLS xvi
LIST OF ACRONYMS/ABBREVIATIONS xx
1. INTRODUCTION 1
1.1. Li-S Battery Principles and Reactions 2
1.2. Drawbacks of Li-S Batteries 4
1.3. Importance of Cathode Design Parameters 6
1.4. Scope of the Current Work 9
2. LITERATURE SURVEY 11
2.1. Effect of the C/S Ratio on the Li-S Battery Performance 11
2.2. Effect of E/S Ratio on the Li-S Battery Performance 13
2.3. Effect of the Sulfur Loading on the Li-S Battery Performance 15
2.4. Effect of the Carbon Type on the Li-S Battery Performance 17
2.5. Modeling for the Li-S performance and Effecting Factors 18
3. EXPERIMENTAL WORK 22
3.1. Chemicals 22
3.2. Electrolyte and Coin Cell Preparation 23
3.3. Experimental Details for the Investigation of the Effect of the E/S Ratio on the Li-S Battery Performance 23
3.3.1. Cathode and Cell preparation 23
3.3.2. Electrochemical Cycling Measurements 25
3.4. Experimental Details for the Investigation of the Effect of the C/S Ratio on the Li-S Battery Performance 27
3.4.1. Cathode and Cell preparation 27
3.4.2. Electrochemical Cycling Measurements 28

3.5. Experimental Details for the Investigation of the Sulfur Loading and Carbon Type on the Li-S Battery Performance 29
3.5.1. Cathode and Cell preparation 29
3.5.2. Electrochemical Cycling Measurements 30
4. MODEL DESCRIPTION 30
4.1. One-Dimensional Electrochemical Performance Model for the Li-S Battery 31
4.2. Cell-Level Performance Model for the Li-S Battery 33
4.3. System-Level Performance Model for the Li-S Battery 38
4.3.1 I-V Relation for System-Level Performance Model 38
4.3.2 I-V Relation with the Maximum Thickness Limitation 40
4.3.3 Battery Pack Design 47
5. RESULTS AND DISCUSSION 48
5.1. The Effect of the E/S Ratio on the Li-S Battery Performance 48
5.1.1. Experimental Characterization of the Effect of the E/S Ratio on the Li-S Cell Performance..... 48
5.1.2. Model Predictions on the Effect of the E/S Ratio on the Li-S Battery Performance 53
5.1.2.1. Cell-Level Performance 54
5.1.2.2. System-Level Performance 56
5.2. The Effect of the C/S Ratio on the Li-S Battery Performance 58
5.2.1. Experimental Characterization of the Effect of C/S Ratio on the Li-S Cell Performance 60
5.2.2. Model Predictions on the Effect of the C/S Ratio on the Li-S Battery Performance 66
5.2.2.1. Cell-Level Performance 66
5.2.2.2. System-Level Performance 68
5.3. The Effect of the Sulfur Loading and Carbon Type on the Li-S Battery Performance 69
5.3.1. Experimental Characterization of the Sulfur Loading and Carbon Type on the Li-S Cell Performance 70
5.3.2. Model Predictions on the Effect of Sulfur Loading and Carbon

Type on the Li-S Battery Performance 79
5.3.2.1. Cell-Level Performance 79
5.3.2.2. System-Level Performance 80
6. CONCLUSIONS AND RECOMMENDATIONS 81
6.1. Conclusions 81
6.2. Recommendations 83
REFERENCES 84
APPENDIX A: SUPPLEMENTARY INFORMATION 1 ……..... 102
APPENDIX B: PERMISSIONS FOR FIGURES USED IN THIS DOCUMENT 111

LIST OF FIGURES

Figure 1.1. Schematic drawing of electrochemistry in Li-S. 22

Figure 1.2. The typical discharge-charge curve for Li-S cell. 24

Figure 3.1. Samples of the prepared cathode films. 47

Figure 3.2. Neware battery cycler. 49

Figure 3.3. Screenshot of the BTS software used to control Neware battery cycler. 49

Figure 5.1. Effect of the E/S ratio on the initial discharge profiles of Li-S cells at 0.1C. The data for each E/S ratio is given for a representative replicate. 72

Figure 5.2. Cycling performance and Coulombic efficiency of Li-S cells a) with varying E/S ratios at a constant S loading (mg cm^{-2}), and b) with varying E/S ratios with different S loadings (mg cm^{-2}) at 0.1C. The data for each E/S ratio is the average of replicates. 73

Figure 5.3. Discharge profiles for the Li-S batteries with different E/S ratios of a) 35 μL mg^{-1}, b) 20 μL mg^{-1}, c) 13 μL mg^{-1}, and d) 6 μL mg^{-1} during cycling at 0.1C. The data for each E/S ratio is given for a representative replicate. 75

Figure 5.4. The effect of the E/S ratio in the cell on the a) discharge capacity and b) cell voltage at the 50% DOD. The data for each E/S ratio is the average of replicates. 76

Figure 5.5. The effect of E/S ratio in the cell on the calculated cell level a) specific energy and b) energy density of Li-S cells with varying sulfur loadings at a C/S ratio of 1, N/P ratio of 1.5, and 0.1C. Experimental peak discharge capacities and cell voltages at 50% DOD are used in the predictions. 77

Figure 5.6. The effect of the E/S ratio in the cell on the calculated cell level a) specific energy and b) energy density of Li-S cells with varying sulfur loadings at a C/S ratio of 1, N/P ratio of 1.5, and 0.1C. Experimental discharge capacities at the 50th cycle of the cell and cell voltages at 50% DOD are used in the predictions. 78

Figure 5.7. The effect of the E/S ratio in the cell on the calculated system level a) specific energy and b) energy density of Li-S cells with varying maximum cathode thicknesses at a C/S ratio of 1 and N/P ratio of 1.5. Experimental peak discharge capacities are used in the predictions. 80

Figure 5.8. The effect of the E/S ratio in the cell on the calculated system level a) specific energy and b) energy density of Li-S cells with varying C/S ratios at a maximum cathode thickness of 150 μm and N/P ratio of 1.5. Experimental peak discharge capacities are used in the predictions. 81

Figure 5.9. Initial discharge profiles of Li-S cells at E/S ratios of (a) 6, (b) 13, (c) 20, and (d) 35 μl mg^{-1} with changing C/S ratios at 0.1C (demonstrative replicate). 83

Figure 5.10. Influence of C/S ratio on a) 50% DOD cell potential and b) peak discharge capacity for different E/S ratios (average of replicates). . 85

Figure 5.11. Voltage curves of Li-S cells at C/S ratios of a) 3.5, b) 2, c) 1, d) 0.5 and e) 0.3 for the 1st, 10th and 100th cycles (demonstrative replicate). E/S ratio is 13 μL mg^{-1}. 86

Figure 5.12. Influence of C/S ratio on the cycle life of Li-S cells a) at 0.1C and (b) at different C-rates for E/S ratio is 13 μL mg^{-1}(average of replicates). …… 87

Figure 5.13. Figure 5.13. Influence of C/S ratio on the projected a) Wh kg-1 and (b) Wh L^{-1} of the Li-S cell for E/S and N/P ratios of 6, 13, 20, and 35 μL mg^{-1}, and 1.5, respectively. ……. 90

Figure 5.14. Influence of the C/S ratio on the projected a) Wh kg-1 and (b) Wh L-1 of the Li-S battery for E/S and N/P ratios of 6, 13, 20, and 35 μL mg^{-1}, and 1.5, respectively. ……. 91

Figure 5.15. First discharge voltage curves for Li-S cells of different carbon cathodes with varying sulfur loadings at 0.1C. …… 94

Figure 5.16. Fig 5.16. Comparison of capacity retention and coulombic efficiency for different carbon cathodes of a) AB, b) KB and c) Super C65 at varying sulfur loadings at 0.1C. ……. 95

Figure 5.17. Comparison of capacity retention and coulombic efficiency for different carbon cathodes of AB, KB and Super C65 with varying sulfur loadings. a) AB as 0.71 mg cm^{-2}, KB as 0.89 mg cm^{-2} and Super C65 as 0.72 mg cm^{-2}, b) AB as 1.13 mg cm^{-2}, KB as 1.33 mg cm^{-2} and Super C65 as 1.48 mg cm^{-2}, c) AB as 1.81 mg cm^{-2}, KB as 2.03 mg cm^{-2} and Super C65 as 2.30 mg cm^{-2}, and d) AB as 3.29 mg cm^{-2} and Super C65 as 3.17 mg cm^{-2}. ……. 96

Figure 5.18. First discharge voltage profiles of Li-S cells of different carbon cathodes of a)AB, b)KB and c)Super C65 with varying E/S ratios of 13 and 20 μl mg^{-1} at 0.1C. S loading in the cathodes are 1.48-1.81 mg cm^{-2}. …… 98

Figure 5.19. Cycling behavior of Li-S batteries with carbon cathodes of AB and KB with E/S ratios of 13 and 20 μl mg^{-1}. …….. 99

Figure 5.20. Comparison of the 1st, 10th, and 100th discharge curves of different carbon cathodes of a) AB with a sulfur loading of 1.13 mg cm^{-2}, b) KB with a sulfur loading of 1.33 mg cm^{-2}, and c) Super C65 with a sulfur loading of 1.48 mg cm^{-2}. ……. 100

Figure 5.21. Influence of carbon type and S loading on the a) peak discharge capacity, b) discharge capacity at the 50th cycle, and c) cell voltage at the 50% DOD. ……... 101

Figure 5.22. Model projections on the cell level a) Wh kg^{-1} and (b) Wh L^{-1} of the Li-S battery with different carbon electrodes at various sulfur loadings. N/P ratio=1.5 and 0.1C. ……. 102

Figure 5.23. Model projections on the system level a) Wh kg^{-1} and (b) Wh L^{-1} of the Li-S battery with different carbon electrodes at various sulfur loadings. N/P ratio=1.5 and 0.1C. ……. 103

LIST OF TABLES

Table 3.1.	The details of the chemicals used. ……	43
Table 3.2.	Experimental Li-S design parameters in the investigation of the effect of the E/S ratio. ……	46
Table 3.3.	Li-S cell properties. ……...	48
Table 3.4.	Summary of the properties of the carbon materials used in the experiments. ……...	50
Table 4.1.	Experimental inputs to the cell-level performance model for the investigation of the effect of the C/S ratio on the Li-S cell performance. ……..	57
Table 4.2	Parameters in the cell-level performance model for the effect of E/S ratio on Li-S cell performance. …….	58
Table 4.3.	Cell-level model inputs used in the investigation of the effect of the sulfur loading on the performance of Li-S batteries. …...……..	59
Table 4.4.	Parameters in the electrochemical and system-level performance models for the investigation of the effect of the E/S ratio on the Li-S cell performance. ……	62
Table 4.5.	1D concentration-independent electrochemical model parameters for the investigation of the effect of the C/S ratio on the Li-S cell performance. …….	64

Table 4.6. 1D concentration-independent electrochemical model parameters for investigation of the effect of sulfur loading on Li-S cell performance. …….. 66

Table 4.7. Parameters in the system-level performance model for investigation of the effect of C/S ratio on Li-S cell performance. …….. 67

Table 4.8. Parameters in the system-level performance model for investigation of the effect of sulfur loading on Li-S cell performance. …….. 67

LIST OF SYMBOLS

a	Cathode electrochemically active area, cm^2/cm^3
$A_{cathode}$	Cathode area, cm^2
A_{cell}	Cell area, cm^2
ASI	Area-specific impedance, Ω cm^2
ASI_{cc+}	Positive current collector ASI, Ω cm^2
ASI_{cc-}	Negative current collector ASI, Ω cm^2
ASI_{cell}	Total ASI of the cell, Ω cm^2
ASI_{ne}	Negative electrode ASI, Ω cm^2
ASI_p	ASI of the cell at rated power, Ω cm^2
ASI_{pe}	Positive electrode ASI, Ω cm^2
ASI_{sep}	Separator ASI, Ω cm^2
C	Cell capacity, Ah
c_{ne}	Negative electrode capacity, mAh/cm^3
$c_{ne,act}$	Negative electrode specific capacity, Ah/g Li
c_{pe}	Positive electrode capacity mAh/cm^3
$c_{pe,act}$	Positive electrode specific capacity, Ah/g S
E	Battery pack energy, kwh
F	Faraday's constant, C/mol
I	Current density, A/cm^2
I_e	Average current density, A/cm^2
I_p	Power current density, A/cm^2
$i_{o,ne}$	Negative electrode exchange current density, A/cm^2
$i_{o,pe}$	Positive electrode exchange current density, A/cm^2
L_{pe}	Positive electrode thickness, cm
$L_{pe,max}$	Maximum cathode electrode thickness, cm

L_{sep}	Separator thickness, cm
L_{cc+}	Positive current collector thickness, cm
L_{cc-}	Negative current collector thickness, cm
L_{ne}	Negative electrode thickness, cm
m_b	Binder loading in the cathode, g/cm^2
m_c	Carbon loading in the cathode, g/cm^2
m_{cell}	Total cell mass per area, g/cm^2
m_{cc+}	Positive current collector mass per area, g/cm^2
m_{cc-}	Negative current collector mass per area, g/cm^2
m_e	Electrolyte loading in the cathode, g/cm^2
m_{ne}	Negative electrode mass per area, g/cm^2
m_{pe}	Positive electrode mass per area, g/cm^2
m_s	Sulfur amount in the cathode, mg
m_{sep}	Separator mass per area, g/cm^2
N_{cell}	Number of cells in a pack
P	Battery pack power, kw
Q	Areal specific capacity, mah/cm^2
R	Gas constant, J/mol K
$S_{loading}$	Sulfur loading in the cathode, g/cm^2
T	Temperature, K
$U_{ocv,p}$	Open-circuit cell voltage, V
U_{batt}	Average open-circuit battery voltage, V
v_b	Binder volume per area, cm^3/cm^2
v_c	Carbon volume per area, cm^3/cm^2
v_{cell}	Total cell volume per area, cm^3/cm^2
v_{cc-}	Negative current collector volume per area, cm^3/cm^2
v_{cc+}	Positive current collector volume per area, cm^3/cm^2
$V_{e,cell}$	Electrolyte volume in the cell, µl

v_e	Electrolyte volume in the cathode per area, cm^3/cm^2
v_{ne}	Negative electrode volume per area,
v_s	Sulfur volume per area, cm^3/cm^2
v_{sep}	Separator volume per area, cm^3/cm^2
V_{cell}	Cell voltage, V
V_e	Voltage at rated energy, V
V_p	Voltage at rated power, V
w_s	Sulfur weight fraction in the cathode
α	Transfer coefficient
β	$\alpha_{pe,c}F/RT$ [1]
δ	$\beta\|I\|L_{pe}(1/\kappa_{eff} + 1/\sigma_{eff})$ [1]
ϵ	$\beta\|I\| L_{pe}/\kappa_{eff}$ [1]
ε	Electrolyte volume fraction in the cathode
ε_{dis}	Discharged volume fraction in the cathode, mah/cm^3
ε_s	Sulfur volume fraction in the cathode
ε_b	Binder volume fraction in the cathode
ε_c	Carbon volume fraction in the cathode
η_{cc-}	Negative current collector overpotential, V
η_{cc+}	Positive current collector overpotential, V
η_{cell}	Total overpotential of the cell, V
η_{ne}	Negative electrode overpotential, V
η_{pe}	Positive electrode overpotential, V
η_{sep}	Separator overpotential, V
θ	First integration constant for Tafel polarization [1]
κ	Positive electrode ionic conductivity, S/cm
κ_{eff}	Positive electrode effective ionic conductivity, S/cm
κ_{sep}	Separator ionic conductivity, S/cm

$\kappa_{sep,eff}$	Separator effective ionic conductivity, S/cm
v	$\sqrt{L_{pe}^2(\alpha_{pe,a}+\alpha_{pe,c})ai_{0,pe}F/R\,T1/\kappa_{eff}+1/\sigma_{eff})}$ for linear polarization [1]
ρ_c	Carbon density, g/cm^3
ρ_b	Binder density, g/cm^3
ρ_{ne}	Negative electrode density, g/cm^3
ρ_{pe}	Positive electrode density, g/cm^3
ρ_{sep}	Separator density, g/cm^3
$\rho_{pe,total}$	Total positive electrode capacity, g/cm^3
σ	Positive electrode electronic conductivity, S/cm
σ_{eff}	Positive electrode effective electronic conductivity, S/cm

LIST OF ACRONYMS/ABBREVIATIONS

AB	Acetylene Black
BatPaC	Battery Performance and Cost Model
BET	Brunauer–Emmett–Teller
DME	Dimethyl Ether
DOD	Depth Of Discharge, %
DOL	1,3-Dioxolane
E/S	Electrolyte-to-Sulfur Ratio (μl mg^{-1})
KB	Ketjen Black
$LiNO_3$	Lithium Nitrate
Li-S	Lithium-Sulfur
LiTFSI	Lithium Bis-Trifluoromethanesulfonimide
NMP	N-Methyl-2-Pyrolidone
OCV	Open Circuit Potential (V)
PVDF	Polyvinylidene Difluoride
SOC	State of Charge
wt.	Weight Percentages

1. INTRODUCTION

Growing energy usage of the world raises a concern as the consumption of fossil fuel-based resources creates damaging consequences on the climate and life quality, resulting in a drastic rise in global temperature due to the increased CO_2 emissions [2]. Therefore, electromobility, electrochemical propulsion achieved by rechargeable batteries providing high energy density, has gained great interest in recent studies [3]. Batteries for portable electronic devices and electric vehicles (electric vehicles (EV), plug-in hybrid electric vehicles (PHEV), hybrid electric vehicles (HEV), etc.) are subjected to increasing demand worldwide [4-7].

Lithium-ion (Li-ion) batteries have been widely used in electric and hybrid vehicles due to their high energy density. Although the development of the Li-ion batteries is still ongoing, there are still critical issues due to the pricing and performance, which might result in challenges to support market demand in the long term [8]. Therefore, new studies have been started to come out with the vision of creating alternative energy storage systems. These new battery chemistries, so-called "beyond lithium-ion", propose better energy density and cost. In contrast, lithium-sulfur (Li-S) batteries have drawn great attention as they can offer high gravimetric energy density and capacity of 2600 Wh kg^{-1} and 1675 mAh g^{-1} (approximately five times higher than Li-ion batteries), respectively (assuming a complete reaction between Li and S to produce Li_2S with an average discharge potential of 2.2 V/cell) [9-14]. The development of Li-S batteries with high energy density and low cost to be used in cars and smart grids will provide a crucial solution to the energy problem of the world.

Herbert and Ulam were the first ones to propose the use of sulfur as the positive electrode. Herbert continued studies on the development of electrolytes, and isopropyl amine was found to be the preferable solvent. Many years later, Nazar *et al.* provided pioneering and strong results to the literature and Li-S batteries have regained attention [15]. Issues regarding the performance of the Li-S batteries have been tried to be addressed, yet important challenges still persist [16]. The biggest issue may be that the energy stored and electrochemical performance of the Li-S batteries diminish when applied in practice. Sion Power and Oxis Energy have developed prototype Li-S cells; specific energies of 350 Wh

kg^{-1} and 400 Wh kg^{-1}, respectively, were achieved. Yet, it was stated that 600 Wh kg^{-1} would be achieved soon [17].

Li-S cells have many advantages besides their high energy density and capacity since they have properties such as;

- Abundant resources of sulfur
- Extensive operating temperature
- Environmentally friendly and non-poisonous
- Safe intrinsic protection mechanism for overcharge [18,19].

Li-S batteries have an opportunity of providing lower costs compared to the other commercial state-of-art lithium-ion batteries since sulfur is produced mainly from reactions of fossil fuels as a by-product of around 60 million tons per year, which can satisfy the requirement for the energy source for nearly 4 billion of 60 kW vehicles [20,21].

1.1. Li-S Battery Principles and Reactions

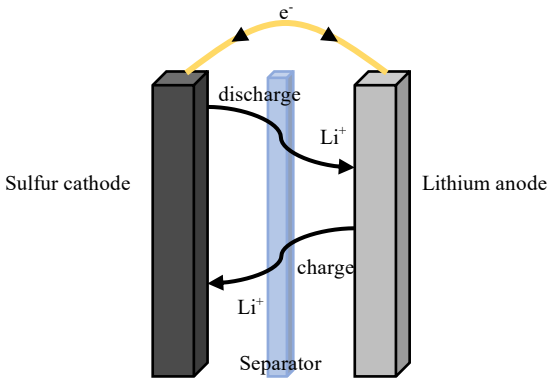

Figure 1.1. Schematic drawing of the electrochemistry in Li-S batteries.

The Li-S battery contains sulfur, Li, and liquid solvent-salt mixture as the cathode, anode, and electrolyte, respectively. During discharge, Li polysulfides Li_2S_x ($6<x\leq8$) are produced by the reduction of S_8 at the upper plateau (2.3-2.4 V vs. Li). Lower order polysulfides Li_2S_x ($2<x\leq6$) evolve due to the further reduction of the polysulfides. Li_2S is produced at the end of discharge, which has no solubility in the electrolyte and is electronically insulating. During charge, this reaction is reversed [22].

The complex reaction mechanism in the li-s batteries is still uncertain however representative reactions are given below [22],

Sulfur (in solid form) is reduced to form high-order polysulfides as

$$Li \rightarrow Li^{+} + e^{-} \tag{1.1}$$

$$\frac{1}{2}S_8 + e^{-} \rightarrow \frac{1}{2}S_8{}^{-} \tag{1.2}$$

$$2Li^{+} + S_8^{2-} \rightarrow Li_2S_8. \tag{1.3}$$

High-order polysulfides are reduced to low order polysulfides as

$$Li_2S_8 + 2Li^{+} + Li_2S_{8-n} \rightarrow Li_2S_n. \tag{1.4}$$

Low-order polysulfides (in liquid form) form insoluble solid Li_2S_2 and Li_2S mixture in the following reduction reactions, which holds the major part of the cathode capacity as

$$2Li_2S_n + (2n-4)Li \rightarrow nLi_2S_2 \tag{1.5}$$

$$Li_2S_n + 6(2n-2)Li \rightarrow nLi_2S. \tag{1.6}$$

Finally, Li_2S_2 transforms into Li_2S in a slow solid to solid transition as

$$Li_2S_2 + 2Li \rightarrow 2Li_2S. \tag{1.7}$$

The overall redox reaction becomes

$$S_8 + 16Li^{+} + 16e^{-} \leftrightarrow 8Li_2S\ (E^0 = 2.2\ V\ vs\ Li^{+}/Li^0). \tag{1.8}$$

To sum up, as intermediate products, Li_2S_x (lithium polysulfides ($8 \geq x \geq 2$)) form during the reduction process of Li and sulfur to produce Li_2S [23,24].

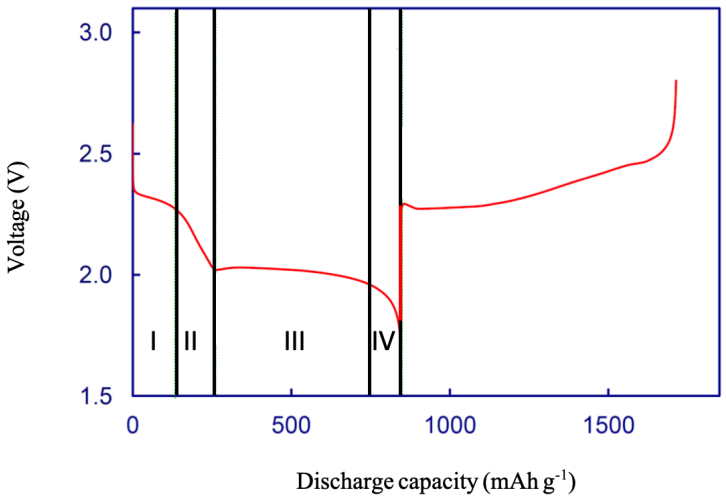

Figure 1.2. The typical discharge-charge curve for Li-S cell.

In Figure 1.2, the typical discharge-charge behavior of Li-S batteries is illustrated. The discharge starts with the reduction of S_8 into soluble S_8^{2-} between the cell voltages of 2.3-2.2 V vs. Li^+/Li (region I). This is followed by a decrease in the cell voltage owing to a complex series of reduction reactions and the formation of Li_2S_4 (region II). Then the cell voltage stays still at around 2.1 V vs. Li^+/Li due to the reduction of Li_2S_4 to Li_2S_2 (region III). Lastly, Li_2S is formed as the final product (region IV).

1.2. Drawbacks of Li-S Batteries

As described above, during the discharge/charge, polysulfides form as intermediate products and participate in the solid-liquid-solid phase transition [25,26]. These polysulfides are highly soluble in the electrolyte; consequently, they may move to the anode surface where they get reduced. After that, these polysulfides may diffuse back to the cathode and get re-oxidized. This phenomenon involving the back and forth diffusion of the polysulfides is called the polysulfide shuttle mechanism, which results in the corrosion of the anode and consequently reduces the cycling stability [27].

There are many studies in the literature for minimizing the effect of the shuttle mechanism. One way is to avoid the production of high soluble long-chain polysulfides by reducing the molecular length of the sulfur [28,29]. Trapping polysulfides with a coating layer for providing a blockage to the diffusion of polysulfides [30,31], using Li_2S as the

active material in the cathode [32], and developing functionalized separators, binders, and new electrolyte systems are some of the approaches taken for lessening the impact of the shuttle effect [33-36].

The addition of $LiNO_3$ as an electrolyte additive is highly common in the literature to overcome the shuttle mechanism by creating a film, called the solid electrolyte interphase (SEI), on the surface of the anode. SEI helps to inhibit the diffusion of the polysulfides into the anode and lower the possibility of the reactions between the anode and the polysulfides [17,37].

Along with the shuttle mechanism, the Li metal anode hosts dissolved electroactive polysulfides due to different concentration levels during discharge, which is called self-discharge. This process resumes even at the OCV (open circuit voltage) and acts as if a current was applied for discharging, resulting in decreased potential and capacity. Since this process is highly dependent on the shuttle mechanism, it may be solved by lowering the solubility of the polysulfide species. Furthermore, concerns related to the restricted amount of Li increase due to high requests for the automotive transportation [38-40].

Li_2S is the main discharge product, yet it is insoluble or inadequately soluble in a variety of organic solvents and electronically and ionically insulating [41,42]. It is believed that the main reason for capacity fade during discharge-charge processes and restraint to have full discharge capacity is the passivation of the cathode due to the precipitation of this insulating product [23,43]. The internal resistance of Li-S battery increases mainly due to Li_2S, which is one of the main products after the discharge process since it is insoluble in aprotic solvents and electronically insulating, as previously explained. Li_2S formation may also lead to significant volume variations owing to varying densities of Li_2S and S_8, which might create harsh safety problems [44].

Another drawback of Li-S cells is the insulating nature of S. In the literature, many efforts have been made to eliminate this effect via encapsulation or infiltration of sulfur into porous carbon; this strategy increases conductivity and decreases polysulfide shuttle mechanism [15,45].

1.3. Importance of Cathode Design Parameters

In Li-S batteries, intelligent cathode design can be a good approach to obtaining high performance. Recently, modeling and characterization of the key materials and cell design parameters such as the electrolyte-to-sulfur (E/S) ratio, sulfur loading, carbon-to-sulfur (C/S) ratio, and carbon properties have been reported in the literature [46-56].

E/S ratio, which is one of the key design parameters in the cell, has a great impact on the electrochemical performance of the Li-S battery since it affects the viscosity of the electrolyte and the polysulfide dissolution in the cell [57,58]. The electrolyte plays a critical role in the Li-S battery performance as it dissolves the polysulfides, the reaction intermediates in the cathode, and carries the lithium ions within the cell. Consequently, it has a great impact on the reaction and polysulfide shuttle mechanisms in the cell. High E/S ratios are required for enhanced sulfur utilization and thus high initial discharge capacity [50,59]. Nevertheless, polysulfide disproportionation should be reduced to achieve good cyclability [37]. As a result of the insulating nature of sulfur and the generation of polysulfides, understanding the reaction and shuttle mechanisms at low electrolyte amounts is a vital challenge that needs to be resolved for the practical use of Li-S batteries [60]. Moreover, increasing the electrolyte amount impacts the system-level performance by decreasing the specific energy and energy density of the battery [61]. Excessive electrolyte amounts, or high E/S ratios, in other words, cause a significant increase in the total weight of the cell, which leads to a decrease in the gravimetric energy density [57]. One of the biggest challenges in the Li-S battery literature is to achieve high specific capacity and cyclability with low electrolyte amounts hence low E/S ratios, which are required for high energy density at the system level [62]. The effect of the E/S ratio on the Li-S battery performance has been investigated experimentally by many studies in the literature [21], [63,64]. The E/S ratio is higher than 10 $\mu l\ mg^{-1}$ in more than half of the investigated studies. Zheng *et al.* presented that the E/S ratio should be 20 $\mu l\ mg^{-1}$ to achieve optimal sulfur utilization and cycling stability with reduced shuttle reactions [65]. Low electrolyte amounts typically cause inadequate wetting of the electrode surface and continuous electrolyte depletion during discharge-charge; thus, only 5 percent of the studies reported E/S ratios lower than 4 $\mu l\ mg^{-1}$ [66]. Recently, different approaches have been taken in the literature to achieve high capacity and improved cycle life at low E/S ratios (<4.5 $\mu l\ mg^{-1}$): designing a

cathode with oxygen-rich dense carbon host to increase the interaction between carbon and sulfur [67], adding polymer gel into the cell as a reservoir to trap polysulfides [68], and developing a solid-state Li_2S_4 cathode to overcome the issue of surface coverage [69]. To sum up, the majority of the studies in the literature focus on enhancing the specific capacity and cycle life of Li-S cells by utilizing very high E/S ratios in the cell. However, as mentioned above, low E/S ratios are required for high energy densities at the cell and system levels. For instance, it was discussed that the E/S ratio should be at most 4 $\mu l\ mg^{-1}$ to pass beyond the energy density of the Li-ion batteries [54]. Hagen *et al.* [57] also reported that the E/S ratio should be 2 $\mu l\ mg^{-1}$ to excel Li-ion batteries with an energy density of 500 Wh kg^{-1}. For this reason, to achieve high-performance Li-S batteries, the influence of the E/S ratio must be studied not only on the specific capacity and cyclability but also on the energy density [70].

C/S ratio is another key factor in Li-S battery design. Sulfur is a desired active material because of its high specific capacity, inexpensiveness, and availability, yet, it requires to be mixed with a conductive agent like carbon in the cell as a consequence of its low electronic conductivity. The addition of carbon into the electrode increases both the cathode active area and electrical conductivity and consequently favors sulfur kinetics. Nevertheless, the cell- and system-level energy densities are affected negatively by the high carbon content in the cathode since it is an inactive material in the battery pack. Previous studies suggest sulfur loadings ~>70% in Li-S batteries to compete with the practical energy densities of the Li-ion batteries [9,71]. In contrast, even though high active material loadings are typically required to attain enhanced energy densities, the agglomeration of sulfur in the cathode at high sulfur loadings may hinder the reaction kinetics and thus worsen the performance [72]. To sum up, there is a trade-off between the carbon and sulfur contents in the cell as high sulfur amounts lead to higher energy densities, whereas low carbon amounts fail to provide sufficient electronic conductivity and thus result in low discharge capacities and poor cycling performance [21,55,73].

Sulfur loading is also one of the essential design parameters in the cathode, which is highly determinative of the Li-S performance; the energy density of Li-S batteries is expected to excel at high levels of sulfur loadings [9]. On the other hand, low S loadings and high E/S ratios are typically desired for Li-S batteries to have high discharge capacities and

prolonged cycle life (S loadings <2 mg cm^{-2} and E/S ratios > 35 µl mg^{-1} are typical in the literature [65,74,75]). Yet, high electrolyte and low active material loadings in the cathode result in deficient energy densities, leading to practically non-competitive Li-S batteries [76,77]. Eroglu *et al.* presented through their analysis that the sulfur loading should be higher than 7 mg cm^{-2} in Li-S batteries in order not to sacrifice high energy density at the pack level [61]. Apart from recent few reports, studies with high sulfur loadings are scarce mainly due to difficulties in obtaining thick and mechanically stable cathodes. For instance, Cheon *et al.* studied the impact of cathode thickness on the Li-S battery performance. They reported that sulfur utilization decreases as the cathode becomes thicker due to the high diffusional resistance caused by the thick Li_2S layer [78].

Another vital parameter for cathode design is the type of carbon used in the composite cathode, which is needed for high cathode electronic conductivity. Furthermore, designing porous carbon architectures with a high surface area can suppress the adverse outcomes due to the polysulfide shuttle mechanism and the insulating nature of sulfur by providing sites for the incorporation of sulfur into the conductive matrix and the adsorption of polysulfides on the surface. Much higher sulfur loadings can be supported by the porous structure of the electrode as reaction kinetics are improved because of the enhanced surface area, and the polysulfide shuttle mechanism is suppressed via the polysulfide adsorption in the pores [79]. Consequently, the battery performance is highly responsive to the properties of the carbon in the cathode. Using cobalt-embedded nitrogen-doped hollow carbon microspheres in the carbon-sulfur cathode offers improved electrochemical performance by providing a high areal sulfur loading [80]. Another study proposes a novel way of cathode design to hinder the regressive outcomes of the shuttle effect of polysulfides by using a hollow carbon skeleton with an interconnected tubular cavity for the encapsulation [81]. A highly porous N-doped C nanofiber cathode design also suggests a high sulfur utilization and electrolyte permeation [82]. Liu *et al.* reported that microcapsules encapsulated with metal organic frameworks (MOFs)-derived Co_3O_4 nanocages provided high coulombic efficiency and rate-performance in the Li-S batteries [83].

Battery modeling is vital for the improvement of new battery chemistries. Despite the fact that models projecting the Li-S battery discharge behavior are widely reported in the literature [84-86], modeling studies investigating the relation between cell design and Li-S

battery performance, especially the pack-level performance, are quite limited [49-50],[87]. One of the earliest examples of a performance model of the Li-S battery at the system level is reported by Eroglu *et al.*, discussing the critical dependence of the pack-level battery performance on the E/S ratio, C/S ratio, and S loading in the cathode [61]. The effect of the E/S ratio on the specific energy and energy density of the Li-S cell is also explored previously by McCloskey [58]. Moreover, Emerce and Eroglu explored the effect of the E/S ratio on the cell and system level performance of a Li-S battery by developing a performance model [48].

1.4. Scope of the Current Work

The aim of this research was to investigate the impact of the critical cathode design parameters, the C/S ratio, E/S ratio, sulfur loading, and carbon type on the electrochemical performance and cell- and system-level energy density and specific energy of the Li-S battery. An integrated research methodology was conducted in this study by using electrochemical characterization and modeling techniques together. This study contributed to the literature in a significant manner since it discusses the critical link between Li-S battery performance and cell design.

First, the electrochemical performance of Li-S cells was determined experimentally by investigating the impact of four critical cathode design parameters, C/S ratio, E/S ratio, S loading, and carbon type in the cathode, on the specific capacity, capacity retention, and cycle life using the galvanostatic cycling method. Following the experimental characterization, a performance model was developed to predict the energy density and specific energy at the cell level as a function of the C/S ratio, E/S ratio, S loading, and carbon properties. Energy density and specific energy at the pack level were also projected as a function of these four design parameters by proposing a system-level performance model.

It is believed that this is a unique study for the investigation of the cell- and system-level performance of the Li-S batteries as a function of important cathode design parameters (C/S ratio, E/S ratio, S loading, and carbon type) coupling a comprehensive material-to-system analysis and electrochemical characterization studies.

Chapter 2 includes a detailed literature review on the effect of key cathode design parameters on the Li-S battery performance. Chapter 3 involves the details of the experimental work for the cathode, electrolyte and cell preparation, and electrochemical tests. The description of the models used in the evaluation of battery performance is given in Chapter 4. Chapter 5 presents the results obtained in the experiments and modeling, along with the discussions. The first part of Chapter 5 includes the effect of the E/S ratio on the performance of the Li-S battery. This part was published in the Journal of Electrochemical Society in 2021 [88]. The second part of Chapter 5 contains the impact of the C/S ratio on the performance of the Li-S battery. This part was published in the International Journal of Energy Research in 2022 [46]. The last part of Chapter 5 covers the results of the examination of the impact of the sulfur loading and carbon type in the cathode on the performance of the Li-S battery (the manuscript is under review). Finally, Chapter 6 displays the conclusions of this study and recommendations for future work.

2. LITERATURE SURVEY

2.1. Effect of the C/S Ratio on the Li-S Battery Performance

Brückner *et al.* studied the effect of C-rate, amount of electrolyte, and sulfur loading on the battery cycle performance. Vertically aligned carbon nanotubes (VA-CNT) were used as a model system, and electrochemical performance was investigated with different amounts of sulfur loading in the range of 20-80% and varying C-rates between 0.1C and 2.5C. It was found that when the sulfur amount was decreased at high electrolyte amounts, C-rate degradation was low and the highest capacity was provided by the sample containing 20wt% sulfur. Furthermore, the study shows that using an excess amount of electrolyte with low sulfur loading and high rate delivers higher cycle life and capacity retention [54].

Gao and Abruna examined the effect of sulfur loading on the gravimetric and volumetric energy densities with a simple model and compared the results with $LiCoO_2$. An increase in the sulfur loading results in a decrease in the discharge capacity, which was explained by having low sulfur utilization when less carbon is utilized. As a result of this study, it was found that the increase in sulfur loading had a much stronger effect on the volumetric energy density than the gravimetric energy density. Moreover, with high sulfur loadings, volumetric energy density can surpass that of a Li-ion cell [9].

The effect of the C/S ratio, sulfur loading, and electrolyte amount on the cyclability and specific capacity was examined by Ding *et al.* The C/S ratio was taken as 3:1, 2:1, 1:1, 1:2, and 1:3, the electrolyte amount was 20 µl, and the sulfur loading was 1.7 mg cm^{-2}. It was observed that when the C/S ratio was decreased, specific capacity was also reduced, which is explained by the strong relationship between sulfur utilization and specific capacity. The accumulation of Li_2S creates an insulating surface on carbon, minimizing the surface area for further reactions, which leads to a lower specific capacity. In addition, it was also concluded that specific capacity is directly related to the E/S ratio and sulfur loading up to a point as an extreme increase in these parameters might result in low battery performance and cyclability [21].

Li *et al.* investigated the impact of the C/S ratio and sulfur loading on the electrochemical performance and used C/S ratios of 1, 2, and 3, corresponding to sulfur loadings of 84, 77, and 60 wt%, respectively. During the experiments, samples with varying C/S ratios of 1:6, 1:4, and 1:2.5, including cathodes fabricated using peapod-like large pore volume mesoporous carbon, were examined. It is stated that the highest specific capacity is obtained with the sample having a C/S ratio of 3 as 1106 mAh g^{-1}, which is close to the theoretical capacity of sulfur. Furthermore, a sudden decrease in the initial discharge capacity with increasing sulfur loading was seen, similar to the previous results in the literature. The capacity continued to drop gradually until 50 cycles. Along with the other studies in the literature, the results also illustrated the increase in the capacity fade as the sulfur loading increased [89].

The impact of the C/S ratio on the electrochemical performance of the Li-S battery, where PEO was used as a binder, was studied by Park *et al.* The carbon amount was changed from 10 to 40 wt%, whereas the sulfur amount was kept constant for the experimental study. Firstly, the initial discharge curve was examined. The outcomes were compatible with the literature; the expected two voltage plateaus were achieved at 2.4 V and 2.1 V due to the reactions throughout discharge. All samples delivered similar first discharge capacities of around 1250 mAh $g^{-1,}$ which decreased after cycling. The cell with the lowest C/S ratio had the highest degradation rate since the electrical contact of carbon has a vital impact through cycling. The optimum capacity was achieved as around 870 mAh g^{-1} with the cell having a 30 wt% carbon loading [90].

Park *et al.* studied the impact of the C/S ratio on the initial discharge capacity and cycling for sulfur and activated carbon matrix. Therefore, cells with varying sulfur loadings were prepared. The results for the initial discharge curves demonstrated that when the sulfur content was increased, the discharge capacity was reduced. It was also explained that the initial discharge profile at the 2.1 V region has a plateau caused by the production of the lower-order polysulfides, which is more apparent in low sulfur loaded cells due to the state and the position of sulfur in the composite. Moreover, the rate capability results displayed that the sample with the lowest C/S ratio offered the highest rate capability along with the highest discharge capacity of 702 mAh g^{-1}, which might be due to high electrical conductivity owing to the homogeneous distribution of sulfur in the carbon matrix [91].

Shim *et al.* demonstrated in their study that when the C/S ratio with a constant sulfur amount was increased, the initial discharge capacity also increased. The higher capacity of the sulfur electrode at higher C/S ratios was explained by a greater contact area for the carbon and sulfur. The carbon amount was changed between 10-25 wt% along with the PEO (as binder) amount of 4-20 wt% while keeping the sulfur content constant at 70 wt%. Furthermore, the ratio of the capacity of the lower plateau to the total capacity was also inspected for all samples. It was observed that up to the first 20 cycles, it went up gradually, whereas, after that point, it decreased [52].

Chen *et al.* examined the influence of the C/S ratio on the specific capacity and capacity retention. It was claimed that the C/S ratio must be chosen carefully since the weight of the inactive material increases with increasing carbon amount. The carbon amount was selected as 40, 50, and 70 wt% by keeping the sulfur amount constant. The highest capacity retention and cycling performance were achieved, with the one having the highest carbon amount. Furthermore, high sulfur-loaded cells delivered a specific capacity of approximately 1000 mAh g^{-1} with an E/S ratio of 5, which is around two times the conventional ones in the literature [92].

2.2. Effect of the E/S Ratio on the Li-S Battery Performance

The impact of the E/S ratio on the cycle life and energy density was examined by Hagen *et al.* [57]. The E/S ratios were selected as 3-8 mL g^{-1} for six different samples to investigate the performance at a sulfur loading of 6.6 mg cm^{-2}. It was found that when the E/S ratio is increased, it directly affects the capacity; the highest capacity is achieved with 7 mL g^{-1}. However, when the E/S ratio is increased to much higher levels, the results illustrated a sudden drop in the discharge capacity. On the other hand, decreasing the E/S ratio resulted in capacity fade caused by the polysulfide shuttle mechanism.

Zhang studied the effect of the E/S ratio on cyclability and proposed an empirical method [37]. Sulfur loading was 2 mg cm^{-2}, and the E/S ratio was 13.3, 10, and 6.5. The sample with an E/S ratio of 13.3 showed high initial capacity, yet, the capacity declined swiftly due to the diffusion of the dissolved PSs into the cell's dead corners. However, the cell with the lowest E/S ratio has low cyclability due to an enhanced shuttle mechanism and

reduced reproducibility. It was claimed in the article that disproportionation should be kept at a minimum by adjusting the E/S ratio.

Urbonaite and Novak investigated the impact of several design parameters, which are the salt concentration, type of electrolyte additive, and amount of electrolyte on the cycling performance of the Li-S battery. For studying the effect of the electrolyte amount, Li-S cells with 100 µl, 50 µl, and 30 µl were prepared and tested to observe their effect on the specific capacity. It was observed that when the electrolyte amount was decreased, specific capacity also declined [93].

The effect of the E/S ratio on the Li_2S electrodeposition kinetics was investigated by Fan and Chiang [94]. E/S ratios were selected as 7.9, 4.2, and 2.4 µl mg^{-1}. The C/S ratio was 0.88, and C-rate was C/4. As a result, specific capacity was found to increase with increasing E/S ratio. This was explained by the relation between the electrolyte amount and the polysulfide concentration since Li_2S electrodeposition during cycling was slow at low E/S ratios due to the dissolved sulfur concentration in the electrolyte.

Yan *et al.* examined the electrochemical performance and capacity depending on the E/S ratio in a Li-S cell. The influence of the electrolyte amount on capacity was determined by preparing three different samples of 5, 8, and 12 µl mg^{-1}. The lowest specific capacity was achieved as 418 mAh g^{-1} with the sample having the lowest electrolyte amount. However, the sample with 5 µl mg^{-1} displayed higher cycling performance compared to the one with 12 µl mg^{-1}. Moreover, the relation between the E/S ratio and reaction kinetics was also scrutinized, and the results showed that higher electrolyte amounts play a crucial role in eliminating internal resistances hence improving the reaction kinetics [95].

Choi *et al.* also analyzed the impact of the electrolyte amount on the discharge capacity and cycling. Outcomes of the study showed that the sample with the highest electrolyte amount provided the highest specific capacity, which was explained by that higher electrolyte amounts deliver a medium for better reaction kinetics resulting in higher sulfur utilization as the electrode surface becomes more wetted and hence charge carriers can be transferred smoothly. The optimum cycling performance, on the other hand, was achieved with 12 µl (out of 4 and 30 µl) [64].

Thieme *et al.* investigated the cycling performance and capacity retention of Li-S batteries by changing the E/S ratio and by the addition of polysulfides into the electrolyte. It was deduced that higher E/S ratios provided long-term cycle life since when the electrolyte amount was high, electrolyte depletion was minimized and capacity was retained successfully after 50 cycles. The addition of polysulfides as a conducting salt leads to a more stabilized capacity and strengthens the performance. 554 mAh g^{-1} was retained as the final capacity (422 mAh g^{-1} was retained without the additive) from an initial capacity of 1100 mAh g^{-1} [96].

2.3. Effect of the Sulfur Loading on the Li-S Battery Performance

Schneider *et al.* examined the impact of the sulfur loading on the areal capacity for binder-free and free-standing highly N-doped C/S cathodes. It was found that the number of available surface sites for the adsorption of the polysulfide precipitates is a restrictive factor since when the sulfur loading changed at a constant E/S ratio, areal capacities achieved were similar [97].

The effect of sulfur loading on the electrochemical performance of a Li-S cell was also studied by Doan *et al.* Experiments with the sulfur-polymer cathode illustrated that when the sulfur amount was raised, a sudden capacity fade was obtained, whereas good cyclability was attained with low sulfur loadings (≤3.1 mg cm^{-2}). Obtaining low discharge capacities at high sulfur loadings was explained as such. Thicker cathodes might be detached from the current collector during cycling. Moreover, higher sulfur amounts lead to higher polysulfide concentrations causing enhanced shuttle mechanism [98].

The relation between the sulfur loading and energy density was analyzed by Kang *et al.* by using cathodes with sulfur loadings of 0.99, 2.98, and 6.80 mg S cm^{-2} and E/S ratios of 1.67, 5, 10, 20, and 40 µl mg^{-1}. At low E/S ratios, Li-S cells exhibited either rapid capacity fade or low sulfur utilization. However, discharge capacity was not affected by the excess electrolyte amount after 400 mAh g^{-1}, which was enlightened as the effect of the cathode thickness surpassing the effect of the electrolyte amount. Hence, it was declared that the best performance was achieved at the optimum conditions, where the sulfur loading and electrolyte amount were 0.99 and 2.98 mg S cm^{-2} and 10 µl mg^{-1}, respectively. Additionally,

it was claimed that cells having low sulfur loading has no benefits in terms of energy density even though achieving high specific capacity owing to the low active material loading [99].

Song *et al.* investigated the impact of cell construction factors on the electrochemical performance of Li-S cells. One of the parameters was the sulfur content; its effect on specific energy was investigated. It was claimed in the article that high specific energies could be achieved with high sulfur loadings if the sulfur utilization is high. Two cells with 50% and 80% S were used in the experiments, and a higher specific capacity based on the total electrode mass was obtained with the one with a higher sulfur loading. Long-term cycling of the cells was also tested, and it was seen that at the 800th cycle, the discharge capacity was 787 mAh g^{-1} at 0.05C, which corresponded to 441 mAh g^{-1} based on the total electrode mass. After this point, capacity started to fade, which was attributed to three reasons: volume variations causing mechanical deterioration of the electrode, the shuttle mechanism , and the polysulfide formation [100].

The effect of cathode thickness on sulfur utilization was also studied by Sun *et al.* In the study, sulfur loading varied between 0.29 and 4.38 mg cm^{-2} and cycling performance was observed. The ones with sulfur loadings lower than 1.40 mg cm^{-2} displayed an initial discharge capacity of 800 mAh g$^{-1,}$ equivalent to 50% of the theoretical capacity of sulfur. Then, the capacity faded until 100 cycles reaching 350 mAh g^{-1}. Medium-level sulfur loaded cells (1.85-2.38 mg cm^{-2}), on the other hand, did not display capacity fade at first. In fact, before the capacity started to fade, it had reached a maximum value. This behavior was explained by the electrode activation process, which was supported by the other studies in the literature with high sulfur loaded prototype cells. Furthermore, sulfur utilization was observed to be linearly dependent on the sulfur loading, signifying that electrochemical performance and active material utilization are significantly affected by the design parameters [101].

Lu *et al.* examined the effect of the cathode thickness on the specific capacity and cycling behavior of Li-S cells. Cathodes with 60, 80, and 120 μm thicknesses were prepared. It was seen that when the cathode thickness was decreased to 80 from 120 μm, better capacity retention was achieved initially; yet, the cell demonstrated capacity fade afterward, which was explained by the diminished electrolyte retention in the dense electrode. Moreover, the

impact of the E/S ratio was also studied. High sulfur utilization was observed at an E/S ratio of 3 µl mg^{-1}. However, a shorter cycle life was seen for cells with controlled E/S ratios. This is generally seen in the studies in the literature due to the instability of the Li anode and the shuttle mechanism consuming the electrolyte at low E/S ratios [59].

2.4. Effect of the Carbon Type on the Li-S Battery Performance

Sun *et al.* stated that carbon particle size and specific pore volume are crucial parameters for achieving high sulfur loading with high sulfur utilization [102]. Barchasz *et al.* found that carbon grain size has a remarkable effect on the amount of polysulfides accumulated on the cathode at the end of discharge. Moreover, high electrode surface area is reported to delay the full electrode passivation, thus, improving the discharge performance of the battery [103]. Many studies in the literature investigated the effect of activated carbon with different surface areas and pore sizes. They concluded that small pore size and high surface area are needed to achieve high discharge capacity and sulfur utilization [104-111].

Zheng *et al.* studied the effect of carbon pore volume and surface area on the electrochemical behavior of Li-S batteries. Four different carbon types with high surface areas (Graphene (nonporous) and Ketjen Black (porous)) and low surface areas (Acetylene black (nonporous) and Hollow Carbon Nano Sphere (porous)) were investigated as the carbon host. The best capacity retention was obtained for the cells with Ketjen Black and Hollow Carbon Nano Sphere, which were the only porous ones in this study. Furthermore, it was found that higher sulfur utilization rates were obtained by using carbons with a high surface area [105].

Jozwiuk *et al.* stated that the polysulfide adsorption ability and specific capacity are highly related to the surface area of the carbon used in the cathode. Electrochemical performance tests were performed with different types of carbon with varying specific surface areas: Ketjenblack EC-600JD, Printex-A, Super C65, and Printex XE-2. Li-S cells with Ketjenblack EC-600JD, which has a high surface area, achieved 800 mAh g^{-1} at 1C over 600 cycles. It was also suggested that preparing cathodes by mixing different carbons having various surface areas would be beneficial for high mechanical stability and performance [106].

Yan *et al.* developed bamboo-derived porous carbon materials with different pore volumes and specific surface areas. Sulfur was encapsulated into the synthesized carbon, and cycling behaviors were observed. It was declared that a high initial capacity of 1453 mAh g^{-1} at 0.1C was achieved with the sample having a sulfur loading of 58.5 wt% [112].

Li-S cells prepared with carbons with different surface areas (Ketjen Black and Super P) were characterized. It was stated that the porous structure achieved by using Ketjen Black as a conductive agent was more beneficial for high electrolyte impregnation. However, due to mechanical constraints with Ketjen Black, a higher initial capacity of 1058 mAh g^{-1} was achieved with the cell with Super P [113].

2.5. Modeling of the Li-S Battery Performance

Xue *et al.* developed a model for the calculation of the gravimetric and volumetric energy densities and to observe the impact of the cell parameters on battery performance. Pouch cell configuration was considered as the type of cell. Packaging materials were disregarded in the model because their volume fraction can be ignored in a multi-electrode pouch cell. The Al and Cu current collectors, the Li anode, the sulfur cathode (carbon, sulfur, and binder), and the separator were the essential parts of the sandwich-structured model. It was assumed to have enough electrolyte to fill the interspaces between the cathode and the separator. Volumetric energy densities calculated by the model for varying cathode thicknesses and excess lithium levels demonstrated that to have a high volumetric energy density, sulfur loading, and sulfur utilization must be increased. Furthermore, sulfur content was discussed to be another vital parameter that linearly affected the volumetric energy density. As a result, it was seen that both of these parameters have a crucial effect on cell-level performance. Moreover, the impact of cathode porosity on the volumetric energy density was investigated, and a reverse relation was obtained; when the porosity increased, volumetric energy density decreased. The maximum value of the volumetric energy density was predicted as 1060 Wh L^{-1} when the porosity was 0.30. The effect of the E/S ratio through the porosity was also examined. It was seen that as the porosity rose, the E/S ratio also increased. This study illustrated that having a high energy density highly depends on having good sulfur utilization, which can be optimized by changing the porosity, E/S ratio, and sulfur content [17].

A mathematical model was developed by Kumaresan *et al.* by taking into account the detailed electrochemical and precipitation reactions, the change in the porosity of the cathode, and the multicomponent transport phenomena in the electrolyte. Li+ ion transport during discharge with respect to time was analyzed; the concentration of Li+ ions increased up to 14 h and then started to decrease. This was explained by the formation of high-order PSs (S_4^{2-}, S_6^{2-}, S_8^{2-}) at the beginning of the discharge process. The shape of the discharge profile was analyzed based on the concentration profiles of the species. In the first plateau, sulfur is reduced into high-ordered polysulfides (S42-, S62-), and the solid phase sulfur turns into the liquid phase. Since this process is kinetically controlled, the concentration of sulfur in the liquid phase remains constant until the dissolution is completed. The second discharge plateau starts when the precipitation of Li_2S on the carbon surface starts and S_2^{2-} concentration becomes apparent [86].

Eroglu *et al.* developed a techno-economic model, which links the material-level reactions to the system-level performance by considering the main cell and electrode design parameters: C/S ratio, electrolyte volume fraction, reaction kinetics, useable specific capacity, and Li amount. The projection of the battery specific energy, energy density, and price were also provided. A 1D, concentration-independent electrochemical performance model was established to predict the current-voltage relation in the techno-economic model. In the electrochemical model, Butler-Volmer kinetics were applied for the anode deposition/dissolution reactions. It was found that when the excess Li amount or the electrolyte vol% increased, energy density and specific energy reduced significantly. Furthermore, the pack-level specific energy and energy density decreased as the specific capacity decreased. The impact of the E/S and C/S ratios were also studied; increasing the amount of the inactive material resulted in an increase in the dead weight in the cell; hence, specific energy and energy density diminished. However, due to its high electronic conductivity and creating more active surface area, increasing the carbon amount led to a better energy density up to a point. Finally, when the electrolyte vol%, excess of Li, or carbon wt% decreased, battery cost was reduced [61].

Michaelis *et al.* established an electrochemical model to predict the effect of the C/S ratio on the electrochemical performance of Li-S batteries. In the study, the C/S ratio varied

between 0.41 to 7.48, and the experimental results were compared with the model. It was found that the capacity achieved with the highest sulfur loading was the lowest. The decrease in the discharge capacity at high sulfur loadings (35.1 and 52.7 wt%) was caused by sulfur agglomeration in the electrode, resulting in electrode polarization. The sulfur utilization was low at high sulfur loadings even though the potential capacity of the electrode was high. Moreover, the results of the model and experiments were compatible [49].

Marinescu *et al.* developed a zero-dimensional model for Li-S batteries, which included two electrochemical reactions and the precipitation and dissolution of one species. In the model, a single electrochemical reaction for each of the two discharge regions was taken. A constant exchange current density and dissolvability of the entire elemental sulfur mass were also assumed. In addition, the anode overpotential caused by the Li oxidation was omitted. Results of the model stated that at high discharge currents, significantly large overpotentials were obtained due to charge transfer and diffusion limitations. The lower plateau voltage diminished at higher C-rates, and less usable capacity was achieved. The effect of the precipitation rate was also investigated [84].

In 2017, it was stated that studies regarding the modeling of the Li-S batteries are nine percent of the reviewed articles [114]. Some examples of these studies are: modeling the effect of cathode design parameters on the self-discharge behavior in Li-S batteries [39], modeling the coupled ion motion in the electrolyte in Li-S batteries [115], modeling the charge and discharge capacities focusing on the polysulfide chemistry and its interaction with the anode while considering self-heating and the impact of salt additives on the shuttle mechanism [85], modeling the self-discharge due to the shuttle mechanism [116], and modeling the polysulfide shuttle mechanism via including additional reactions at the anode and nonreversible precipitation [117].

3. EXPERIMENTAL WORK

3.1. Chemicals

The details of the chemicals used in this work are given in Table 3.1.

Table 3.1. The details of the chemicals used.

Chemical	Function	Source
Super C65	Conductive carbon black	MTI
Ketjen Black EC-600J	Conductive carbon black	Nanografi
Acetylene Black	Conductive carbon black	Nanografi
Sulfur	Active material	Sigma Aldrich
PVDF (polyvinylidene difluoride)	Binder	MTI
NMP (N- methyl-2-pyrolidone)	Solvent	MTI
Al Foil	Current collector	MTI
Li Foil	Anode	MTI
Cu Foil	Current collector	MTI
DOL (1,3-Dioxolane)	Electrolyte	Sigma Aldrich
DME (1,2-dimethoxyethane)	Electrolyte	Sigma Aldrich
Lithium nitrate ($LiNO_3$)	Electrolyte	Sigma Aldrich
LiTFSI (lithium bis-trifluoromethanesulfonimide)	Electrolyte	Sigma Aldrich
Polymer-based separator	Separator	Celgard

Li-S cells consist of the carbon-sulfur cathode, electrolyte, Li anode, separator, and current collectors. The preparation of the electrolyte and coin cells is explained below.

3.2. Electrolyte and Coin Cell Preparation

In order to prepare the electrolyte, 1,3-Dioxalane (DOL) and 1,2-dimethoxyethane (DME) were mixed in equal volumes in a glove box under Ar atmosphere. Then, 1 M lithium bis-trifluoromethanesulfonimide (LiTFSI) and 0.1 M lithium nitrate ($LiNO_3$) were added to the solution:

- 5 ml DOL and 5 ml DME were mixed
- 2.871 g LiTFSI and 0.06895 g $LiNO_3$ were dissolved in the 10 mL DOL&DME mixture to obtain 1 M LiTFSI and 0.1 M $LiNO_3$
- The solution was stirred in a magnetic stirrer for 1 hour

Coin cells (CR2032) were prepared in the glove box under Ar atmosphere. In the assembly of the coin cells, first steel O-ring was placed into the bottom case, and after that ,the flat steel sheet was placed on top of it. Next, cthe opper foil was placed before the lithium anode, and a certain amount of electrolyte was dropped onto the lithium anode (2.01 cm^2, 170 μm). Then, the Celgard polymeric separator (3.1 cm^2, 25 μm) was placed, and the rest of the electrolyte was poured into the separator. The cathode was placed next, keeping the aluminum side pointing up. Finally, one more flat steel sheet was placed, and after putting the top case, the coin cell was closed in the cell crimping machine.

3.3. Experimental Details for the Investigation of the Effect of the E/S Ratio on the Li-S Battery Performance

3.3.1. Cathode and Cell Preparation

Cathodes were prepared by adjusting carbon/sulfur/binder weight ratios to 45/45/10. First, conductive carbon black (Super C65, MTI) and sulfur (Sigma Aldrich) were mixed in a mortar and pestle for 5 minutes. Afterward, polyvinylidene fluoride (PVDF, MTI) was added to the mixture as a binder. N-methyl-2-pyrrolidone (NMP, MTI) was then mixed with the solid mixture until a homogenous medium with an NMP/solid mixture ratio of 7:1 wt/wt was obtained. In order to achieve a well-mixed solution, the slurry was first mixed in a magnetic stirrer overnight, then heated to 50°C for 2 hours, and then mixed in an ultrasonic

mixer for 2 more hours. Next, the solution was cast onto an aluminum foil (MTI) with a doctor blade. The cathode slurry cast on the aluminum foil was dried overnight and then at 50°C for 4 hours in the oven to remove the NMP. The thickness of the cathodes after drying was around 90 μm. Finally, the cathode films were cut as 2.01 cm^2 disks by using a puncher. Figure 3.1 illustrates the prepared cathode films and samples. Table 3.2 presents the experimental design parameters used in this study.

Figure 3.1. Samples of the prepared cathode films.

So, as to study the effect of the E/S ratio on the electrochemical performance of the battery, Li-S cells with E/S ratios of 6-35 μl mg^{-1} were prepared. The cathode composition and thickness, thus the sulfur loading, were kept constant for all Li-S cells with varying electrolyte amounts.

Table 3.2. Experimental Li-S design parameters in the investigation of the effect of the E/S ratio.

E/S ($\mu l\ mg^{-1}$)*,[a]	S loading ($mg\ cm^{-2}$)*	Electrolyte Amount (μl)
35	0.70	50
20	0.74	30
13	0.76	20
6	0.79	10

*Average of three replicates
[a] C/S/Binder wt%: 45/45/10

3.3.2. Electrochemical Cycling Measurements

Galvanostatic cycling measurements were performed at room temperature to assess the electrochemical performance of the coin cells by using a Neware battery cycler (Figure 3.2and Figure 3.3). First, each cell was rested for 16 h at its open circuit voltage. The cells were then cycled for 100 cycles at a C-rate of 0.1C (C-rate was calculated based on the theoretical capacity of the Li-S cell). The lower and upper cut-off voltages were set as 1.5 and 3 V, respectively. Each experiment was replicated three times, and all results were reported as the average of the three replicates.

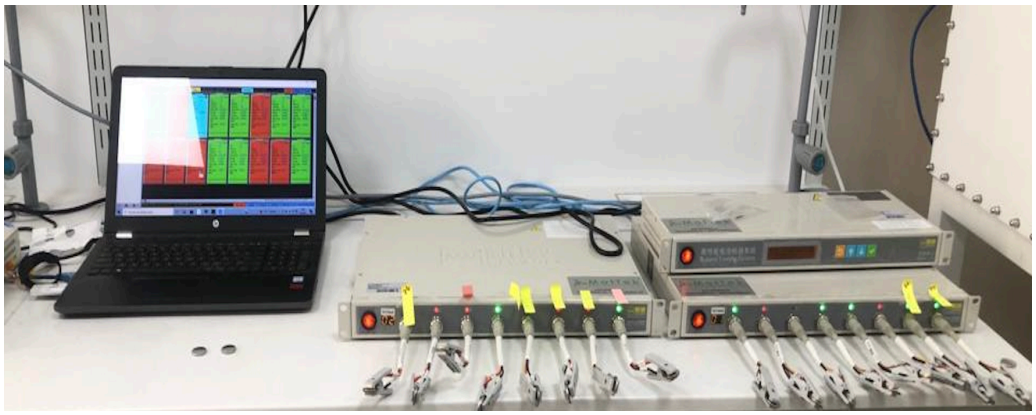

Figure 3.2. Neware battery cycler.

Figure 3.3. Screenshot of the BTS software used to control Neware battery cycler.

3.4. Experimental Details for the Investigation of the Effect of the C/S Ratio on the Li-S Battery Performance

3.4.1. Cathode and Cell Preparation

Cathodes with different C/S ratios (0.5, 1, 2, and 3.5) were prepared by modifying the carbon and sulfur amounts in the electrodes. The electrodes were prepared at a specified thickness; consequently, the S loading in the cathode for each C/S ratio was different. E/S ratio was kept constant at 6, 13, 20, or 35 µl mg^{-1}. Table 3.3. reports the design parameters employed in the preparation of the Li-S cells.

Carbon black (Timcal Super C65, MTI), sulfur (Sigma Aldrich), and binder (PVDF, MTI) were ground in a mortar and pestle for 5 min. Then, N-methyl-2-pyrrolidone (NMP, MTI) solvent was added to the mixture. The slurry was mixed in a magnetic stirrer overnight, followed by mixing at 50ºC for 2 hours to achieve uniform mixing. Afterward, the slurry was mixed in an ultrasonic mixer for 2 hours at room temperature, and the resulting solution was cast on an Al foil (15 µm thick, MTI) with a doctor blade at a specified thickness. Cathode films were dried overnight and then at 50ºC in the oven until all the remaining NMP was dried out. Cathode films with an area of 2.01 cm^2 were punched out and weighed.

Table 3.3. Li-S cell properties.

E/S ratio (µl mg^{-1})	C/S ratio	S Loading (mg cm^{-2})[a]	Electrolyte amount (µl)[a]
6	0.5	1.75	21
	1	0.75	9
	2	0.61	7
	3.5	0.37	5
13	0.3	4.42	150
	0.5	1.48	39

Table 3.3. Li-S cell properties. (cont.)

E/S ratio ($\mu l\ mg^{-1}$)	C/S ratio	S Loading ($mg\ cm^{-2}$)[a]	Electrolyte amount (μl)[a]
13	1	0.75	20
	2	0.63	17
	3.5	0.34	9
20	0.5	1.75	70
	1	0.75	30
	2	0.63	25
	3.5	0.30	12
35	0.5	1.75	120
	1	0.70	50
	2	0.64	45
	3.5	0.30	20

[a]Average of three replicates

3.4.2. Electrochemical Cycling Measurements

The cells were cycled via the galvanostatic cycling method at room temperature by using a Neware battery cycler. The lower and upper cut-off voltages were set as 1.7 and 3 V, respectively. Each cell rested for 16 h at its open circuit voltage and then cycled for 100 cycles at 0.1C, which was calculated based on the theoretical capacity of the Li-S cell. Each experiment was repeated at least three times, and the average results of the replicates were reported. All capacities were reported per g of sulfur in the cathode.

3.5. Experimental Details for the Investigation of the Sulfur Loading and Carbon Type on the Li-S Battery Performance

3.5.1. Cathode and Cell Preparation

The cathode composite was prepared by mixing different carbons with sulfur (Sigma Aldrich) and binder (PVDF, MTI) in the N-methyl-2-pyrrolidone (NMP, MTI) solvent. Carbon black (Super C65, MTI), acetylene black (AB, Nanografi), or Ketjen black (KB, Nanografi) was used as the carbon source. After homogenization, the slurry was cast onto an aluminum current collector (15 μm thick, MTI) by the doctor blade technique. The sulfur loading in the cathode was adjusted by regulating the thickness of the slurry during casting (wet thicknesses of the cathodes were 200, 350, 500, 700, or 850 μm). The resulting electrodes were dried overnight and then at 50 ºC in the oven for 4 hours. A list of the examined carbon black materials, along with some of the important characteristics, are displayed in Table 3.4.

Table 3.4. Summary of the properties of the carbon materials used in the experiments.

Name	**Grade and supplier**	**Specific surface area (BET) (m^2g^{-1})**	**Particle size (nm)**
Super C65	Carbon Black, Super C65 Timcal, MTI	60	40
KB	Ketjen Black, EC-600J, Nanografi	1000-1400	180
AB	Conductive Acetlyene Black, Nanografi	70-75	35-40

3.5.1. Electrochemical Cycling Measurements

The electrochemical performance of the cells was monitored by a galvanostatic battery cycler between 1.7 and 3.0 V at room temperature at 0.1C. Before cycling, the cells were kept at rest at the open-circuit voltage for 16h to allow equilibration.

4. MODEL DESCRIPTION

Following the experimental part, the effect of critical cathode design parameters on the cell- and system-level performance of a Li-S battery was investigated by developing performance models as described in this chapter. Design parameters used in the experiments, as well as experimentally measured cell capacities and voltages, were fed into the models to capture the dependence of the electrochemical performance of the Li-S cell on the cell design in the performance models.

4.1. One-Dimensional Electrochemical Performance Model for the Li-S Battery

A one-dimensional, concentration-independent electrochemical model was proposed for the constant-current, isothermal discharge of the Li-S cell. The model described the Li-S cell as the cathode composed of carbon, sulfur, binder, and an organic electrolyte, the porous separator, the Li-metal anode, and the positive and the negative current collectors as reported in our previous models [48,50]. In the model, the ASI and the overpotential were calculated at a specified DOD for each component of the cell; cathode, anode, current collectors, and porous separator, individually.

One of the crucial assumptions in the model was that there is a single electrochemical reaction for each of the two discharge plateaus [84,85]. The high and the low discharge plateaus are described as

$$\frac{1}{4}S_8^0 + e^- \leftrightarrow \frac{1}{2}S_4^{2-} \tag{4.1}$$

$$\frac{1}{4}S_4^{2-} + e^- \leftrightarrow \frac{1}{2}S^{2-} + \frac{1}{4}S_2^{2-}. \tag{4.2}$$

For the porous positive electrode, the overpotential was calculated as in the model of Newman and Tobias [1].Based on the current density, either Tafel ($|I| > ai_{0,pe}L_{pe}$,) or linear ($|I| < ai_{0,pe}L_{pe}$) kinetics is applied to calculate the cathode overpotential and ASI of the positive electrode is determined accordingly as

$$\eta_{pe} = \frac{1}{\beta}\left\{(\delta-\epsilon)\left[\frac{\epsilon}{\delta}+\frac{2}{\delta}lnsec(\theta-\psi)\right]+\frac{2\epsilon}{\delta}lnsec\psi + ln\left(\frac{2|I|\theta^2}{ai_{0,pe}L_{pe}\delta}\right)\right\} \tag{4.3}$$

$$\eta_{pe} = \frac{I\times L_{pe}}{\kappa_{eff}+\sigma_{eff}}\left[1+\frac{2+\left(\frac{\sigma_{eff}}{\kappa_{eff}}+\frac{\kappa_{eff}}{\kappa_{eff}}\right)coshv}{vsinhv}\right] \tag{4.4}$$

$$ASI_{pe} = \frac{\eta_{pe}}{I} \tag{4.5}$$

where η_{pe} is overpotential of the cathode and calculated according to current density for Tafel (Equation (4.3)) or linear (Equation (4.4)) kinetics and ASI_{pe} is the ASI of the positive electrode provided in Equation (4.5).

Butler-Volmer equation was applied to calculate the anode overpotential according to electrochemical reaction occurring in the anode and Ohm's law was applied to calculate overpotential for porous separator where the Ohmic losses resulting from the transport of Li^+ ions were included. Moreover, the ASI of the negative electrode and separator is calculated using following equations

$$Li^+ + e^- \rightarrow Li^0 \tag{4.6}$$

$$I = i_{o,ne}\left[exp\left(\frac{\alpha_{ne,a}F}{RT}\eta_{ne}\right)-exp\left(\frac{-\alpha_{ne,c}F}{RT}\eta_{ne}\right)\right] \tag{4.7}$$

$$ASI_{ne} = \frac{\eta_{ne}}{I} \tag{4.8}$$

$$\eta_{sep} = ASI_{sep}\times I \tag{4.9}$$

$$ASI_{sep} = \frac{L_{sep}}{\kappa_{eff,sep}} \tag{4.10}$$

where η_{ne} is overpotential of negative electrode, ASI_{ne} is ASI for negative electrode, η_{sep}

is overpotential of porous separator and ASI_{sep} is ASI for porous separator, respectively. Furthermore, Equation (4.6) describes the electrochemical reaction occurring in the anode.

Cell voltage at a constant-current density was predicted by the model through the total overpotential and ASI of the cell given as

$$V_{cell} = U - \eta_{cell} \tag{4.11}$$

$$\eta_{cell} = \eta_{ne} + \eta_{sep} + \eta_{pe} + \eta_{cc-} + \eta_{cc+} \tag{4.12}$$

$$ASI_{cell} = ASI_{ne} + ASI_{sep} + ASI_{pe} + ASI_{cc-} + ASI_{cc+}. \tag{4.13}$$

4.2. Cell-Level Performance Model for the Li-S Battery

The impact of key parameters (E/S ratio, C/S ratio, sulfur loading, and carbon properties) on the cell-level energy density and specific energy was examined by developing a cell-level performance model. The Li-S cell in the model is composed of the positive and negative current collectors, the separator, and the positive and the negative electrodes. In the calculation of the specific energy and energy density, cell capacity and the mass and volume of each cell component were normalized to the cathode area [48,58].

E/S ratio was calculated by using experimentally measured electrolyte volume and sulfur amount. Sulfur amount (m_s) was computed by using the mass of the cathode measured ($m_{cathode}$) and sulfur weight fraction. Next, sulfur loading in the cathode and C/S ratio was calculated. The positive electrode thickness and positive electrode capacity were then determined based on the experimentally measured properties as described in

$$E/S = \frac{V_{e,cell}}{m_s} \tag{4.14}$$

$$m_s = w_s \times m_{cathode} \tag{4.15}$$

$$S_{loading} = \frac{m_s}{A_{cathode}} \tag{4.16}$$

$$C/S = \frac{w_c}{w_s} \tag{4.17}$$

where $^{E}/_{S}$ is the electrolyte-to-sulfur ratio in µl mg^{-1}, $V_{e,cell}$ is the volume of the electrolyte in the cell in µl, m_s is the sulfur amount in mg, w_s is the sulfur weight fraction in the cathode, $m_{cathode}$ is the mass of the cathode excluding the mass of aluminum foil measured experimentally for each cell, $S_{loading}$ is the sulfur loading in the cathode in mg cm^{-2}, and $A_{cathode}$ is the area of the cathode in cm^2.

The positive electrode thickness and positive electrode capacity were then determined based on the experimentally measured properties as described in

$$L_{pe} = \frac{S_{loading}}{\rho_s \times \varepsilon_s} \tag{4.18}$$

$$c_{pe} = c_{pe,act} \times \rho_{pe,total} \times w_s \tag{4.19}$$

respectively, where L_{pe} is the positive electrode thickness in cm, ρ_s is the density of the sulfur in g S cm^{-3} S, ε_s is the sulfur volume fraction in the cathode, c_{pe} is the positive electrode capacity in mAh cm^{-3}, $c_{pe,act}$ is the positive electrode specific capacity measured experimentally in mAh g^{-1}, and $\rho_{pe,total}$ is the total cathode density in g cm^{-3}.

Next, the negative electrode capacity was formulated based on the positive electrode capacity and negative electrode thickness was determined based on positive electrode thickness as

$$c_{ne} = c_{ne,act} \times \rho_{ne} \tag{4.20}$$

$$L_{ne} = \frac{L_{pe} \times c_{pe}}{c_{ne}} \times N/P \tag{4.21}$$

respectively, where c_{ne} is the anode capacity in Ah cm^{-3}, $c_{ne,act}$ is the anode specific capacity in Ah/g, ρ_{ne} is the anode density in g cm^{-3}, L_{ne} is the anode thickness in cm, and *N/P* is the negative-to-positive capacity ratio.

Total mass, total volume, cell capacity and cell-level performance, namely the specific energy and energy density of a Li-S cell, was calculated by using following equations

$$m_{cell} = S_{loading} + m_c + m_b + m_{sep} + m_{ne} + m_e + m_{cc^-} + m_{cc^+} \quad (4.22)$$

$$v_{cell} = v_s + v_c + v_b + v_{sep} + v_{ne} + v_e + v_{cc^-} + v_{cc^+} \quad (4.23)$$

$$Q = c_{pe} \times L_{pe} \quad (4.24)$$

where v_{cell} is the total volume of the cell in cm^3/cm^2 and m_{cell} is the total mass of the cell in g/cm^2. Q is the areal specific capacity in mAh/cm^2. Volume of each component is calculated by dividing its mass by its density.

Finally, cell-level specific energy and energy density is calculated according to areal specific capacity and cell voltage given in

$$Cell - level\ specific\ energy = \frac{Q \times V_{cell}}{m_{cell}} \quad (4.25)$$

$$Cell - level\ energy\ density = \frac{Q \times V_{cell}}{v_{cell}} \quad (4.26)$$

where cell-level specific energy in Wh kg^{-1}, energy density in Wh L^{-1} and V_{cell} is the cell voltage measured experimentally at 50% depth of discharge (DOD) in V.

Table 4.1. Experimental inputs to the cell-level performance model for the investigation of the effect of the C/S ratio on the Li-S cell performance.

E/S ratio	C/S ratio	Cathode electrode specific capacity, ($c_{pe,act}$) (mAh g^{-1})[a,b]	Cell voltage at 50% DOD, (V)[a,b]
6	0.5	825	2.06
	1	856	2.03
	2	772	2.06
	3.5	747	2.09
13	0.5	1051	2.06
	1	1081	2.11
	2	1165	2.12
	3.5	951	2.10
20	0.5	718	2.07
	1	969	2.11
	2	1013	2.11
	3.5	997	2.21
35	0.5	936	2.06
	1	942	2.07
	2	1073	2.11
	3.5	1058	2.13

[a]Average of three replicates
[b]Standard deviations provided in Figure 5.10

Table 4.2. Parameters in the cell-level performance model for the effect of E/S ratio on Li-S cell performance.

E/S ratio in the cathode ($\mu l\ mg^{-1}$)[a]	35	20	13	6
Positive electrode specific capacity, $c_{pe,act}$ (mAh g^{-1} S)[a]	1034	1104	1073	809
Positive electrode specific capacity at 50th cycle[a]	593	717	820	-
Cell voltage at 50% DOD, V_{cell} (V)[a]	2.07	2.08	2.1	1.9
Negative electrode specific capacity, $c_{ne,act}$ (mAh g^{-1} Li)	3860			
N/P ratio	1.5			
C/S ratio in the cathode[b]	1			

[a]Experimental values
[b]Cathode with 10 wt% binder

Table 4.3. Cell-level model inputs used in the investigation of the effect of the sulfur loading on the performance of Li-S batteries.

Carbon Type	S Loading (mg cm^{-2})	Cathode specific capacity, $c_{pe,act}$ (mAh g^{-1})[a,b]	Cell voltage at 50% DOD, (V)[a,b]
AB	0.71	761.43	2.08
	1.13	743.09	2.07
	1.81	826.23	2.09
	3.29	746.44	2.04
KB	0.89	719.24	2.05
	1.33	893.83	1.99
	2.03	252.87	1.82
Super C65	0.72	750.38	2.06
	1.48	1051.41	2.06
	2.30	863.88	1.99
	3.17	894.81	1.96

[a]Average of three replicates
[b]Standard deviations provided in Figure 5.21

4.3. System-Level Performance Model for the Li-S Battery

The effect of key design parameters on the system-level performance was modeled in this section as described below.

4.3.1. I-V Relation for System-Level Performance Model

System-level specific energy and energy density of a Li-S battery were projected by a modified model of publicly available design and cost model, Battery Performance and Cost (BatPaC) [118]. In the system-level performance model, the area-specific impedance (ASI) and overpotential for each cell component were calculated by a one-dimensional electrochemical model. Detailed governing equations of the electrochemical model are provided in Section 4.1.

The battery pack was designed based on the essential inputs of power, energy, and voltage of the battery as shown in the following design equations

$$A_{cell} = \frac{P}{I_p \times V_p \times N_{cell}} \tag{4.27}$$

$$N_{cell} = \frac{U_{batt}}{U_{ocv,p}} \tag{4.28}$$

$$C = \frac{E}{V_e \times N_{cell}} \tag{4.29}$$

$$L_{pe} = \frac{C}{A_{cell} \times \varepsilon_{dis} \times \varepsilon_s} \tag{4.30}$$

$$V_p = U_{ocv,p} \times 0.8 \tag{4.31}$$

$$I_p = \frac{U_{ocv,p}}{ASI_p} \times (1 - \left[\frac{V}{U_{ocv,p}}\right]) \tag{4.32}$$

$$I_e = \frac{C}{A_{cell} \times 5} \tag{4.33}$$

where A_{cell} is cell area in cm^2 obtained by using power requirements, I_p is the pulse power current density in A cm^{-2}, V_p is the voltage at rated power in V, N_{cell} is the number of cells in a battery pack calculated by using pack voltage specifications, $U_{ocv,p}$ is the open-circuit cell voltage in V, U_{batt} is the average open-circuit battery voltage, C is the cell capacity in Ah obtained by using energy requirements, V_e is the voltage at rated energy in V, ε_{dis} is the discharged volume fraction in the cathode in mAh cm^{-3}, ε is the electrolyte volume fraction (or the porosity in other words) in the cathode, ASI_p is the ASI of the cell at rated power in Ω cm^2 and I_e is the average current density at a C/5 rate in A cm^{-2}.

As a rule of thumb, 80% DOD and 50% DOD were used in the model for the power and energy specifications, respectively [61]. The model defines all variables both for the rated power (subscript p) and the rated energy (subscript e). As given in the design equations, the power requirement determines the cell area Equation (4.27), while the pack voltage necessity defines the number of cells in the battery pack Equation (4.28). On the other hand, the energy specification sets the required cell capacity and the cathode thickness Equation

(4.29) and Equation (4.30), respectively). Accordingly, the current density at rated power was iterated until the target cell voltage at rated power was accomplished Equation (4.31) and Equation (4.32). Lastly, the cell voltage at rated energy was iterated at a current density at rated energy of C/5 Equation (4.33).

4.3.2. I-V Relation with the Maximum Thickness Limitation

Electrode thickness is a crucial design parameter which affects the performance of the battery significantly. Thus, a practical limit set by the battery performance and life is typically defined as the maximum electrode thickness [119]. Positive electrode thickness was calculated by the cell capacity as described. However, the model was developed so that when the calculated thickness exceeds the maximum limit, the cell area was recalculated accordingly. The maximum electrode thickness was set as 150 μm for the cathode; this limitation was only implemented to the positive electrode since it was the only porous electrode in the cell [61]. Therefore, it was assumed that thicker cathodes than the ones used in traditional Li-ion batteries (<100 μm) could be allowed without a decrease in the battery performance and life [48,61]. The cell area was recalculated in accordance with the maximum electrode thickness limit and revealed as

$$A_{cell} = \frac{C}{L_{pe,max} \times c_{pe}}. \tag{4.34}$$

Table 4.4. Parameters in the electrochemical and system-level performance models for the investigation of the effect of the E/S ratio on the Li-S cell performance.

Open-circuit cell voltage, $U_{ocv,p}$ (V)	2.2
Power, P (kW)	80
Energy, E (kWh)	118
Maximum cathode thickness, $L_{pe,max}$ (μm)	150
Average battery open-circuit voltage, U_{batt} (V)	360
Target voltage efficiency at rated power, [V/$U_{ocv,p}$]	0.8
Useable state of charge window (%)	85
Temperature, T (K)	298
Separator thickness, L_{sep} (μm)	20
Separator effective ionic conductivity,$\kappa_{eff,sep}$ (S cm^{-1})	6.5×10^{-4}
Cathode transfer coefficient, $\alpha_{pe,a}$, $\alpha_{pe,c}$	0.5
Anode exchange current density, $i_{0,ne}$ (A cm^{-2})	10^{-3}
Anode charge transfer coefficients $\alpha_{ne,a}$, $\alpha_{ne,c}$	0.5
Cathode electrochemically active area, a (cm^{-1})[a]	$a=650000\ .\rho_c^{1.5}.\varepsilon_c^{1.5}$
Cathode effective ionic conductivity κ_{eff} (S cm)[b]	$\kappa_{eff}=\kappa\ .\varepsilon^{1.5}$
Cathode effective electronic conductivity σ_{eff} (S cm^{-1})[b]	$\sigma_{eff}=\sigma\ .\varepsilon_c^{1.5}$
Cathode exchange current density, $i_{0,pe}$ (A/cm^2)	10^{-6}
Cathode electronic conductivity κ (S/cm)	100
Cathode ionic conductivity σ(S/cm)	0.01
C/S ratio in the cathode[c]	0.3-3.5

Table 4.4. Parameters in the electrochemical and system-level performance models for the investigation of the effect of the E/S ratio on the Li-S cell performance. (cont.)

E/S ratio in the cathode (μl mg^{-1})[d]	35	20	13	6
Positive electrode specific capacity, $c_{pe,act}$ (mAh g^{-1} S)[d]	1034	1104	1073	809
Electrolyte volume fraction in the cathode, ε	0.64-0.98			
C-rate (mA g^{-1} S)	C/5			

[a] a is defined as a function of Brunauer-Emmett-Teller surface area (650000 cm^2 g^{-1})
[b]Effective electronic and ionic conductivities in the porous cathode are achieved using Bruggeman's expression, density (ρ_c) and volume fraction of the carbon (ε_c) in the cathode
[c] Cathode contains 10 wt% binder.
[d] Experimental values.

Table 4.5. 1D concentration-independent electrochemical model parameters for the investigation of the effect of the C/S ratio on the Li-S cell performance.

Open-circuit cell voltage, $U_{ocv,p}$ (V)	2.2
Power, P (kW)	80
Energy, E (kWh)	118
Maximum cathode thickness, $L_{pe,max}$ (μm)	150
Average battery open-circuit voltage, U_{batt} (V)	360
Target voltage efficiency at rated power, [V/$U_{ocv,p}$]	0.8
Useable state of charge window (%)	85
Temperature, T (K)	298
Separator thickness, L_{sep} (μm)	20
Separator effective ionic conductivity,$\kappa_{eff,sep}$ (S cm^{-1})	6.5×10^{-4}
Cathode transfer coefficient, $\alpha_{pe,a}$, $\alpha_{pe,c}$	0.5
Anode exchange current density, $i_{0,ne}$ (A cm^{-2})	10^{-3}
Anode charge transfer coefficients $\alpha_{ne,a}$, $\alpha_{ne,c}$	0.5
Cathode electrochemically active area, a (cm^{-1})[a]	$a=650000 .\rho_c^{1.5}.\varepsilon_c^{1.5}$
Cathode effective ionic conductivity κ_{eff} (S cm)[b]	$\kappa_{eff}=\kappa .\varepsilon^{1.5}$
Cathode effective electronic conductivity σ_{eff} (S cm^{-1})[b]	$\sigma_{eff}=\sigma .\varepsilon_c^{1.5}$
Cathode exchange current density, $i_{0,pe}$ (A/cm^2)	10^{-6}
Cathode electronic conductivity κ (S/cm)	100
Cathode ionic conductivity σ(S/cm)	0.01
E/S ratio in the cathode (μl mg^{-1})[c]	6-35

Table 4.5. 1D concentration-independent electrochemical model parameters for the investigation of the effect of the C/S ratio on the Li-S cell performance. (cont.)

C/S ratio in the cathode[d]	0.5	1	2	3.5
Electrolyte volume fraction in the cathode, ε	86-97	82-96	75-95	6-92

[a] a is defined as a function of Brunauer-Emmett-Teller surface area (650000 cm^2 g^{-1})
[b]Effective electronic and ionic conductivities in the porous cathode are achieved using Bruggeman's expression, density (ρ_c) and volume fraction of the carbon (ε_c) in the cathode
[c] Experimental values.
[d] Cathode contains 10 wt% binder.

Table 4.6. 1D concentration-independent electrochemical model parameters for investigation of the effect of sulfur loading on Li-S cell performance.

E/S ratio in the cathode (μl mg^{-1})[a]	13
C/S ratio in the cathode[b]	0.5
Electrolyte volume fraction in the cathode, ε	93
Separator thickness, L_{sep} (μm)	20
Separator effective ionic conductivity,$\kappa_{eff,sep}$ (S cm^{-1})	6.5×10^{-4}
Cathode transfer coefficient, $\alpha_{pe,a}$, $\alpha_{pe,c}$	0.5
Anode exchange current density, $i_{0,ne}$ (A cm^{-2})	10^{-3}
Anode charge transfer coefficients $\alpha_{ne,a}$, $\alpha_{ne,c}$	0.5
Cathode electrochemically active area, a (cm^{-1})	$a=S_{BET}{}^{c} .\rho^{1.5}.\varepsilon^{1.5}$
Cathode effective ionic conductivity κ_{eff} (S cm)[d]	$\kappa_{eff}=\kappa .\varepsilon^{1.5}$
Cathode effective electronic conductivity σ_{eff} (S cm^{-1})[d]	$\sigma_{eff}=\sigma .\varepsilon^{1.5}$
Cathode exchange current density, $i_{0,pe}$ (A/cm^2)	10^{-6}
Cathode electronic conductivity κ (S/cm)	100
Cathode ionic conductivity σ (S/cm)	0.01
C-rate (mA g S^{-1})	C/5

[a]Experimental values
[b] Cathode contains 10 wt% binder
[c] S_{BET} is taken from Table 3.4 for each carbon Brunauer-Emmett-Teller surface area, density (ρ_c) and volume fraction of the carbon (ε_c) in the cathode
[d] Effective electronic and ionic conductivities in the porous cathode are achieved using Bruggeman's expression.

Table 4.7. Parameters in the system-level performance model for investigation of the effect of C/S ratio on Li-S cell performance

Open-circuit cell voltage, $U_{ocv,p}$ (V)	2.2
Power, P (kW)	80
Useable Energy, E (kWh)	100
Maximum cathode thickness, $L_{pe,max}$ (μm)	150
Average battery open-circuit voltage, U_{batt} (V)	360
Target voltage efficiency at rated power, [$V/U_{ocv,p}$]	0.8
Useable state of charge window (%)	85
Negative electrode specific capacity, cne,act (mAh g^{-1})	3860
N/P ratio	1.5

Table 4.8. Parameters in the system-level performance model for investigation of the effect of sulfur loading on Li-S cell performance

Open-circuit cell voltage, $U_{ocv,p}$ (V)	2.2
Power, P (kW)	80
Useable Energy, E (kWh)	100
Average battery open-circuit voltage, U_{batt} (V)	360
Target voltage efficiency at rated power, [$V/U_{ocv,p}$]	0.8
Useable state of charge window (%)	85
Anode specific capacity, $c_{ne,act}$ (mAh g^{-1} Li)	3860
N/P ratio	1.5

4.3.3. Battery Pack Design

In the model, after the cell was designed according to the energy and power requirements, the components of packaging and thermal management were also calculated to predict the system-level performance of the Li-S battery by adapting the BatPac model [61,118]. The battery pack consists of modules, and modules consist of cells. Battery mass was calculated by considering the battery coolant mass within the jacket, battery jacket mass, pack integration unit (BMS& disconnects), and module mass. Battery volume was calculated by considering the volume of pack integration unit (BMS&disconnects) and battery pack volume. All the module and pack design equations are provided in detail in Appendix A. Usable energy, system-level energy density and specific energy was provided as

$$Usable\ energy = Usable\ SOC\ window(\%) \times E \tag{4.35}$$

$$System - level\ energy\ density = \frac{Usable\ energy}{Battery\ volume} \tag{4.36}$$

$$System - level\ specific\ energy = \frac{Usable\ energy}{Battery\ mass} \tag{4.37}$$

where usable energy is in kWh, system-level energy density in Wh L^{-1}, system-level specific energy in Wh kg^{-1},battery volume in L and battery mass in kg.

5. RESULTS AND DISCUSSION

5.1. The Effect of the E/S Ratio on the Li-S Battery Performance

In this chapter, we present an integrated research methodology combining electrochemical characterization and modeling techniques to characterize the impact of the E/S ratio on the cell -and system level performance of the Li-S battery. First, we demonstrate an experimental investigation of the electrochemical performance of the Li-S cells, namely the initial discharge capacity and cycling performance, with varying E/S ratios. Then, cell and system level performance models predicting the impact of the E/S ratio on the energy density and specific energy of the Li-S battery are developed based on our experimental observations. This part of the chapter was published as a paper [46] and the original manuscript has been adapted for this dissertation.

5.1.1. Experimental Characterization of the Effect of the E/S Ratio on the Li-S Cell Performance

Electrolyte amount has a great impact on the electrochemical performance of a Li-S cell since it provides a medium for the transportation of the Li ions between the electrodes. As previously discussed, adequate wetting of the surface and accelerated charge transfer can be achieved with high amounts of electrolyte. The effect of the E/S ratio on the cycling behavior and discharge capacity of a Li-S cell is examined for E/S ratios of 35, 20, 13, and 6 $\mu L\ mg^{-1}$. The initial discharge curves for the respective cells with varying E/S ratios and their cycling performance are demonstrated in Figure 5.1 and 5.2, respectively.

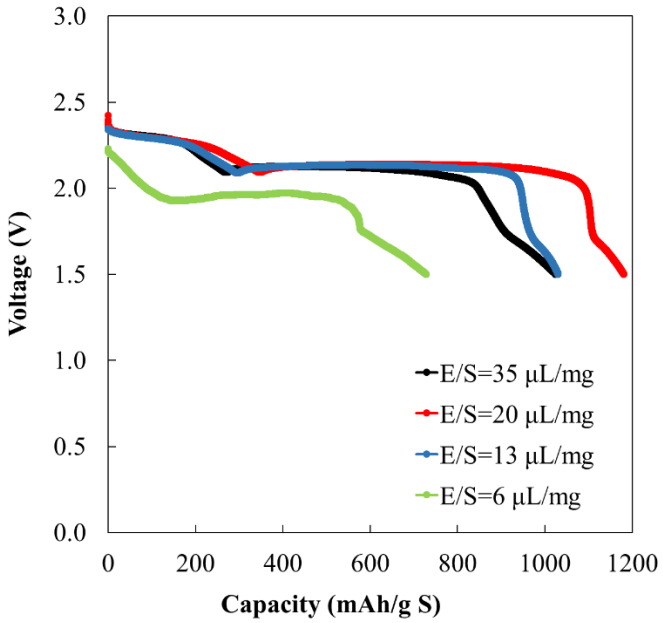

Figure 5.1. Effect of the E/S ratio on the initial discharge profiles of Li-S cells at 0.1C. The data for each E/S ratio is given for a representative replicate.

As seen in Figure 5.1, the highest initial capacity is obtained with an E/S ratio of 20 µl g^{-1}. It is clearly illustrated that both the cell capacity and voltage increase up to a certain level with an increasing E/S ratio. This can simply be explained by the enhanced kinetics and sulfur utilization at higher electrolyte amounts in the cathode [95]. However, a further increase in the E/S ratio leads to a decrease in the cell capacity, while not impacting the cell voltage to any further extent [65,87].

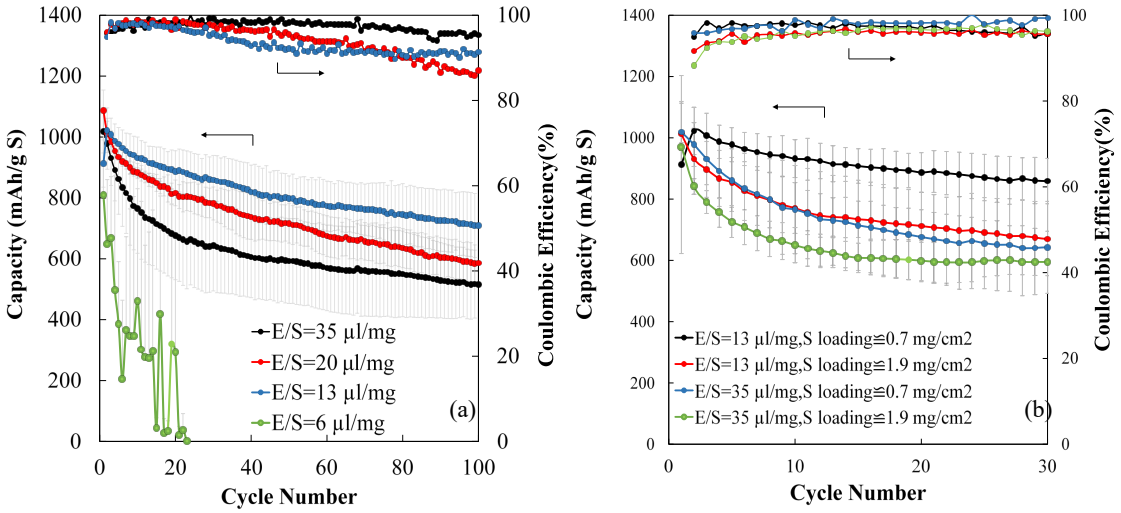

Figure 5.2. Cycling performance and Coulombic efficiency of Li-S cells a) with varying E/S ratios at a constant S loading (mg cm^{-2}), and b) with varying E/S ratios with different S loadings (mg cm^{-2}) at 0.1C. The data for each E/S ratio is the average of replicates.

The electrolyte amount in the cell is highly related to the polysulfide amount in the medium as stated before. Although the initial capacity is high in cells with high electrolyte content, a sharp decrease in the capacity is observed for these cells as the number of cycles increases (Figure 5.2). At a higher level of E/S ratio with a relatively excess electrolyte amount, capacity declines rapidly, which can be explained by that the polysulfides dissolved in the electrolyte diffuse into the cell's dead corners during cycling resulting in poor capacity retention [37]. Consequently, the best cycling performance is obtained for the Li-S cell with an E/S ratio of 13 µL mg^{-1}.

Even though the Li-S cell with the lowest E/S ratio of 6 µl mg^{-1} shows a similar initial discharge profile to the others, the cycling performance of this cell is significantly bad. The capacity fades completely after the 20^{th} cycle as seen in Figure 5.2a. This can be explained by the fact that when the electrolyte amount is insufficient in the cell, polysulfide concentration increases considerably leading to a highly viscous medium and inadequate wetting of the surface of the carbon/sulfur composite cathode; hence, the reaction kinetics is hindered [57,65]. It should be noted that due to the low sulfur loading used in this study, 10

μL electrolyte is used in the cell to achieve the targeted E/S ratio of 6 μL mg^{-1}. This electrolyte amount is fairly low to attain sufficient wetting of the electrode and the separator in a coin cell; this may also contribute to the extremely poor cycling performance obtained for this E/S ratio. Yet, the trends observed in Figure 5.2a on the effect of the E/S ratio on the cycling performance are expected to be independent of the S loading of the cathode, as will be discussed below in Figure 5.2b.

Another factor contributing to the capacity fade observed in Figure 5.2a may be the irreversible reduction of $LiNO_3$ forming a passivation layer on the cathode at low cut-off voltages (<1.7V) [120-122]. It is previously reported in the literature that narrowing the voltage window leads to a better cycling performance of the Li-S batteries [120-122]. Nevertheless, the impact of the E/S ratio on the cycling performance is expected to be independent of the voltage window chosen for the cycling measurements.

Figure 5.2a also presents the Coulombic efficiencies of the Li-S cells with different E/S ratios as a function of cycle number. It can be seen in the figure that the Coulombic efficiencies are higher for higher E/S ratios. This may be explained by the presence of excess $LiNO_3$ in the cell at higher electrolyte amounts [123]. It is also apparent in the figure that the reported Coulombic efficiencies are higher than 90% for almost all E/S ratios during the first 100 cycles, which may be also explained by the availability of $LiNO_3$ in the cell.

In Figure 5.2b, the cycling performance of Li-S cells with a higher S loading is shown for two different E/S ratios. Similar conclusions to the ones stated above can be drawn from the figure; while the initial discharge capacity of the cell with an E/S=35 μL mg^{-1} is slightly higher than the one with an E/S=13 μL mg^{-1}, the capacity retention for the lower E/S ratio is much better. This trend seems to be independent of the sulfur loading of the cathode; consequently, it can be discussed that the conclusions we report in this study can be extended for Li-S cells with higher S-loaded cathodes. The impact of sulfur loading on the performance is also apparent in the figure. It is clear that the capacity fade becomes more prominent at higher sulfur loadings. On the other hand, the effect of sulfur loading on the initial discharge capacity is less pronounced.

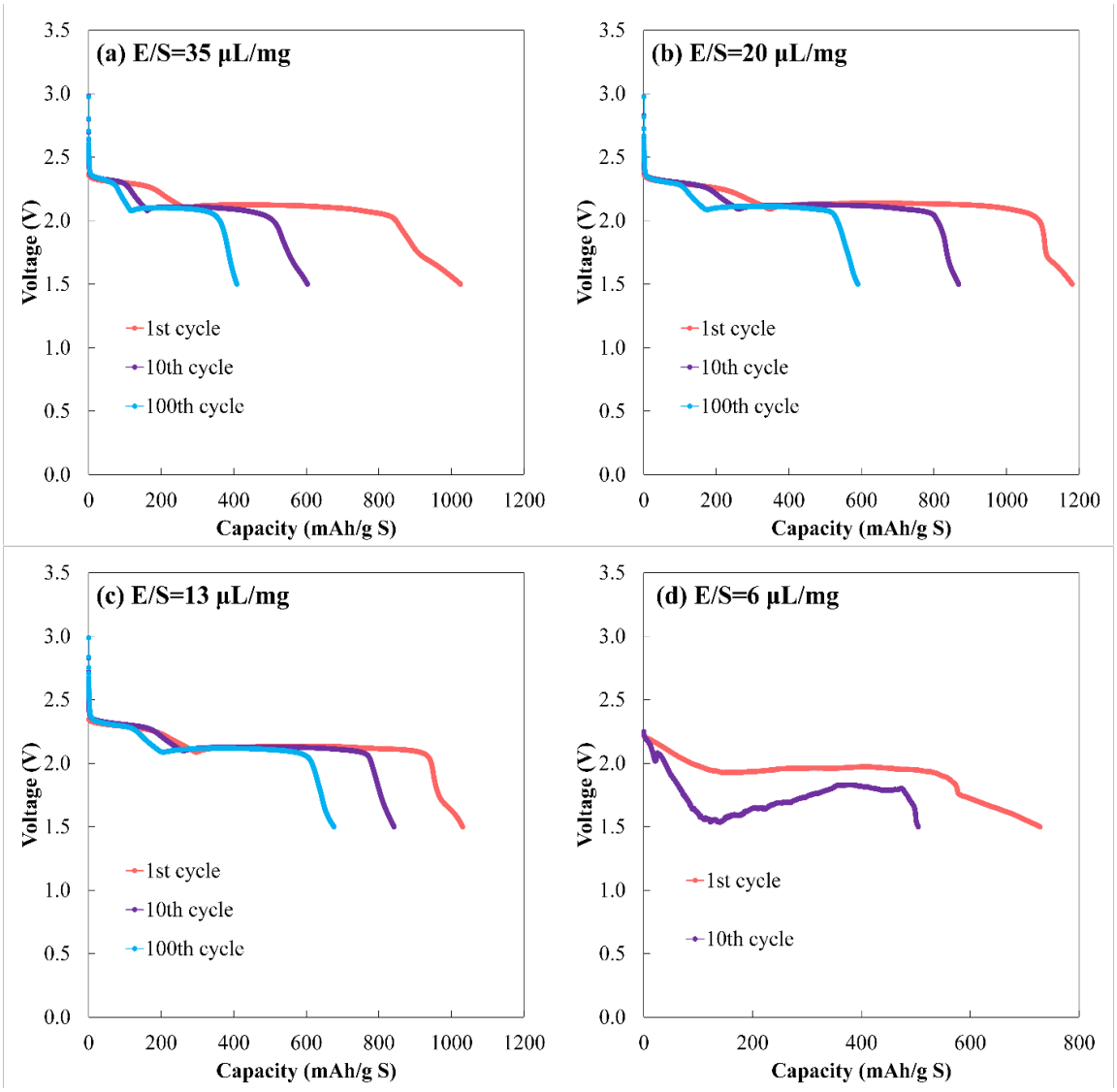

Figure 5.3. Discharge profiles for the Li-S batteries with different E/S ratios of a) 35 µL mg^{-1}, b) 20 µL mg^{-1}, c) 13 µL mg^{-1}, and d) 6 µL mg^{-1}during cycling at 0.1C. The data for each E/S ratio is given for a representative replicate.

In Figure 5.3, the discharge behavior of the Li-S batteries with different E/S ratios is demonstrated at the 1st, 10th, and 100th cycles. It is apparent in the figures that in almost all E/S ratios there is a considerable capacity decay at the 10th and 100th cycles. Especially, the cell with an E/S ratio of 35 µL mg^{-1}displays a significant decrease in the capacity through cycling since the shuttle mechanism increases at elevated electrolyte amounts, which may cause corrosion on the surface of the lithium anode. As expected from Figure 5.2a, the best capacity retention is achieved with an E/S ratio of 13 µL mg^{-1}. As the electrolyte amount

decreases, discharge profiles are relatively well preserved; the negative effect of the polysulfide shuttle mechanism over the capacity retention may be diminished with a limited amount of dissolved species [65].

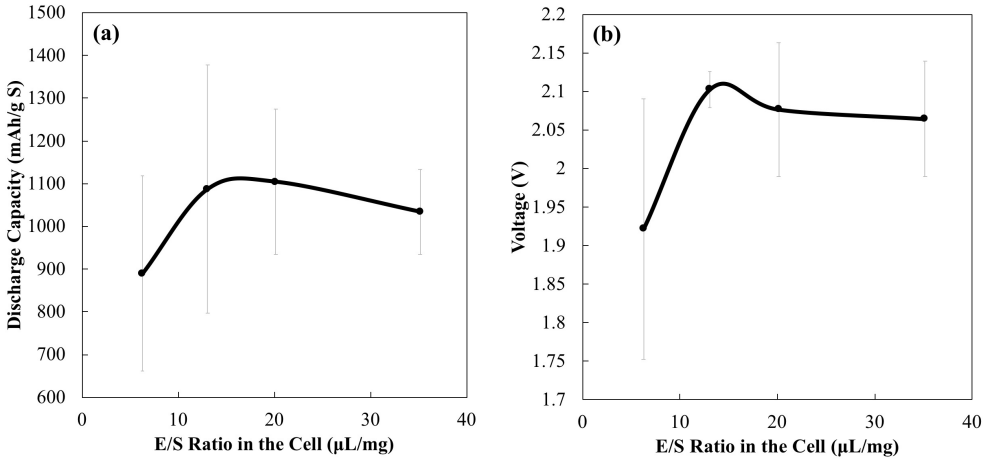

Figure 5.4. The effect of the E/S ratio in the cell on the a) discharge capacity and b) cell voltage at the 50% DOD. The data for each E/S ratio is the average of replicates.

Figure 5.4 summarizes the experimental results obtained on the influence of the E/S ratio on the Li-S cell performance. As also discussed above, the amount of electrolyte has a considerable impact on the discharge capacity (Figure 5.4a). It can be observed in the figure that increasing the E/S ratio increases the discharge capacity up to a certain level. Figure 5.4b illustrates the relation of the cell voltage at 50% DOD with the E/S ratio; increasing the E/S ratio leads to a sharp increase in the cell voltage, which can be explained by the domination of kinetic limitations at low E/S ratios. However, since kinetic limitations become more submissive at higher E/S ratios, cell voltage does not change considerably with a further increase in the E/S ratio.

5.1.2. Model Predictions on the Effect of the E/S Ratio on the Li-S Battery Performance

As mentioned previously, the majority of the literature focuses on the effect of E/S ratio on the discharge capacity and cycling performance of the Li-S battery. However, one should also consider the specific energy and energy density at the cell and system levels

while optimizing the electrolyte amount. In order to do so, both cell- and system-level performances of the Li-S battery are projected here, as discussed next.

5.1.2.1. Cell-Level Performance

Figure 5.5 demonstrates the specific energy and energy density of a Li-S cell as a function of the E/S ratio. It can be seen in the figure that at very high E/S ratios specific energy and energy density at the cell level decreases significantly. Even though our experimental results clearly present that the specific capacity is the highest for an E/S ratio of 20 µL mg^{-1}, the best cell level energy density and specific energy are achieved at lower E/S ratios. This observation suggests that the increase in the cell weight and volume with an increasing E/S ratio has a more prominent effect on the performance than the improvement in the discharge capacity. This critical discussion proves that the E/S ratio should be optimized not only based on the discharge capacity but also on the energy density.

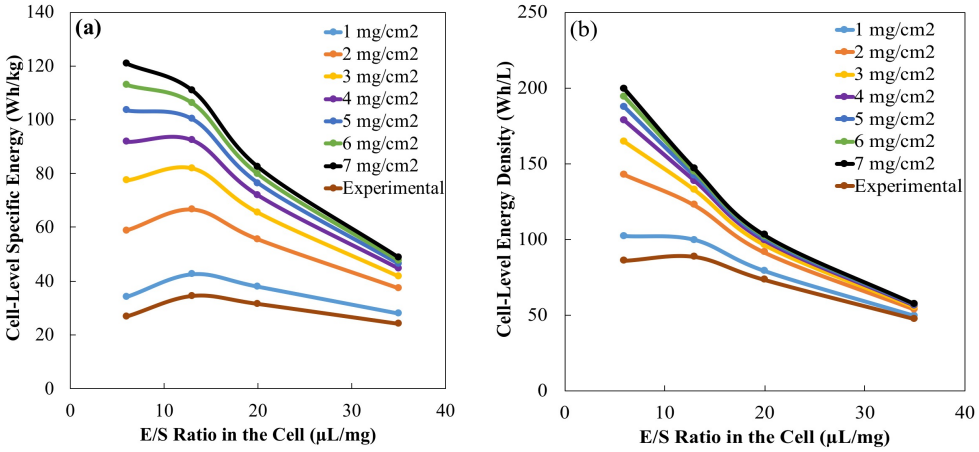

Figure 5.5. The effect of E/S ratio in the cell on the calculated cell level a) specific energy and b) energy density of Li-S cells with varying sulfur loadings at a C/S ratio of 1, N/P ratio of 1.5, and 0.1C. Experimental peak discharge capacities and cell voltages at 50% DOD are used in the predictions.

Since sulfur loading is another key design parameter affecting the performance of Li-S batteries considerably, its effect on the performance is also discussed in Figure 5.5. It is clear that when sulfur loading increases cell performance is enhanced remarkably. High sulfur loadings are required to attain higher specific energies and energy densities as also predicted in the literature [21,37]. It can be also discussed that the enhancement in the cell performance with increasing sulfur loading is specifically pronounced at low sulfur loadings; Li-S cells present similar energy densities at higher sulfur loadings. Another interesting observation in Figure 5.5 is that at low S loadings (including the experimental S loading in this study), the effect of discharge capacity on the specific energy is more pronounced as the highest specific energies are obtained for an E/S ratio of 13 µL mg^{-1}. On the other hand, energy densities are not as much affected; it may be discussed that the best energy densities are projected for the lowest E/S ratio for almost all S loadings.

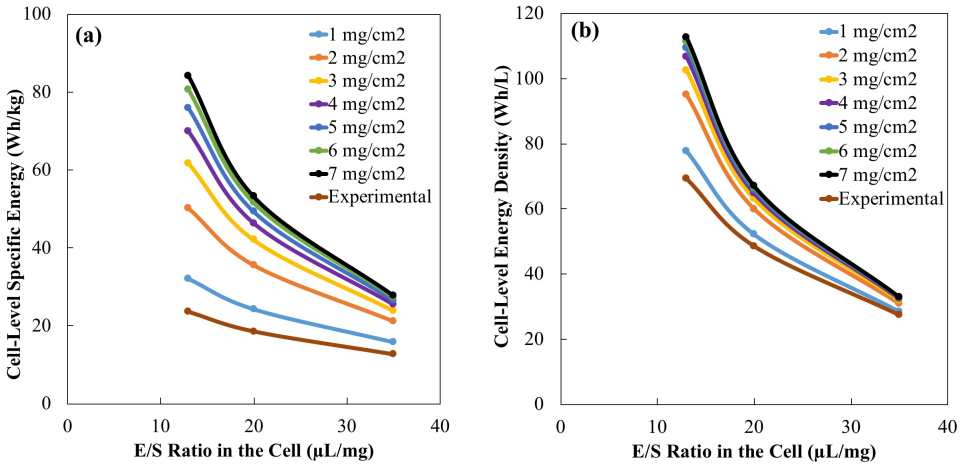

Figure 5.6. The effect of the E/S ratio in the cell on the calculated cell level a) specific energy and b) energy density of Li-S cells with varying sulfur loadings at a C/S ratio of 1, N/P ratio of 1.5, and 0.1C. Experimental discharge capacities at the 50th cycle of the cell and cell voltages at 50% DOD are used in the predictions.

In Figure 5.6, the effect of the E/S ratio on the cell level performance of Li-S cells with varying sulfur loadings is investigated by using the 50th cycle discharge capacities. This is mainly done to compare the performance of the cells based on their reversible capacity rather than the peak one and thus to include the cycling performance of the cells in the model

projections. Similar trends are obtained with Figure 5.5, but this time the predicted specific energies and energy densities are the highest for an E/S ratio of 13 μL mg^{-1} for all S loadings.

Here, it should be emphasized that in the predictions reported in Figures 5.5 and 5.6, the variation of the discharge capacity with S loading is not taken into consideration and the same discharge capacity at a certain E/S ratio is fed into the model for all S loadings. It is an optimistic assumption to take the discharge capacities constant with varying sulfur loading (as discussed in Figure 5.2b); however, our focus here is to determine the impact of the E/S ratio on the cell level performance. Therefore, in Figures 5.5 and 5.6 we aim to provide a roadmap for high energy density and specific energy Li-S cells and emphasize that Li-S batteries should be designed to have high S loadings at low E/S ratios in order to achieve high performance. Yet, we will focus on developing performance models considering the influence of S loading on the discharge capacity in our future studies.

5.1.2.2. System-Level Performance

As stated previously, higher electrolyte amounts lead to better battery capacity, yet it should be optimized by considering the overall mass and volume of the battery. Figures 5.7 and 5.8 show the predicted specific energy and energy density of a Li-S battery at the system level as a function of the E/S ratio in the cell. Similar to our discussions in the previous part, both specific energy and energy density decrease significantly with increasing electrolyte amounts in the cell. This suggests that the increase in the specific capacity of the cell with an increasing E/S ratio is less influential on the system performance compared to the increase in the pack weight and volume.

The impact of the E/S ratio on the system level performance is investigated for different maximum cathode thicknesses and C/S ratios using the developed model. As the scope of this work is studying the effect of the E/S ratio on battery performance, the effect of cathode thickness and C/S ratio is not examined experimentally in this study and the same cathode specific capacities are fed into the model for all electrode thicknesses and C/S ratios. Consequently, the influence of these two critical design factors is investigated by changing the maximum cathode thickness limitation (100, 150, and 200 μm) or the weight percentages

of carbon and sulfur (20:70, 30:60, 45:45, 60:30, 70:20) in the system level performance model.

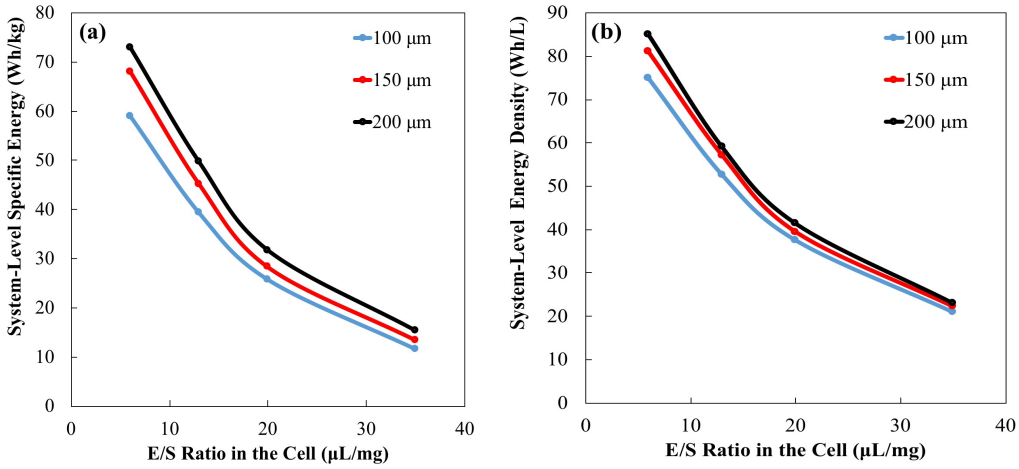

Figure 5.7. The effect of the E/S ratio in the cell on the calculated system level a) specific energy and b) energy density of Li-S cells with varying maximum cathode thicknesses at a C/S ratio of 1 and N/P ratio of 1.5. Experimental peak discharge capacities are used in the predictions.

The effect of maximum cathode thickness on the system level performance is also investigated in Figure 5.7. The figure exhibits that when the cathode thickness increases, the specific energy and energy density of the Li-S battery also increase. This is expected based on our discussion on the impact of sulfur loading; higher sulfur loadings can be achieved with increasing cathode thicknesses. Thus, higher cathode thicknesses result in higher cell capacities, thereby, better system level performance. It is also seen in the figure that the influence of the E/S ratio on the specific energy and energy density is clearer at higher cathode thicknesses due to prevailing kinetic limitations at these high cathode thicknesses.

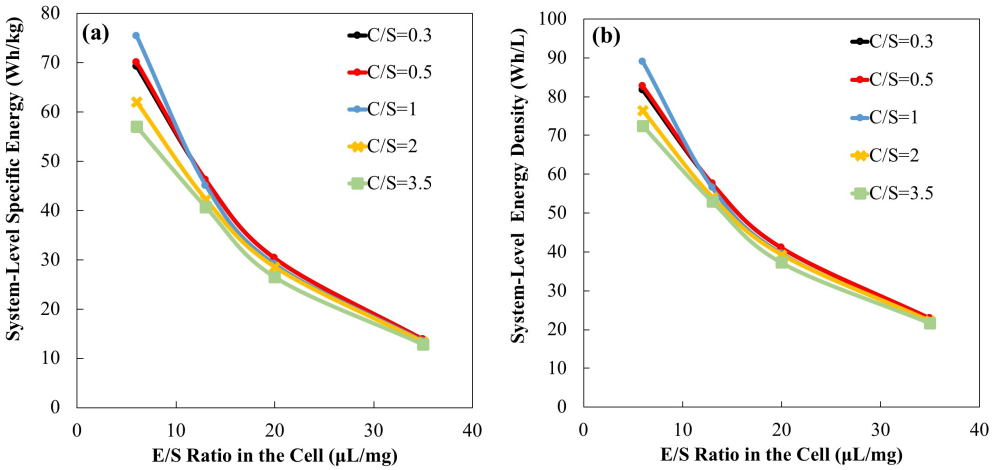

Figure 5.8. The effect of the E/S ratio in the cell on the calculated system level a) specific energy and b) energy density of Li-S cells with varying C/S ratios at a maximum cathode thickness of 150 µm and N/P ratio of 1.5. Experimental peak discharge capacities are used in the predictions.

Finally, in Figure 5.8 the impact of the C/S ratio on the battery performance is also considered. Carbon is needed in the cell in excess amounts due to its good electronic conductivity. Increasing carbon amount increases the discharge capacity and cyclability of the cell since it is a vital parameter affecting the electrochemically active surface area and electronic conductivity in the cathode. Consequently, there is a direct relation between the carbon amount and the cell voltage. However, since it is an inactive material in the cell as the electrolyte, it should be optimized considering the specific energy and energy density of the battery. As displayed in Figure 5.8, when the E/S ratio is low, decreasing the carbon amount, thus the C/S ratio, enhances the specific energy and energy density. This impact is less significant at higher E/S ratios. When the C/S ratio decreases, cell capacity increases due to an increase in the active material amount in the cell. It is clear that the effect of the C/S ratio on the system performance is noticeably observed at low E/S ratios.

5.2. The Effect of the C/S Ratio on the Li-S Battery Performance

Here, a novel approach combining experimental investigation and modeling to project the influence of the C/S ratio on the Li-S battery performance at the cell and system level is

proposed. Experimental characterization of the reliance of the cycling behavior and useable capacity of a Li-S battery on the C/S ratio is presented first. Then, performance models projecting the Li-S battery performance at the cell and pack level based on the C/S ratio are reported. These models are developed by taking into consideration the experimental variance of the battery performance with the carbon amount in the cell. Consequently, proposed models successfully capture and project the critical impact of cathode design on the Li-S battery performance. This part of the chapter was published as a paper [46] and the original manuscript has been adapted for this dissertation.

5.2.1. Experimental Characterization of the Effect of the C/S Ratio on the Li-S Cell Performance

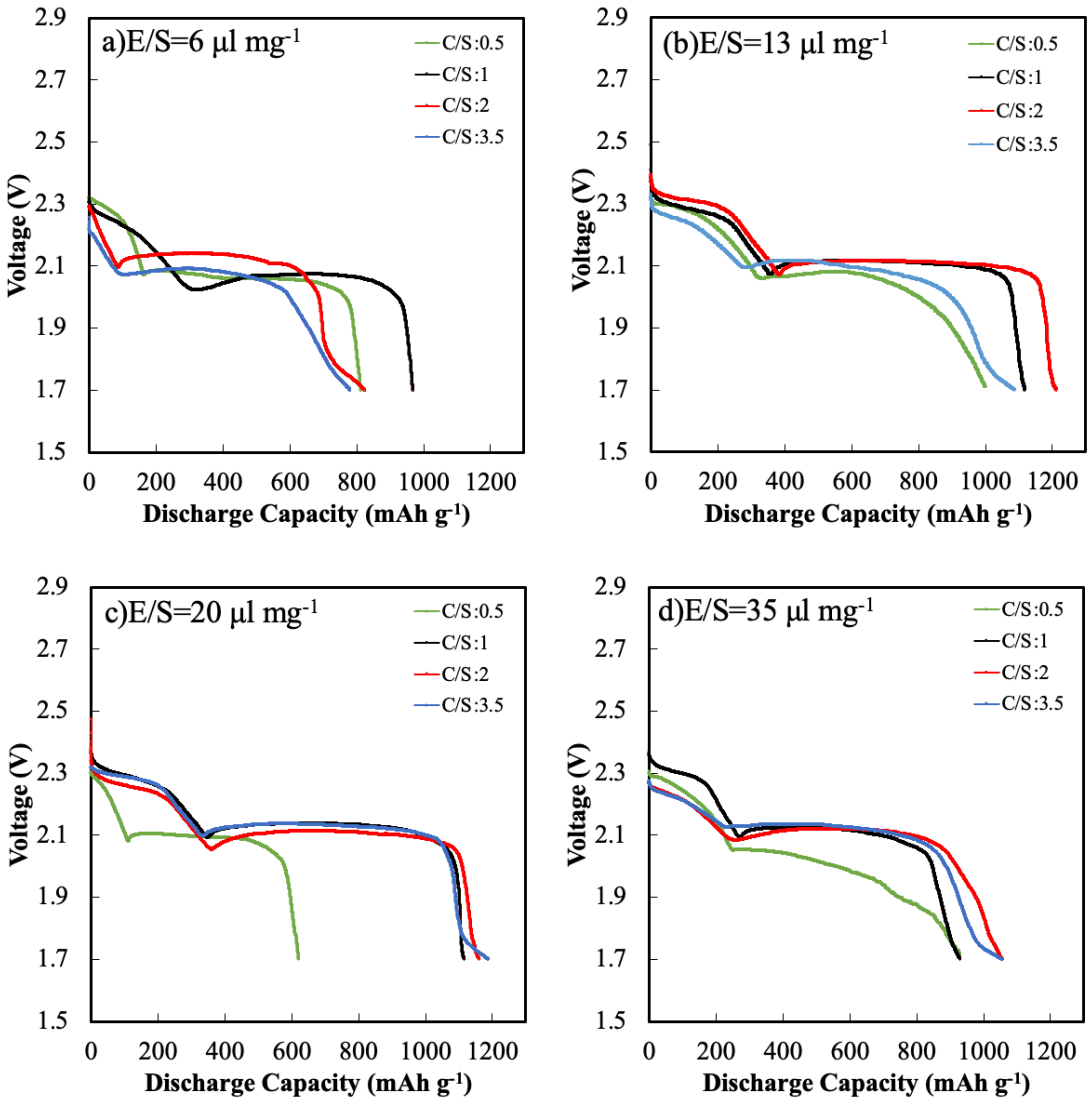

Figure 5.9. Initial discharge profiles of Li-S cells at E/S ratios of (a) 6, (b) 13, (c) 20, and (d) 35 µl mg^{-1} with changing C/S ratios at 0.1C (demonstrative replicate)

Herein, the reliance of the Li-S battery performance on the C/S ratio is discussed for various E/S ratios since the electrolyte amount in the cell is also a crucial factor in describing the battery performance through the reduction and shuttle mechanisms in the cathode and the total pack weight. Consequently, how the C/S ratio influences the battery performance

is presented here for various E/S ratios. Figure 5.9 illustrates the first discharge behavior of the Li-S cells as a function of the C/S ratio for various E/S ratios. For almost all C/S ratios, the two discharge plateaus around 2.4 V and 2.1 V are apparent in the figure; as known, the first plateau corresponds to the reaction of S forming higher-order polysulfides, and the second plateau represents the conversion of higher-order polysulfides into the lower ones [124]. The figure presents that the useable capacity increases with increasing carbon loading to a certain level, mainly because of the better kinetics and thus improved sulfur utilization at higher carbon amounts. It is previously shown that the C/S ratio has a great influence on the Li-S cell resistance (both transport and kinetic resistances), particularly in the excess or scarcity of sulfur in the cell [47]. Interestingly, the E/S ratio influences how the C/S ratio affects the specific capacity in a great manner. For instance, the highest capacity is attained at a different C/S ratio for each E/S ratio. For low or moderate E/S ratios (Figures 5.9a and 5.9b), Li-S cells with moderate C/S ratios provide the best performance. For instance, the highest initial specific capacity is obtained as 1165 mAh g^{-1} for the Li-S cell with a C/S ratio of 2 at an E/S ratio of 13 μl mg^{-1} corresponding to a sulfur utilization of ~70%. Moreover, for these low or moderate E/S ratios, the Li-S cell with C/S=3.5 presents poor performance mainly due to the low amount of electrolyte (Table 3.3.) and thus poor wetting of the cathode. On the other hand, capacities comparable to other C/S ratios are achieved for C/S=3.5 at higher E/S ratios (Figures 5.9c and 5.9d). Contrastingly, too low C/S ratios such as 0.5 lead to inferior capacities at almost all electrolyte amounts. Finally, it may be discussed that the influence of the C/S ratio is less pronounced at excessive E/S ratios (Figure 5.9d). These discussions on the impact of C/S and E/S ratios on the discharge profiles may also be extended based on the solubility and reduction kinetics of polysulfides in the cathode. First, it may be discussed that at low E/S ratios (Figure 5.9a), the capacity of the first discharge plateau is much lower than the theoretical value of 418 mAh g^{-1} for almost all C/S ratios, suggesting that the reduction of cyclo-S_8 to soluble high-order polysulfides is restricted [21]. This may be explained by the limited solubility of the polysulfides in the electrolyte at low electrolyte amounts, which may cause a shift in the reaction pathway in the first plateau [125]. Moreover, for low C/S ratios, the second voltage plateau presents a lower capacity and a decreasing trend for almost all E/S ratios indicating that the conversion of soluble Li_2S_n into Li_2S is quite sensitive to the C/S ratio. At low C loadings, the limited carbon surface area may hinder the precipitation of Li_2S_2 into Li_2S restraining the discharge capacity [21].

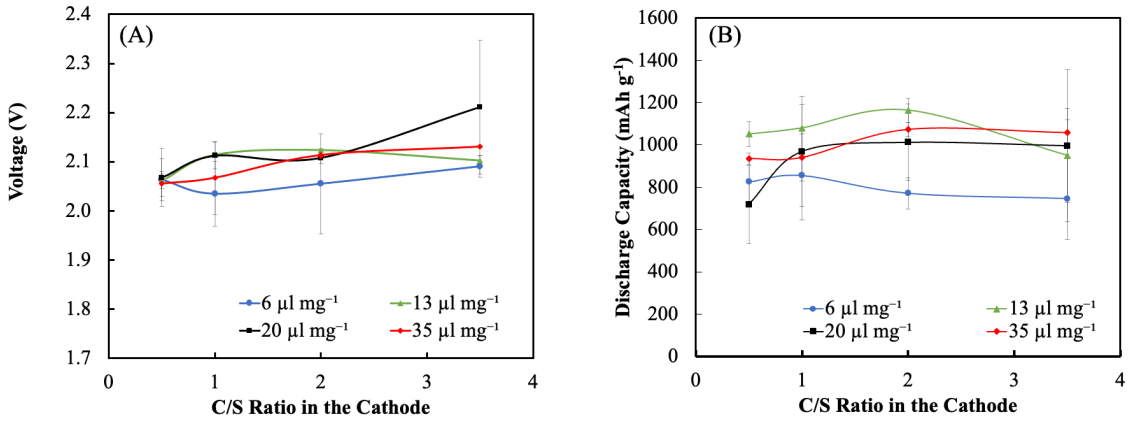

Figure 5.10 . Influence of C/S ratio on a) 50% DOD cell potential and b) peak discharge capacity for different E/S ratios (average of replicates).

The influence of the C/S ratio on discharge performance is summarized in Figure 5.10 as a function of the E/S ratio. As evident in the figure, different trends for the influence of the C/S ratio on the specific capacity and cell potential are obtained for different E/S ratios. For high E/S ratios, the discharge capacity and cell potential are both enhanced with an increasing C/S ratio. However, for moderate or low E/S ratios (13 and 6 µl mg^{-1}), capacity and cell voltage are improved only at moderate C/S ratios. As discussed above, high electrode polarization and limited S utilization as a result of the agglomeration of S in the electrode at excessive sulfur loadings cause poor performance at low C/S ratios [49]. Conversely, the insufficient amount of electrolyte at low sulfur loadings (or high C/S ratios) for moderate or low E/S ratios also results in detrimental cell performance.

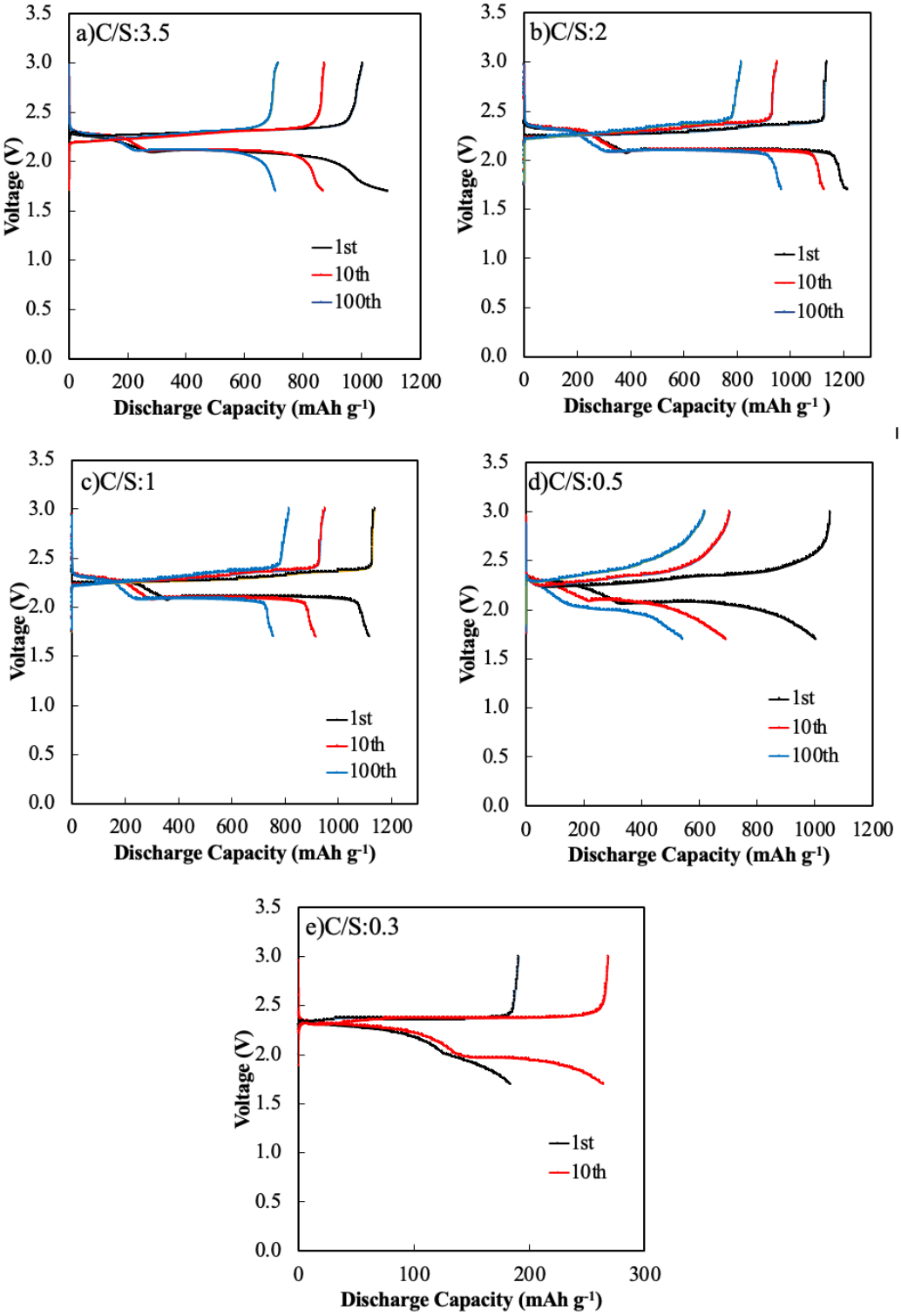

Figure 5.11. Voltage curves of Li-S cells at C/S ratios of a) 3.5, b) 2, c) 1, d) 0.5 and e) 0.3 for the 1st, 10th and 100th cycles (demonstrative replicate). E/S ratio is 13µl mg^{-1}.

The 1st,10th, and 100th cycle discharge and charge curves are shown in Figure 5.11 for various C/S ratios at a specific E/S ratio (13 µl mg^{-1}). The given E/S ratio is chosen to further investigate the effect of the C/S ratio on the discharge behavior of Li-S cells as the aforementioned effect is much more prominent here. It is clear in the figure that both the first and the second plateaus are sustained even for the 100th cycle for moderate C/S ratios (Figures 5.11b and 5.11c), whereas the second voltage plateau is not evidently detected for the others. Moreover, high capacity degradation is seen for very low or high carbon amounts in Figures 5.11a and 5.11e, respectively. The highest capacity retention is attained with a C/S ratio of 2. Furthermore, the cell with C/S=0.3 does not exhibit a clear first discharge plateau, mostly due to deficient cathode electronic conductivity (Figure 5.11e). Additionally, due to the low carbon loading in this sample, the reaction kinetics is severely hindered and thus, a sulfur utilization of ~11% is obtained.

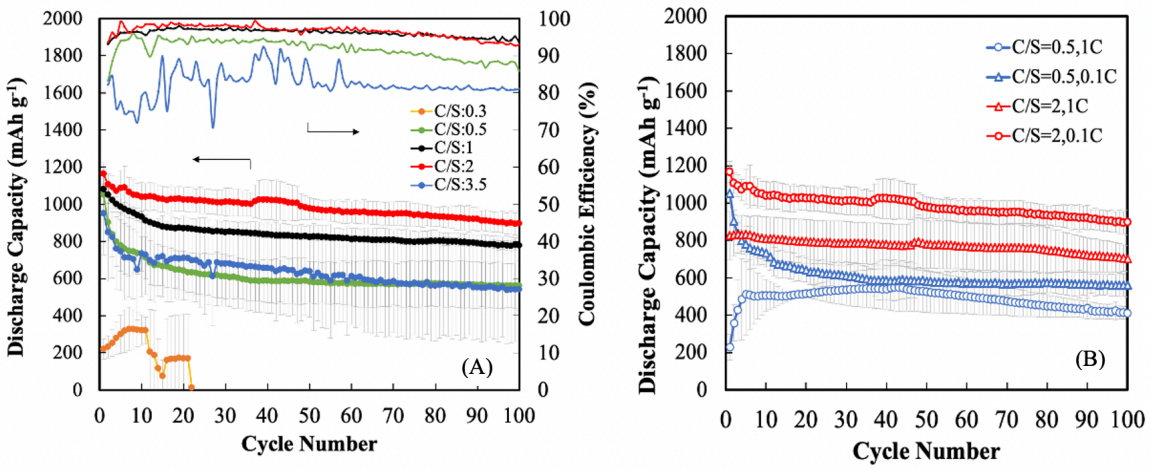

Figure 5.12. Influence of C/S ratio on the cycle life of Li-S cells a) at 0.1C and (b) at different C-rates for E/S ratio=13µL mg^{-1} (average of replicates).

Figure 5.12 presents the Li-S cell cycling behavior with changing C loadings. As evident in the figure, the cycling behavior is greatly affected by the carbon content in the cathode. The sample with C/S=2 demonstrates the best capacity retention as well as the highest initial discharge capacity (Figure 5.12a). The highest coulombic efficiency is also achieved with this sample. As evident in the figure, the capacity retention decreases as the C/S ratio decreases from 2 to 0.3. For instance, although the sample with a C/S ratio of 0.5 shows a high initial discharge capacity, a sharp capacity fade and a decrease in the coulombic

efficiency are seen for this cell with cycling. Moreover, the sample having a C/S ratio of 0.3 shows very poor performance; cycling could only be achieved until ~20 cycles. Relatively lower coulombic efficiencies in addition to the deficient cycling behavior observed at low carbon loadings indicate that the polysulfide shuttle mechanism is enhanced at higher S loadings [53]. It can also be discussed that there is a significant difference in the cycling performances of Li-S cells with C/S=0.5 and C/S=0.3. This may be explained such that the cell with a C/S ratio of 0.3 has a much higher S loading compared to that of C/S=0.5 (4.42 vs 1.48 mg cm^{-2} as seen in Table 3.4.). Consequently, the performance worsens much more drastically when the C/S ratio is decreased from 0.5 to 0.3. Increasing the C/S ratio from 2 to 3.5 also leads to inferior cycling performance as Figure 5.12a presents. Previously, we reported that the best capacity retention and cell and system level performance are achieved for the Li-S cell with an E/S ratio of 13 µl mg^{-1} [88]. Thus, herein, the impact of the C/S ratio on the cycling behavior is examined for this specific E/S ratio. Accordingly, 9 µl electrolyte is added into the cell with a C/S ratio of 3.5 to reach the desired E/S ratio. This low electrolyte amount in the cathode leads to exceedingly deficient cycling performance because of the inadequate wetting of the cathode; our calculations indicate that the minimum amount of electrolyte required to fully wet the cathode and the separator would be in the range of 13-21 µl. Moreover, the S loading in this sample with a C/S ratio of 3.5 is extremely low; the scarcity of the active material in the cell also contributes to the observed poor cycling performance. Additionally, in these carbon-rich cells, carbon may also contribute to the discharge capacity at low voltages (<1.8V) leading to the CEI formation and thus worsening the cycling performance; the tails seen in the voltage profiles in Figure 5.11 for C/S=3.5 indicates that the CEI formation may be substantial here. As also seen in the figure, much lower coulombic efficiencies are observed for this cell; at such high C/S ratios, sulfur scarcity in the cathode and low polysulfide concentration in the electrolyte may lead to isolated and inhomogeneous Li_2S formation, which may cause irreversibility in the charge/discharge processes and consequently low coulombic efficiencies [47,89,127,128]. Finally, it can be discussed that for moderate C/S ratios (2, 1, and 0.5) a reversible capacity is attained after approximately 15 cycles, which can connote that there is an equilibrium achieved between the sulfur content in the electrolyte and the electrode. Figure 5.12b presents the impact of the C/S ratio on the cycling performance of Li-S cells at a higher C-rate of 1C. In parallel to our discussions above, the Li-S cell with a C/S ratio of 2 offers a

better performance also for higher C-rates. This suggests that our conclusions on the impact of the C/S ratio on cycling performance can be extended for higher C-rates.

It should be noted that in this study the influence of the C/S ratio on the performance is discussed for varying S loadings in the cathode. An alternative way to investigate the impact of the C/S ratio on the battery performance would be to keep the S loading constant (and thus adjust the cathode thickness for each C/S ratio).

5.2.2. Model Predictions on the Effect of the C/S Ratio on the Li-S Battery Performance

Most studies address the influence of the C/S ratio on the cycle life and specific capacity. Nevertheless, the link connecting the C/S ratio to the Wh kg^{-1} and Wh L^{-1} should also be discussed. Here, the experimentally obtained peak discharge capacities, cell voltages, and sulfur loadings are fed into the proposed models and the Li-S battery performance is reported for the Li-S cell and pack based on the E/S and C/S ratios.

5.2.2.1. Cell-Level Performance

The significance of the effect of S and C loadings on the discharge behavior of the Li-S battery was discussed above. Electrolyte amount is another vital factor that must be considered while analyzing the Li-S battery performance. Limited E/S ratios are typically desired to reach enhanced Wh L^{-1}, whereas Li-S cells necessitate high electrolyte amounts to prevent electrolyte depletion and shuttle mechanism. Here, the impact of the C/S ratio on cell level performance will be deliberated together with the influence of the E/S ratio. Table 4.1. presents the experimental inputs used in the cell performance model.

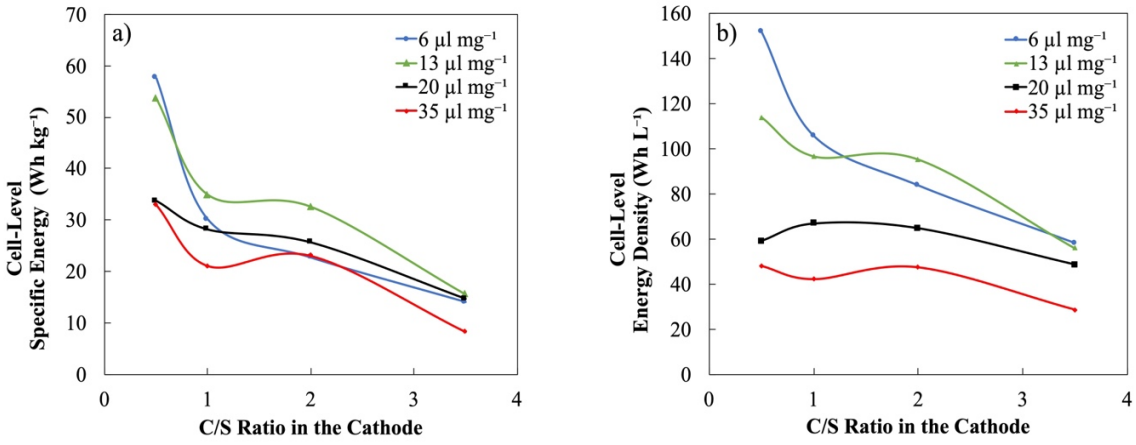

Figure 5.13. Influence of C/S ratio on the projected a) Wh kg^{-1} and (b) Wh L^{-1} of the Li-S cell for E/S and N/P ratios of 6, 13, 20, and 35 µL mg^{-1}, and 1.5, respectively.

The reliance of the cell performance on the C/S ratio is clear in Figure 5.13, especially for low or moderate E/S ratios (6 and 13 µl mg^{-1}). As the C/S ratio increases, the cell level performance worsens. For instance, even though the peak discharge capacities obtained at a C/S ratio of 0.5 are lower compared to the others (Figures 5.9a and 5.9b), the cell with this C/S ratio shows the best cell level performance. This indicates that the effect of carbon amount on the battery volume or mass is more dominant than its effect on the discharge capacity for low or moderate E/S ratios. On the contrary, the influence of C/S ratio on Wh L^{-1} is less noteworthy for higher E/S ratios. Similarly, the variance of the Wh L^{-1} or Wh kg^{-1} with the electrolyte amount is much more significant at low C/S ratios; they both increase with decreasing E/S ratio as the figure presents. Consequently, we may conclude that the cell level performance greatly depends on the cathode design factors, especially at low E/S and C/S.

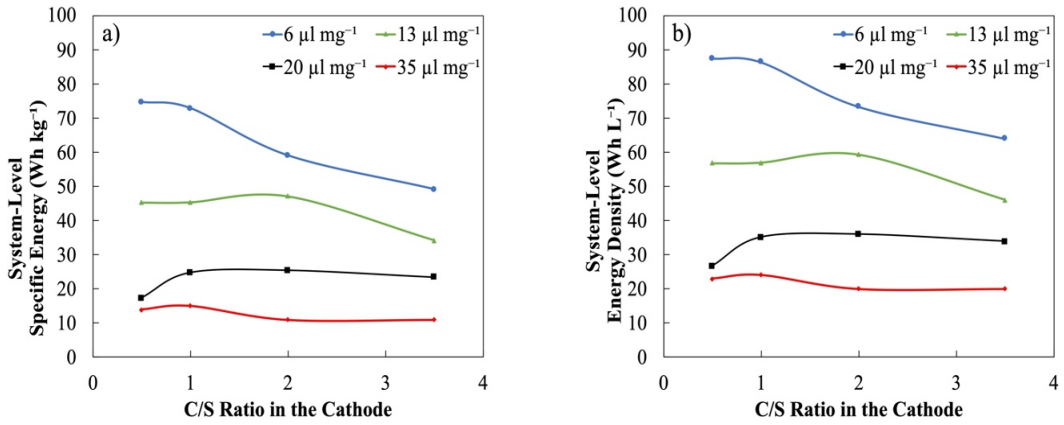

Figure 5.14. Influence of the C/S ratio on the projected a) Wh kg^{-1} and (b) Wh L^{-1} of the Li-S battery for E/S and N/P ratios of 6, 13, 20, and 35 µL mg^{-1}, and 1.5, respectively.

5.2.2.2. System-Level Performance

The development of practical Li-S batteries necessitates the consideration of the pack-level Wh L^{-1} and Wh kg^{-1} in addition to the cycling performance or the discharge capacity. Li-S battery performance calculated by using the experimentally achieved peak discharge capacities are displayed in Figure 5.14 based on the C/S ratio for various E/S ratios. Parallel to our previous discussions, Figure 5.14 presents dissimilar trends for the impact of the C/S ratio on the system level specific energy and energy density for different E/S ratios. The reliance of the Wh kg^{-1} and Wh L^{-1} on the C/S ratio is obvious for limited electrolyte amounts, whereas this trend is less pronounced at excessive E/S ratios. For low E/S ratios (6 µl mg^{-1}), energy density decreases with increasing C/S ratio, whereas for medium E/S ratios (13 and 20 µl mg^{-1}) a C/S ratio of 2 gives the best performance even though the difference between C/S=2 and C/S=1 is subtle. The reason for the slight increase seen when the C/S ratio increases from 1 to 2 for medium E/S ratios can be explained by the discharge capacity results reported in Figure 5.10b. We observe an increase in the discharge capacity when the C/S ratio increases from 1 to 2 for E/S ratios of 13 and 20 µl mg^{-1}; energy density projections follow this trend. Consequently, we can conclude that at medium E/S ratios, energy density predictions obey the discharge capacity trends. On the other hand, at low E/S ratios the change in the weight/volume of the pack with increasing C/S ratio has a more determinative influence on the calculated energy density. Finally, we may discuss that at the highest E/S

ratio of 35 μl mg^{-1}, the effect of C/S ratio on the energy density is almost nonexistent. As discussed in the previous chapter, for high E/S ratios, the electrolyte weight/volume dominates the pack weight/volume and the system level performance becomes less sensitive to the other design factors [46]. The best system level metrics are projected with the lowest C/S and E/S ratios of 0.5 and 6 μl mg^{-1}, respectively, even though this cell provided a lower peak discharge capacity compared to the others. This result supports our discussion that the Wh L^{-1} or Wh kg^{-1} for the battery packs should be a prior concern in Li-S cathode design; optimizing the E/S or C/S ratio based on the peak discharge capacities may be misleading. Our model projections validate that electrolyte-starved cells with high S loadings are required to accomplish high-performing Li-S batteries.

It should be noted that herein the system level performance projections are based on the experimental performance results of Li-S coin cells. As known, the E/S ratios used in coin cells are typically much higher compared to pouch cells [129]. It would be interesting to run the system level performance model developed here using the experimental performance results of pouch cells; this will be focused on in our future studies. Nevertheless, this study provides a detailed discussion on the impact of C/S and E/S ratios on the electrochemical performance and energy density of a Li-S battery and the conclusions can be easily extended to other cell designs.

5.3. The Effect of the Sulfur Loading and Carbon Type on the Li-S Battery Performance

Herein, we investigated the impact of S loading and carbon type on the electrochemical, cell- and system-level performance of the Li-S battery via employing experimental and modeling methods together. First, we examined the impact of carbon properties and sulfur loading on the capacity and cycle performance of the Li-S battery experimentally for cathodes containing carbons with different pore volumes, particle sizes, and specific surface areas prepared at different thicknesses (thus at varying S loadings). Furthermore, the dependency of the cell and system level energy density on the carbon properties and the S loading is inspected with the help of an experimentally-driven system level performance model for the Li-S battery. This part of the chapter is under review to be published and the original manuscript has been adapted for this dissertation.

5.3.1. Experimental Characterization of the Sulfur Loading and Carbon Type on the Li-S Cell Performance

Figure 5.15 displays the voltage profiles during the initial discharge of Li-S cells with different carbon cathodes of AB, KB, and Super C65 with varying sulfur loadings. For each illustration, the result of a representative replicate is provided. Figure 5.15 presents that the initial discharge capacity increases with increasing sulfur loading up to a point for almost all different carbon samples; the highest capacity is obtained for moderate S loadings (1.3-1.8 mg cm^{-2}) for all cases. On the other hand, a further increase in the active material loading results in a decrease in the capacity. This may be explained firstly by the excess sulfur in the pores constraining lithium interaction. Moreover, increasing cathode thickness hence sulfur loading causes polysulfide anions to agglomerate on the carbon surface and be converted into shorter and less soluble polysulfides blocking the remaining sulfur to contact with the carbon [37]. Sufficient wetting of thick sulfur cathodes is also challenging owing to the hydrophobic properties of both carbon and sulfur. Consequently, sulfur utilization worsens with increasing S loading also due to slow electrolyte infiltration and inadequate electrolyte uptake [59]. Furthermore, as the cathode thickness increases voltage drop becomes more visible; this is mainly due to hindered reaction kinetics at decreased cathode electronic conductivity. Notably, for Li-S cells with high S loadings the low voltage plateau, where the reduction of S_4^{2-} into solid Li_2S_2 and Li_2S occurs, is not clearly achieved. As known, the reduction of Li_2S_2 to Li_2S is necessary for high capacity and hence high energy density [130].

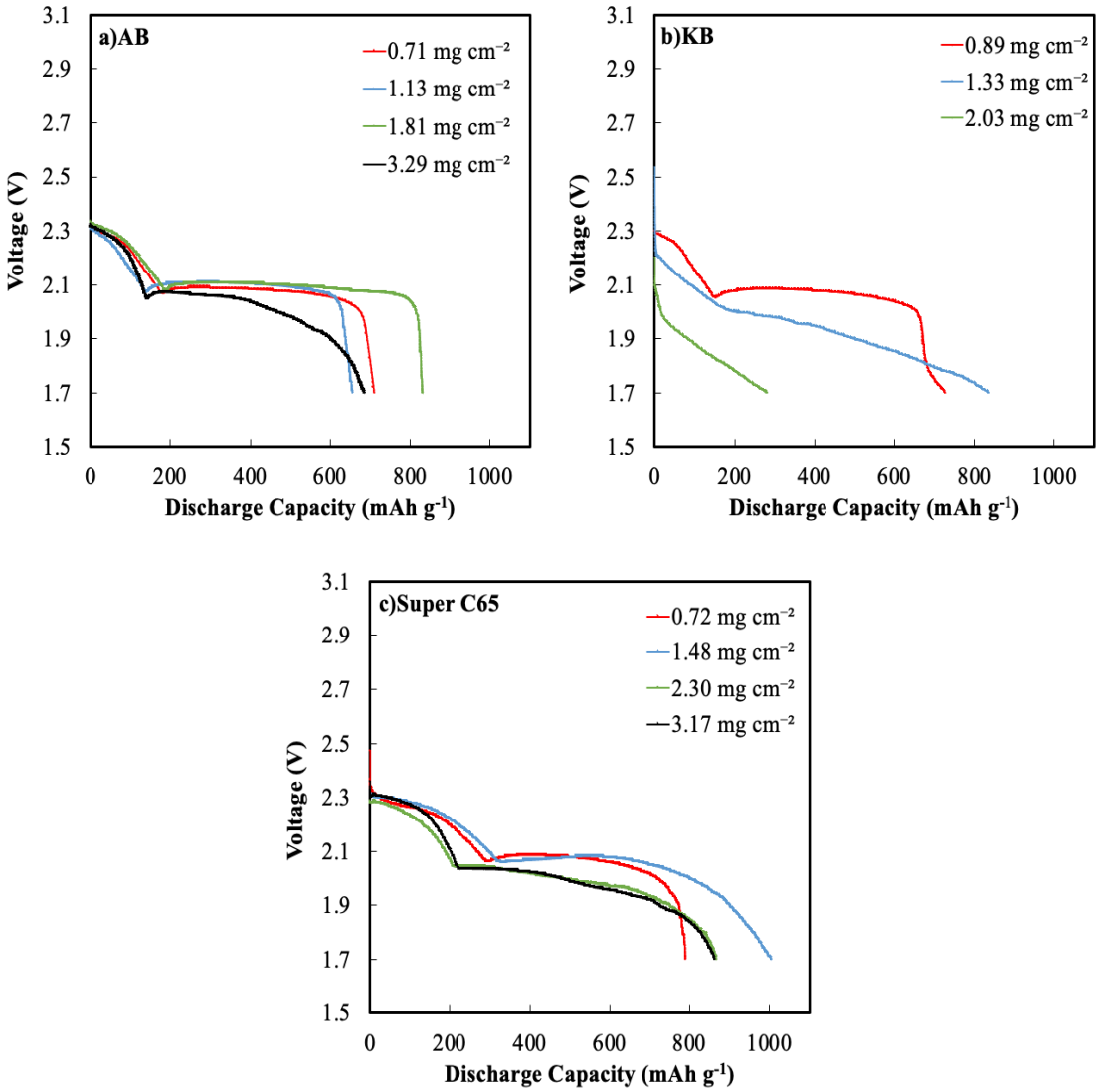

Figure 5.15. First discharge voltage curves for Li-S cells of different carbon cathodes with varying sulfur loadings at 0.1C.

The cycling behavior of Li-S cells with changing S loadings for all three carbon types is illustrated in Figure 5.16. The type of carbon used in the cathode has a determinative effect on how the S loading impacts capacity retention. For instance, it can be seen that S loading does not have a significant influence on the cycling behavior of Li-S cells with AB [131]. On the other hand, for Li-S cells with Super C65, the capacity retention is much better at higher S loadings (2.30 and 3.17 mg cm^{-2}) although the best initial discharge capacity was achieved for the S loading of 1.48 mg cm^{-2}. This may be explained by higher S-loaded cells

displaying higher capacity retention due to the delayed capacity fading because of the activation process [101]. For Li-S cells with KB, the dependence of the cycling behavior on the S loading is also different; much lower capacities are obtained at the highest S loading of 2.03 mg cm^{-2}. This result is rather surprising as KB has a significantly higher surface area compared to the other two types of carbon and thus it is expected to accommodate much higher S loadings in the cathode. This may be due to the inhomogeneous distribution of S in the cathode and fractures on the surface causing volume change and material loss with the cycling [59]. Moreover, there may be significant volume shrinkage in these high surface area materials during the solvent removal process in the cathode preparation [77].

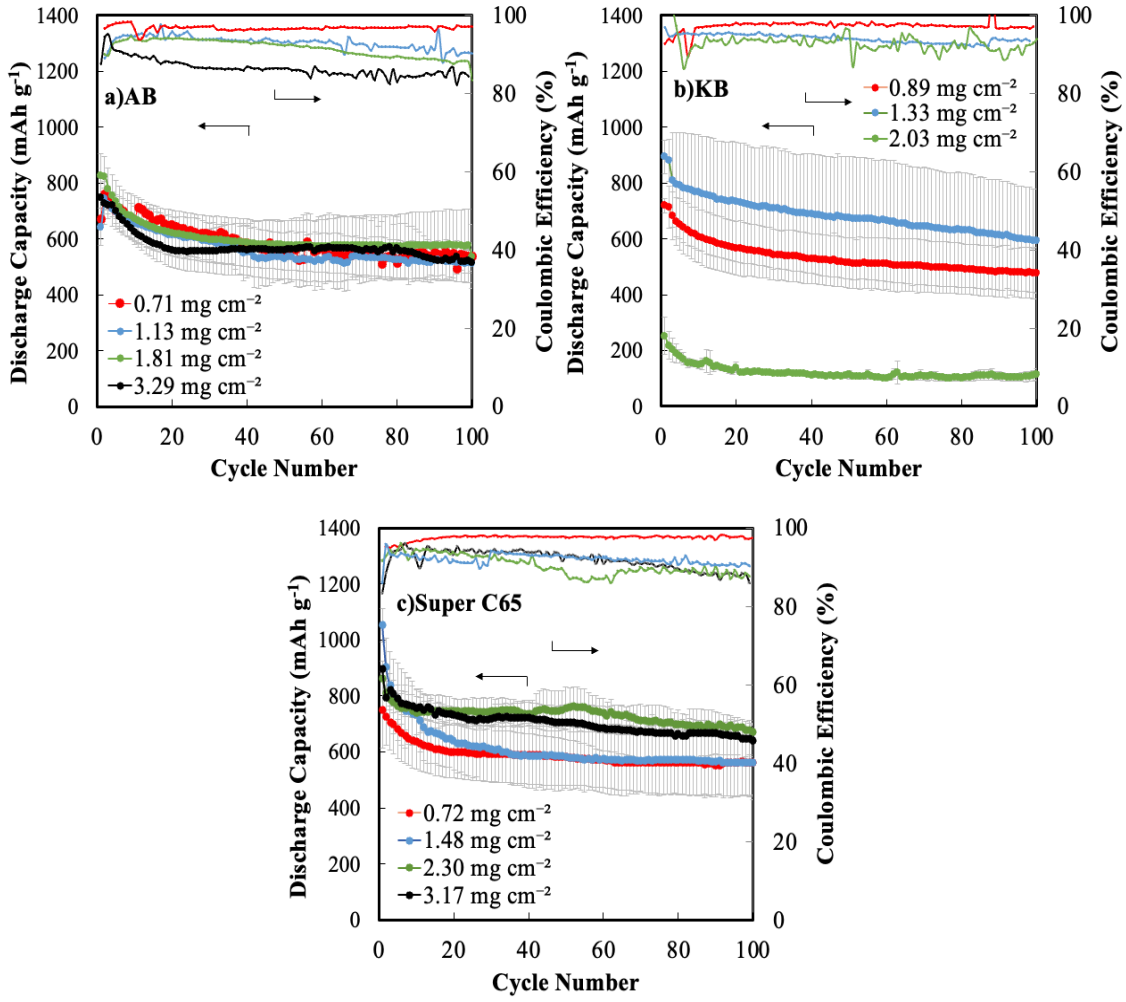

Figure 5.16. Comparison of capacity retention and coulombic efficiency for different carbon cathodes of a) AB, b) KB and c) Super C65 at varying sulfur loadings at 0.1C.

The effect of S loading on the coulombic efficiency is much clearer; coulombic efficiency decreases with increasing active material loading for all carbon types. This is expected since enhanced shuttle rates are expected for higher S-loaded cathodes.

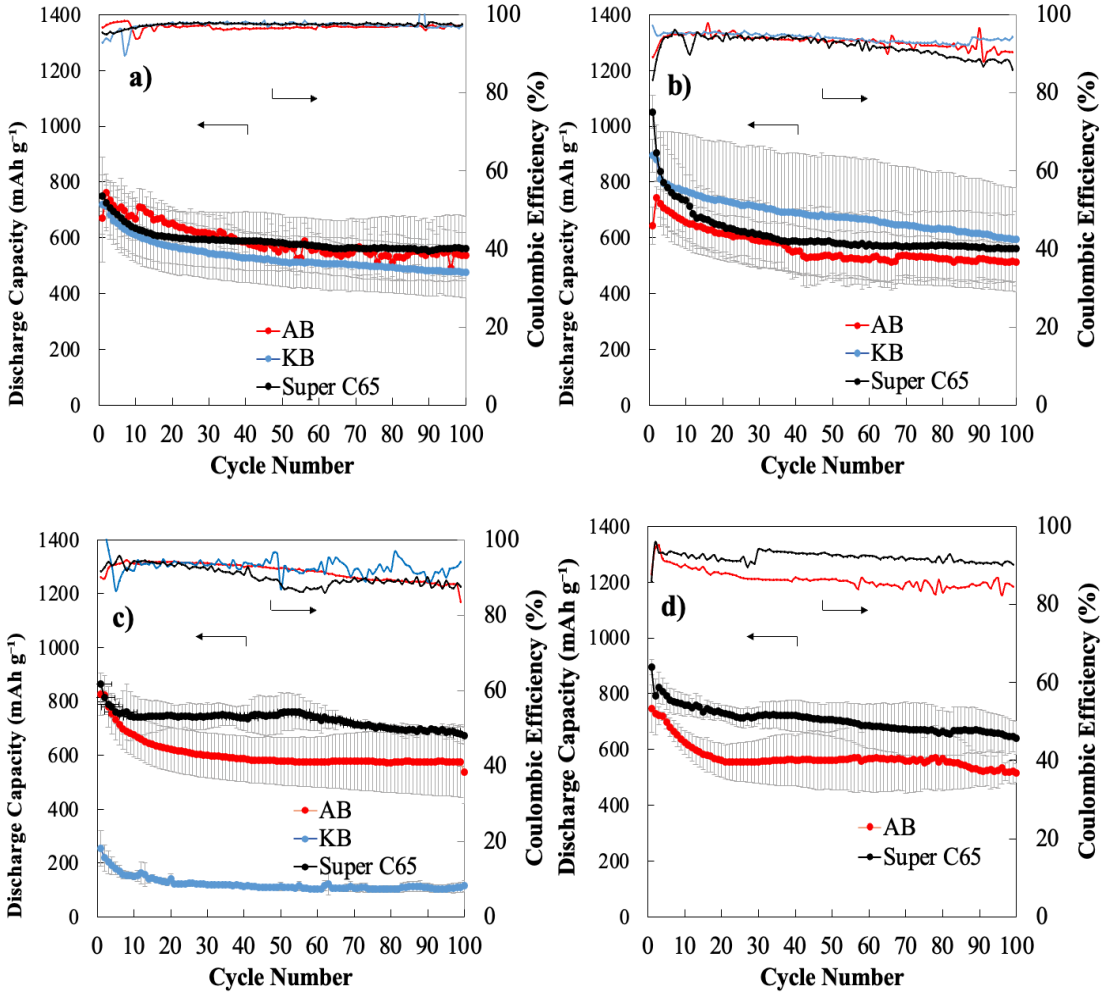

Figure 5.17. Comparison of capacity retention and coulombic efficiency for different carbon cathodes of AB, KB and Super C65 with varying sulfur loadings. a) AB as 0.71 mg cm^{-2}, KB as 0.89 mg cm^{-2} and Super C65 as 0.72 mg cm^{-2}, b) AB as 1.13 mg cm^{-2}, KB as 1.33 mg cm^{-2} and Super C65 as 1.48 mg cm^{-2}, c) AB as 1.81 mg cm^{-2}, KB as 2.03 mg cm^{-2} and Super C65 as 2.30 mg cm^{-2}, and d) AB as 3.29 mg cm^{-2} and Super C65 as 3.17 mg cm^{-2}.

So as to observe the impact of the carbon type on the battery performance in a more obvious manner, the cycling behavior of Li-S cells with different carbon cathodes is

compared for 4 different S loadings in Figure 5.17. As seen in Figure 5.17a, the cycling behavior of the cells with comparatively low S loadings shows no remarkable difference between the carbon variants. However, for medium S loadings (Figure 5.17b), the highest capacity retention is achieved with KB although it provides a relatively lower initial capacity of 894 mAh g^{-1}. Here, the highest initial discharge capacity is attained with Super C65 as 1051 mAh g^{-1}; yet, capacity fade for the cell with Super C65 is notable at the given S loading. Carbons with a larger specific surface area could deliver more electrochemical reaction sites available for the adsorption of the soluble lithium polysulfides and host of the lithium sulfide, and thus typically provides a better cycle life [74]. This may be the reason that the cell with KB gives the best capacity retention.

In contrast, as presented in Figure 5.17c, as the sulfur loading hence the cathode thickness increases, much lower capacities are achieved with KB. Super C65 exhibits the best capacity retention and the highest capacities among the other carbons at a S loading of ~2 mg cm^{-2}. Similar discussions can be made as the sulfur loading increases to almost 3 mg cm^{-2}; no significant change is observed for the cells with AB and Super C65. Yet, the cycling of the Li-S cell with KB cannot be achieved at this S loading due to problems with the cathode surface. As the carbon surface area increases, the discharge capacity and cycling behavior should be enhanced [106]. Although KB has superior features regarding its much higher surface area, surprisingly it did not provide the highest discharge capacity in our study. Moreover, as discussed above, it was not possible to increase the S loading of the cathodes with KB. The use of high surface area carbons may result in brittle electrodes with cracks over the surface, which becomes more distinct as the sulfur loading gets higher. Cathodes prepared with KB were non-homogenous and brittle, leading to poor performance. A different approach in electrode preparation might be needed to achieve high performance in KB containing cells; melt diffusion or encapsulation strategies may be more effective in incorporating S more homogeneously at higher loadings into the cathodes. Moreover, using conventional casting methods may result in cracking on the cathode surface after drying in addition to detachment during cycling due to poor interparticle adhesion [132].

Since the electrolyte amount is another decisive factor in the Li-S battery performance, an E/S ratio of 20 µl mg^{-1} is also investigated for different carbon types. As seen in Figure 5.18, as the E/S ratio increases from 13 to 20 µl mg^{-1}, the initial discharge capacities worsen;

this trend is more visible for AB and Super C65. The cycling performance of different carbon cathodes is also examined (Figure 5.19); better cycling performance is achieved with the lower E/S ratio for all carbon types. Moreover, our prior discussions on the impact of carbon type on battery performance are shown to be valid also for higher E/S ratios.

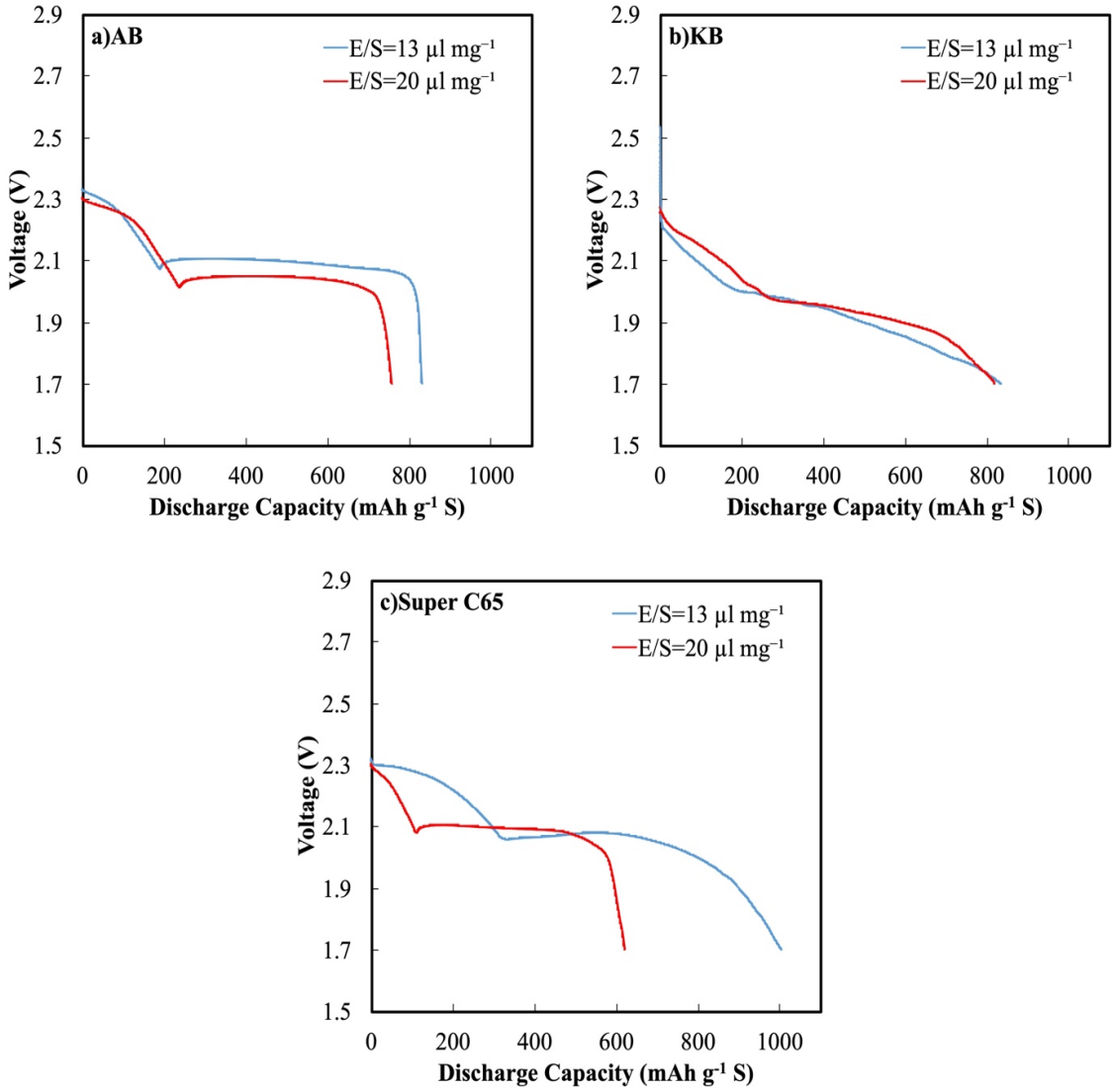

Figure 5.18. First discharge voltage profiles of Li-S cells of different carbon cathodes of a)AB, b)KB and c)Super C65 with varying E/S ratios of 13 and 20 µl mg^{-1} at 0.1C. S loading in the cathodes are 1.48-1.81 mg cm^{-2}.

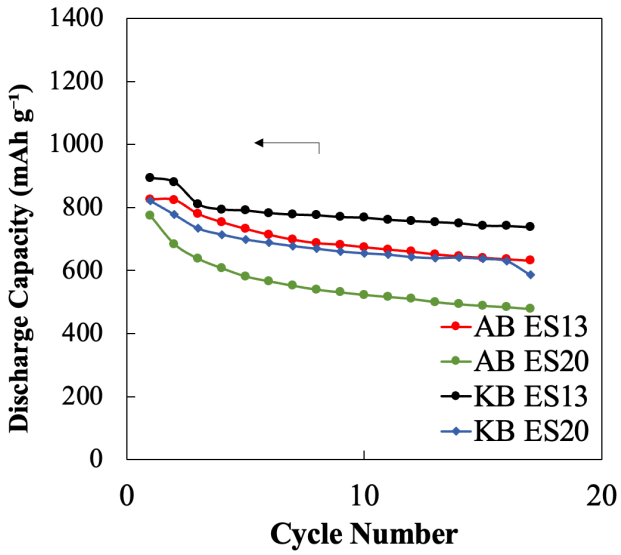

Figure 5.19. Cycling behavior of Li-S batteries with carbon cathodes of AB and KB with E/S ratios of 13 and 20 µl mg^{-1}.

Figure 5.20 presents the change of the voltage profiles with cycling for Li-S cells with different carbon cathodes. As known, the two plateaus at 2.4 V and 2.1 V correspond to the conversion of sulfur to higher-order polysulfides and the conversion of these to lower-order ones, respectively. It is apparent in the figure that these two plateaus are not distinctive for KB; the cell voltage decreases continuously during discharge. Interestingly, the two discharge plateaus become more well-defined at the 100^{th} cycle. On the contrary, Li-S cells with AB present a stable cell voltage throughout the low voltage plateau. In parallel with our previous discussions, even though the uppermost initial discharge capacity is attained for the Super C65 electrode (1051 mAh g^{-1}), capacity fade is more pronounced for this cell at the given S loading, and the Li-S cell with KB presents better capacity retention as evident in the figure.

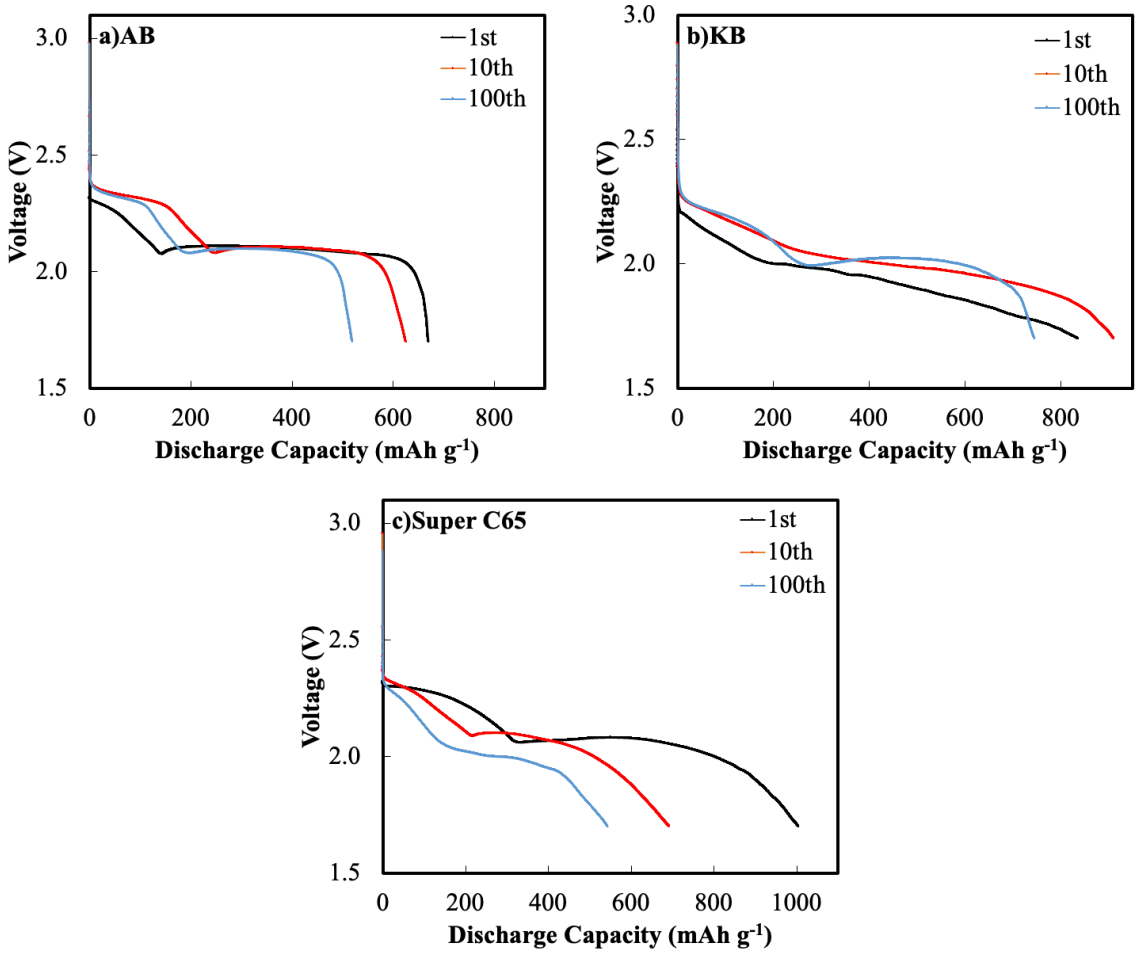

Figure 5.20. Comparison of the 1st, 10th, and 100th discharge curves of different carbon cathodes of a) AB with a sulfur loading of 1.13 mg cm^{-2}, b) KB with a sulfur loading of 1.33 mg cm^{-2}, and c) Super C65 with a sulfur loading of 1.48 mg cm^{-2}.

Peak and 50th cycle discharge capacities and cell voltages at the 50% depth of discharge (DOD) of Li-S cells for various sulfur loadings on different carbon electrodes are displayed in Figure 5.21. For all carbon electrodes, it is seen that as the sulfur loading increases, peak discharge capacity also increases up to a sulfur loading of approximately 2 mg cm^{-2}. However, a further increase in the S loading causes a decline in the discharge capacity, and this behavior is more distinct with the KB electrode. As explained above, KB cathodes at higher thicknesses are very stiff and brittle, and thus the battery performance is severely affected at higher S loadings. Similar behavior is attained with the discharge capacities at the 50th cycle, except that Li-S cells with KB electrodes show superior

capacities than the others at low S loadings due to their advantage in capacity retention. Despite that, Figure 21b presents that the highest capacity is obtained with the Li-S cell containing Super C65 with a S loading of 2.3 mg cm^{-2}. Moreover, cell voltage decreases with increasing sulfur loading in all cases because of lower electronic conductivity and surface area and increasing current density and overpotential.

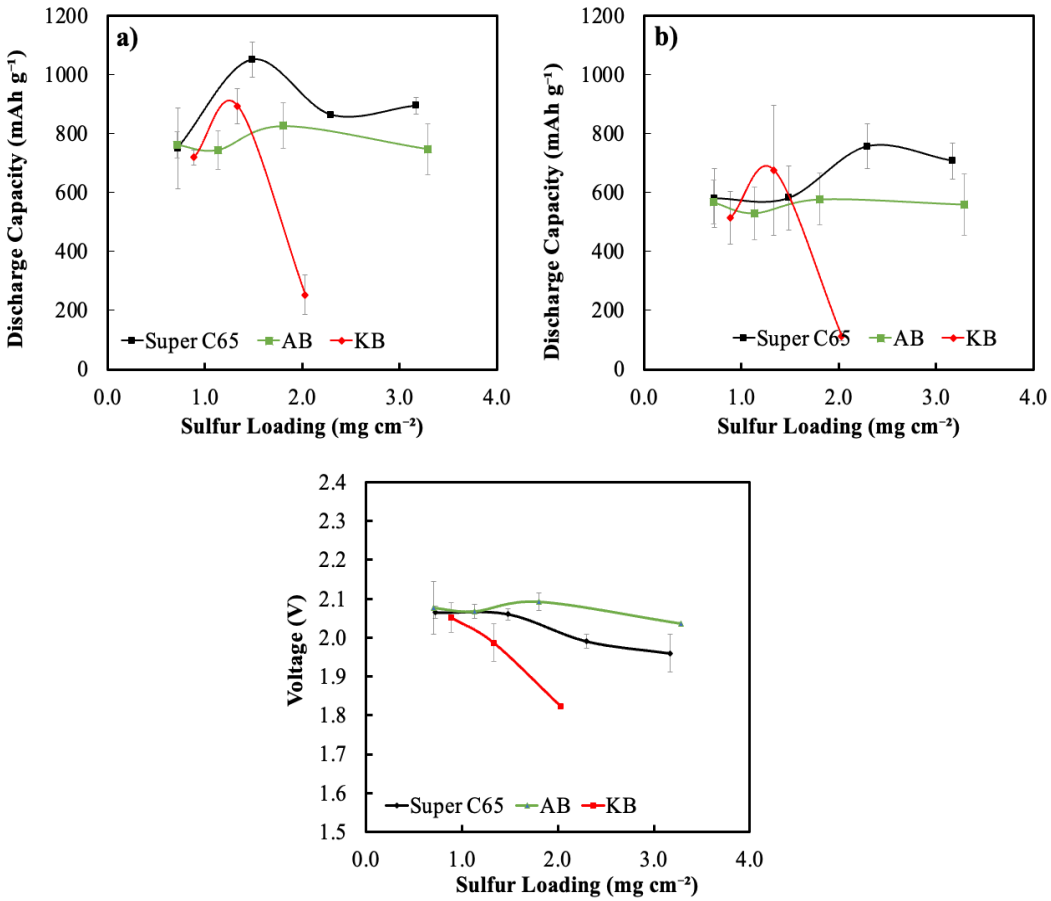

Figure 5.21. Influence of carbon type and S loading on the a) peak discharge capacity, b) discharge capacity at the 50th cycle, and c) cell voltage at the 50% DOD.

5.3.3. Model Predictions on the Effect of Sulfur Loading and Carbon Type on the Li-S Battery Performance

5.3.3.1. Cell-Level Performance

The impact of sulfur loading and carbon type on the cell level performance is projected via the model, of which parameters are given in Table 4.3. The cell level model uses experimental peak discharge capacities and cell voltages at the 50% DOD. As seen in Figure 5.22, increasing sulfur loading improves the cell level performance until a certain level of sulfur loading. Interestingly, Li-S cells with AB and Super C65 cathodes show slightly different trends of energy density and specific energy at higher S loadings. For instance, higher sulfur loadings with AB and Super C65 cathodes increase the specific energy, whereas cell level energy density decreases with a further increase in the S amount. This suggests that the weight of the cell is more sensitive to the active material loading; the decrease in the cell weight with increasing S loading is more influential than the decrease in the cell capacity. The deficient performance of the cell with KB at high S loadings is obviously due to the low discharge capacity.

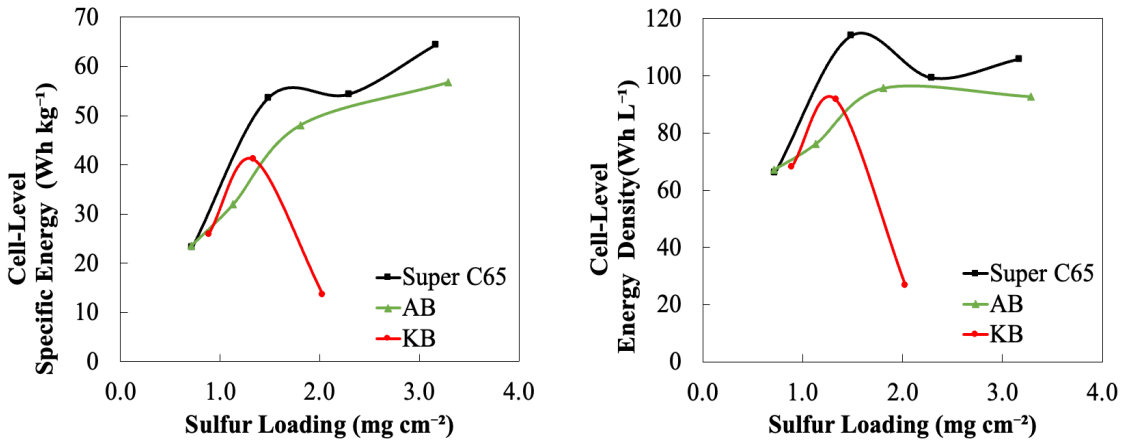

Figure 5.22. Model projections on the cell level a) Wh kg^{-1} and (b) Wh L^{-1} of the Li-S battery with different carbon electrodes at various sulfur loadings. N/P ratio=1.5 and 0.1C.

5.3.3.2. System Level Performance

High practical energy densities are required for Li-S batteries for their commercialization in the future; consequently, projecting the performance at the pack level is critical for Li-S batteries. Figure 5.23 displays the effect of sulfur loading with different carbon electrodes on the system level performance, modeled using the experimentally measured peak discharge capacities. Higher S loadings are expected to enhance energy density due to the minimized amount of inactive material. However, this trend is not fully captured here. For Li-S cells with both AB and Super C65 cathodes, the highest metrics at the pack level are projected at medium S loadings, where the discharge capacities are maximized. A better design of electrodes is probably required to improve discharge capacities and thus energy densities at higher S loadings. Lastly, it is evident in the figure that the highest pack performance is achieved with the use of Super C65 in the cathode.

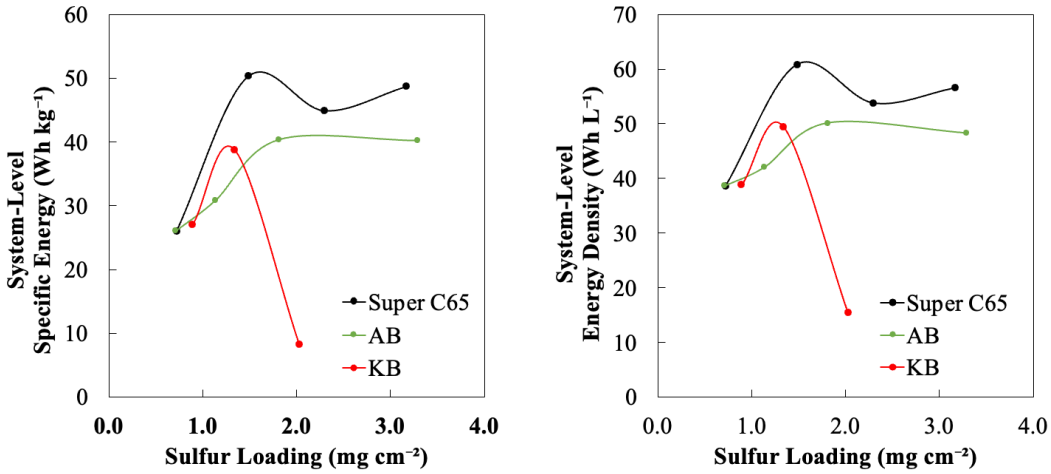

Figure 5.23. Model projections on the system level a) Wh kg^{-1} and (b) Wh L^{-1} of the Li-S battery with different carbon electrodes at various sulfur loadings. N/P ratio=1.5 and 0.1C.

6. CONCLUSIONS AND RECOMMENDATIONS

6.1. Conclusions

In this study, the effect of key cathode design parameters, E/S ratio, C/S ratio, sulfur loading, and carbon type, on the Li-S battery performance is assessed through electrochemical characterization and performance modeling.

First, electrochemical characterization of Li-S cells with varying E/S ratio was performed and the experimental results were fed into the developed cell-and-system level performance models to project the effect of the E/S ratio on the specific energy and energy density of the Li-S battery. Experimental results demonstrated that even though the highest initial discharge capacity was obtained for an E/S ratio of 20 μL mg^{-1}, the highest capacity retention was achieved with an E/S ratio of 13 μL mg^{-1}. Cell- and system-level energy density and specific energy projections clearly suggested that lower E/S ratios were better for higher performance. The impact of sulfur loading, cathode thickness, and C/S ratio on the energy density and specific energy was also investigated along with the E/S ratio with the developed performance models. To conclude, when the influence of the E/S ratio not only on the initial discharge capacity and cycling performance but also on the specific energy and energy density at the cell and system level were considered, an E/S ratio of 13 μL mg^{-1} showed the best performance. Our approach has clearly shown that achieving enhanced cycle life at low E/S ratios and high S loadings is crucial to attain high specific energy and energy density at the system level, thus, to succeed practical Li-S batteries.

Next the impact of the C/S ratio on the battery cycling behavior and discharge profiles for varying E/S ratios was performed. It was concluded that moderate C/S ratios (1 or 2) achieve the best performance, mainly due to a trade-off between high electronic conductivity (thus high sulfur utilization) and high active material loading. The highest initial discharge capacity and the best capacity retention were achieved for the Li-S cell having C/S=2 and E/S=13 μl mg^{-1}. Next, performance models for Li-S cells and packs were developed by incorporating the experimental dependence of the discharge capacities on the C/S ratio. Wh L^{-1} and Wh kg^{-1} at the cell and pack level were projected for the Li-S battery based on the

E/S and C/S ratios. C loading affects the battery performance more dominantly at low E/S ratios; as the electrolyte amount increases, this trend is less likely to be captured. To conclude, the projection of the Li-S battery Wh L^{-1} and Wh kg^{-1} is critical in the optimization of the cell design.

Finally, the influence of carbon properties on Li-S battery discharge behavior and cycling performance was investigated experimentally for cathodes prepared at various thicknesses using three different carbons (Super C65, AB, and KB) with varying pore volumes, particle sizes, and specific surface areas. Furthermore, the impact of sulfur loading on the electrochemical performance of a Li-S cell was discussed for these three carbons. Following experimental characterization, a system level performance model was presented by adapting the publicly available BatPaC model to estimate the Wh L^{-1} and Wh kg^{-1} of the battery pack based on carbon type and S loading. The performance model considers the experimental relationship between the discharge capacity and the carbon type. It also contains a one-dimensional electrochemical model that predicts the variance of the current-voltage association as a function of carbon characteristics. The cycling behavior of Li-S cells with various S loadings suggested that the carbon utilized in the cathode significantly influences how the S loading impacts the battery performance. Li-S cells with AB, for example, exhibited no significant sensitivity toward S loading, but Li-S cells with Super C65 retained more capacity at higher S loadings. Li-S cells with KB, on the other hand, were unable to attain good performance at higher S loadings, which was surprising given their significantly larger surface area. This poor performance might be due to an inhomogeneous distribution of S in the cathode. Our findings also implied that carbon characteristics are more important in determining the cycling performance for higher S loadings. Moreover, Super C65 was projected to have the best pack performance. Li-S cells with both AB and Super C65 cathodes attained the highest system-level metrics when discharge capacities are maximized at medium S loadings. Our results demonstrate that enhancing the battery pack's energy density and specific energy is crucial and focusing exclusively on discharge performance for Li-S cell design might be deceptive.

6.2. Recommendations

The impact of critical cathode design parameters on the electrochemical, cell-and system-level performance of Li-S batteries has been investigated in this thesis. The following recommendations can be considered in future research to deepen the presented analysis.

- The effect of the E/S ratio, C/S ratio, sulfur loading and carbon type in the cathode on the Li-S battery performance was examined in this study. The effect of other key factors such as the electrolyte material, binder type and separator type can also be investigated.
- Li-S battery resistance for the key design parameters investigated in this study can be examined
- High sulfur loadings and low E/S ratios are desired in the matter of achieving high-performance Li-S batteries. Therefore, the encapsulation of cathodes can be examined to improve the cell- and- system level performance of Li-S batteries.
- The effect of different carbon types can also be studied by improving the cathode preparation method.
- Electronic conductivity and surface morphology analysis can be done for the different carbons used in the study.

REFERENCES

1. J. S. Newman and C. W. Tobias, “Theoretical Analysis of Current Distribution in Porous Electrodes”, *Journal of the Electrochemical Society*, Vol. 109, No. 12, p. 1183, 1962.

2. B. Scrosati and J. Garche, “Lithium Batteries: Status, Prospects And Future”, *Journal of Power Sources,* Vol. 195, No. 9, pp. 2419–2430, 2010.

3. A. Rosenman, E. Markevich, G. Salitra, D. Aurbach, A. Garsuch, and F. F. Chesneau, “Review on Li-Sulfur Battery Systems: An Integral Perspective”, *Advanced Energy Materials*, Vol. 5, No. 16, p. 1500212, 2015.

4. Z. Yang, J. Zhang, M. Kintner-Meyer, X. Lu, D. Choi, J. Lemmon, W. Liu,, “Electrochemical Energy Storage for Green Grid”, *Chemical Reviews*, Vol. 111, No. 5, pp. 3577–3613, 2011.

5. A. F. Burke, “Batteries and Ultracapacitors for Electric, Hybrid, and Fuel Cell Vehicles”, *Proceedings of the IEEE*, Vol. 95, No. 4, pp. 806–820, 2007.

6. J. M. Tarascon and M. Armand, “Issues and Challenges Facing Rechargeable Lithium Batteries”, *Nature*, Vol. 414, No. 6861, pp. 359–367, 2001.

7. M. S. Whittingham, “Materials Challenges Facing Electrical Energy Storage”, *MRS Bulletin*, Vol. 33, No. 4, pp. 411–419, 2008.

8. X. Chen, Y. Zhang, “The Main Problems and Solutions in Practical Application of Anode Materials for Sodium Ion Batteries and the Latest Research Progress”, *International Journal of Energy Research*, Vol. 45, pp. 9753-9779, 2021.

9. J. Gao and H. D. Abruña, “Key Parameters Governing the Energy Density of Rechargeable Li/S Batteries”, *Journal of Physical Chemistry Letters*, Vol. 5, No. 5, pp. 882–885, 2014.

10. H. D. Abruña, Y. Kiya, and J. C. Henderson, “Batteries and Electrochemical Capacitors”, *Physics Today*, Vol. 61, No. 12, pp. 43–47, 2008.

11. A. Zhamu, G. Chen, C. Liu, D. Neff, Q. Fang, Z. Yu, W. Xiong, Y. Wang, X. Wang, B. Jang, “Reviving Rechargeable Lithium Metal Batteries: Enabling Next-Generation High-Energy and High-Power Cells”, *Energy and Environmental Science*, Vol. 5, No. 2, pp. 5701–5707, 2012.

12. B. L. Ellis, K. T. Lee, and L. F. Nazar, “Positive Electrode Materials for Li-Ion and Li-Batteries”, *Chemistry of Materials*, Vol. 22, No. 3, pp. 691–714, 2010.

13. E. Peled, Y. Sternberg, A. Gorenshtein, and Y. Lavi, “Lithium-Sulfur Battery: Evaluation of Dioxolane-Based Electrolytes”, *Journal of the Electrochemical Society*, Vol. 136, No. 6, pp. 1621–1625, 1989.

14. D. Aurbach, “Introduction to the Focus Issue on Lithium-Sulfur Batteries: Materials, Mechanisms, Modeling, and Applications”, *Journal of the Electrochemical Society*, Vol. 165, No. 1, pp. Y1–Y1, 2018.

15. X. Ji, K. T. Lee, and L. F. Nazar, “A Highly Ordered Nanostructured Carbon-Sulphur Cathode for Lithium-Sulphur Batteries”, *Nature Materials*, Vol. 8, No. 6, pp. 500–506, 2009.

16. V. Thangavel, K.-H. Xue, Y. Mammeri, M. Quiroga, A. Mastouri, C. Guéry, P. Johansson, M. Morcrette, A.A. Franco,“A Microstructurally Resolved Model for Li-S Batteries Assessing the Impact of the Cathode Design on the Discharge Performance”, *Journal of the Electrochemical Society*, Vol. 163, No. 13, pp. A2817–A2829, 2016.

17. W. Xue, L. Miao, L. Qie, C. Wang, S. Li, J. Wang, J. Li, “Gravimetric and Volumetric Energy Densities Of Lithium-Sulfur Batteries”, *Current Opinion in Electrochemistry*, Vol. 6, No. 1, pp. 92–99, 2017.

18. V. S. Kolosnitsyn and E. V. Karaseva, “Lithium-Sulfur Batteries: Problems and Solutions”, *Russian Journal of Electrochemistry*, Vol. 44, No. 5, pp. 506–509, 2008.

19. M. Hagen, D. Hanselmann, K. Ahlbrecht, R. Maça, D. Gerber, and J. Tübke, “Lithium-Sulfur Cells: The Gap between the State-of-the-Art and the Requirements for High Energy Battery Cells”, *Advanced Energy Materials*, Vol. 5, No. 16, 2015.

20. W.J. Chung, J.J. Griebel, E.T. Kim, H. Yoon, A.G. Simmonds, H.J. Ji, P.T. Dirlam, R.S. Glass, J.J. Wie, N.A. Nguyen, B.W. Guralnick, J. Park, Á. Somogyi, P. Theato, M.E. Mackay, Y.E. Sung, K. Char, J. Pyun, “The Use of Elemental Sulfur as an Alternative Feedstock for Polymeric Materials”, *Nature Chemistry*, Vol. 5, No. 6, pp. 518–524, 2013.

21. N. Ding, S. W. Chien, T. S. A. Hor, Z. Liu, and Y. Zong, “Key Parameters in Design of Lithium Sulfur Batteries”, *Journal of Power Sources*, Vol. 269, pp. 111–116, 2014.

22. S. S. Zhang, “Liquid Electrolyte Lithium/Sulfur Battery: Fundamental Chemistry, Problems, and Solutions”, *Journal of Power Sources*, Vol. 231, pp. 153–162, 2013.

23. C. Barchasz, J. C. Leprêtre, F. Alloin, and S. Patoux, “New Insights into the Limiting Parameters of the Li/S Rechargeable Cell”, *Journal of Power Sources*, Vol. 199, pp. 322–330, 2012.

24. Y. Zhang, Y. Zhao, K. E. Sun, and P. Chen, “Development in Lithium/Sulfur Secondary Batteries”, *Open Materials Science Journal*, Vol. 5, No. 1, pp. 215–221, 2011.

25. Y. Diao, K. Xie, S. Xiong, and X. Hong, “Shuttle Phenomenon-the Irreversible Oxidation Mechanism of Sulfur Active Material in Li-S Battery”, *Journal of Power Sources*, Vol. 235, pp. 181–186, 2013.

26. M. Barghamadi, A.S. Best, A.I. Bhatt, A.F. Hollenkamp, M. Musameh, R.J. Rees, T. Rüther, “Lithium-Sulfur Batteries - The Solution is in the Electrolyte, but is the Electrolyte a Solution?”, *Energy and Environmental Science*, Vol. 7, No. 12, pp. 3902–3920, 2014.

27. W. Ren, W. Ma, S. Zhang, and B. Tang, “Recent Advances in Shuttle Effect Inhibition for Lithium Sulfur Batteries”, *Energy Storage Materials*, Vol. 23, No. January, pp. 707–732, 2019.

28. S. Zheng, F. Yi, Z. Li, Y. Zhu, Y. Xu, C. Luo, J. Yang, C. Wang, “Copper-Stabilized Sulfur-Microporous Carbon Cathodes for Li-S Batteries”, *Advanced Functional Materials*, Vol. 24, No. 26, pp. 4156–4163, 2014.

29. S. Moon, Y. H. Jung, W. K. Jung, D. S. Jung, J. W. Choi, and D. K. Kim, “Encapsulated Monoclinic Sulfur for Stable Cycling of Li-S Rechargeable Batteries”, *Advanced Materials*, Vol. 25, No. 45, pp. 6547–6553, 2013.

30. B. Yan, X. Li, Z. Bai, X. Song, D. Xiong, M. Zhao, D. Li, S. Lu, “A Review of Atomic Layer Deposition Providing High Performance Lithium Sulfur Batteries”, *Journal of Power Sources*, Vol. 338, pp. 34–48, 2017.

31. B. Campbell, J. Bell, H. Hosseini Bay, Z. Favors, R. Ionescu, C.S. Ozkan, M. Ozkan, “SiO_2-Coated Sulfur Particles with Mildly Reduced Graphene Oxide as a Cathode Material for Lithium-Sulfur Batteries”, *Nanoscale*, Vol. 7, No. 16, pp. 7051–7055, 2015.

32. M. Yu, Z. Wang, Y. Wang, Y. Dong, and J. Qiu, “Freestanding Flexible Li_2S Paper Electrode with High Mass and Capacity Loading for High-Energy Li–S Batteries”, *Advanced Energy Materials*, Vol. 7, No. 17, p. 1700018, 2017.

33. M. Li, Y. Zhang, Z. Bai, W.W. Liu, T. Liu, J. Gim, G. Jiang, Y. Yuan, D. Luo, K. Feng, R.S. Yassar, X. Wang, Z. Chen, J. Lu, "A Lithium–Sulfur Battery using a 2D Current Collector Architecture with a Large-Sized Sulfur Host Operated under High Areal Loading and Low E/S Ratio", *Advanced Materials*, Vol. 30, No. 46, p. 1804271, 2018.

34. J. Q. Huang, Q. Zhang, and F. Wei, "Multi-Functional Separator/Interlayer System for High-Stable Lithium-Sulfur Batteries: Progress and Prospects", *Energy Storage Materials,* Vol. 1, pp. 127–145, 2015.

35. X. Yao, N. Huang, F. Han, Q. Zhang, H. Wan, J.P. Mwizerwa, C. Wang, X. Xu, "High-Performance All-Solid-State Lithium–Sulfur Batteries Enabled by Amorphous Sulfur-Coated Reduced Graphene Oxide Cathodes", *Advanced Energy Materials*, Vol. 7, No. 17, p. 1602923, 2017.

36. W. Chen, T. Lei, T. Qian, W. Lv, W. He, C. Wu, X. Liu, J. Liu, B. Chen, C. Yan, J. Xiong, "A New Hydrophilic Binder Enabling Strongly Anchoring Polysulfides for High-Performance Sulfur Electrodes in Lithium-Sulfur Battery", *Advanced Energy Materials*, Vol. 8, No. 12, p. 1702889, 2018.

37. S. S. Zhang, "Improved Cyclability of Liquid Electrolyte Lithium/Sulfur Batteries by Optimizing Electrolyte/Sulfur Ratio", *Energies,* Vol. 5, No. 12, pp. 5190–5197, 2012.

38. P. G. Bruce, S. A. Freunberger, L. J. Hardwick, and J. M. Tarascon, "Li-O_2 and Li-S batteries with high energy storage", *Nature Materials,* Vol. 11, No. 1, pp. 19–29, 2012.

39. S. M. Al-Mahmoud, J. W. Dibden, J. R. Owen, G. Denuault, and N. Garcia-Araez, "A Simple, Experiment-Based Model of the Initial Self-Discharge of Lithium-Sulphur Batteries", *Journal of Power Sources*, Vol. 306, pp. 323–328, 2016.

40. R. Demir-Cakan, “Li-S Batteries: The Challenges, Chemistry, Materials, and Future Perspectives”, *World Scientific Publishing Company*, Singapore, 2017.

41. R. Xu, J. Lu, and K. Amine, “Progress in Mechanistic Understanding and Characterization Techniques of Li-S Batteries”, *Advanced Energy Materials*, Vol. 5, No. 16, p. 1500408, 2015.

42. Z. Lin, Z. Liu, N. J. Dudney, and C. Liang, “Lithium Superionic Sulfide Cathode for All-Solid Lithium-Sulfur Batteries”, *ACS Nano,* Vol. 7, No. 3, pp. 2829–2833, 2013.

43. L. Yuan, X. Qiu, L. Chen, and W. Zhu, “New Insight into the Discharge Process of Sulfur Cathode by Electrochemical Impedance Spectroscopy”, *Journal of Power Sources*, Vol. 189, No. 1, pp. 127–132, 2009.

44. Y. X. Yin, S. Xin, Y. G. Guo, and L. J. Wan, “Lithium-Sulfur Batteries: Electrochemistry, Materials, and Prospects”, *Angewandte Chemie - International Edition,* Vol. 52, No. 50, pp. 13186–13200, 2013.

45. E. Peled, A. Gorenshtein, M. Segal, and Y. Sternberg, “Rechargeable Lithium-Sulfur Battery”, *Journal of Power Sources*, Vol. 26, No. 3–4, pp. 269–271, 1989.

46. H. M. Bilal and D. Eroglu, “Carbon-to-Sulfur Ratio in the Cell Controls the Discharge Capacity, Cycling Performance and Energy Density of a Lithium-Sulfur Battery”, *International Journal of Energy Research*, Vol. 46, No. 11, pp. 15926-15937, 2022.

47. Kilic and D. Eroglu, “Characterization of the Effect of Cell Design on Li−S Battery Resistance Using Electrochemical Impedance Spectroscopy”, *ChemElectroChem*, Vol. 8, No. 5, pp. 963–971, 2021.

48. N. B. Emerce and D. Eroglu, “Effect of Electrolyte-to-Sulfur Ratio in the Cell on the Li-S Battery Performance”, *Journal of the Electrochemical Society*, Vol. 166, No. 8, pp. A1490–A1500, 2019.

49. C. Michaelis, N. Erisen, D. Eroglu, and G. M. Koenig, “Electrochemical Performance and Modeling of Lithium-Sulfur Batteries with Varying Carbon to Sulfur Ratios”, *International Journal of Energy Research*, Vol. 43, No. 2, pp. 874–883, 2019.

50. N. Erisen, N. B. Emerce, S. C. Erensoy, and D. Eroglu, “Modeling the Effect of Key Cathode Design Parameters on the Electrochemical Performance of a Lithium-Sulfur Battery”, *International Journal of Energy Research*, Vol. 42, No. 8, pp. 2631–2642, 2018.

51. B. Abdulkadiroglu, H. Bektas, and D. Eroglu, “How to Model the Cathode Area in Lithium-Sulfur Batteries?”, *ChemElectroChem*, Vol. 9, No. 4, 2022.

52. J. Shim, K. A. Striebel, and E. J. Cairns, “The Lithium/Sulfur Rechargeable Cell”, *Journal of the Electrochemical Society*, Vol. 149, No. 10, p. A1321, 2002.

53. R. Xu, J. C. M. Li, J. Lu, K. Amine, and I. Belharouak, “Demonstration of Highly Efficient Lithium–Sulfur Batteries”, *Journal of Material Chemistry A*, Vol. 3, No. 8, pp. 4170–4179, 2015.

54. J. Brückner, S. Thieme, H. T. Grossmann, S. Dörfler, H. Althues, and S. Kaskel, “Lithium–Sulfur Batteries: Influence of C-Rate, Amount of Electrolyte and Sulfur Loading on Cycle Performance”, *Journal of Power Sources*, Vol. 268, pp. 82–87, 2014.

55. S.-R. Chen, Y.-P. Zhai, G.-L. Xu, Y.-X. Jiang, D.-Y. Zhao, J.-T. Li, L. Huang, S.-G. Sun, “Ordered Mesoporous Carbon/Sulfur Nanocomposite of High Performances as Cathode for Lithium–Sulfur Battery”, *Electrochimica Acta*, Vol. 56, No. 26, pp. 9549–9555, 2011.

56. A.Bhargav, J. He, A. Gupta, and A. Manthiram, “Lithium-Sulfur Batteries: Attaining the Critical Metrics”, *Joule*, Vol. 4, No. 2, pp. 285–291, 2020.

57. M. Hagen, P. Fanz, and J. Tübke, “Cell Energy Density and Electrolyte/Sulfur Ratio in Li-S Cells”, *Journal of Power Sources*, Vol. 264, pp. 30–34, 2014.

58. B. D. McCloskey, “Attainable Gravimetric and Volumetric Energy Density of Li-S and Li Ion Battery Cells with Solid Separator-Protected Li Metal Anodes”, *Journal of Physical Chemistry Letters,* Vol. 6, No. 22. American Chemical Society, pp. 4581–4588, 2015.

59. D. Lu, Q. Li, J. Liu, J. Zheng, Y. Wang, S. Ferrara, J. Xiao, J.G. Zhang, J. Liu, “Enabling High-Energy-Density Cathode for Lithium-Sulfur Batteries”, *ACS Applied Materials and Interfaces*, Vol. 10, No. 27, pp. 23094–23102, 2018.

60. G. Li, S. Wang, Y. Zhang, M. Li, Z. Chen, and J. Lu, “Revisiting the Role of Polysulfides in Lithium–Sulfur Batteries”, *Advanced Materials*, Vol. 30, No. 22, p. 1705590, 2018.

61. D. Eroglu, K. R. Zavadil, and K. G. Gallagher, “Critical Link between Materials Chemistry and Cell-Level Design for High Energy Density and Low Cost Lithium-Sulfur Transportation Battery”, *Journal of the Electrochemical Society*, Vol. 162, No. 6, pp. A982–A990, 2015.

62. L. Cheng, L. A. Curtiss, K. R. Zavadil, A. A. Gewirth, Y. Shao, and K. G. Gallagher, “Sparingly Solvating Electrolytes for High Energy Density Lithium-Sulfur Batteries”, *ACS Energy Letters*, Vol. 1, No. 3, pp. 503–509, 2016.

63. J. E. Kim, C. S. Jin, K. H. Shin, and S. H. Yeon, “Optimized Cell Conditions for a High-Energy Density, Large-Scale Li-S Battery”, *International Journal of Energy Research*, Vol. 40, No. 5, pp. 670–676, 2016.

64. J. W. Choi, J. K. Kim, G. Cheruvally, J. H. Ahn, H. J. Ahn, and K. W. Kim, “Rechargeable Lithium/Sulfur Battery with Suitable Mixed Liquid Electrolytes”, *Electrochimica Acta*, Vol. 52, No. 5, pp. 2075–2082, 2007.

65. J. Zheng, D. Lv, M. Gu, C. Wang, J.-G. Zhang, J. Liu, J. Xiao, “How to Obtain Reproducible Results for Lithium Sulfur Batteries?”, *Journal of the Electrochemical Society* ,Vol. 160, No. 11, pp. A2288–A2292, 2013.

66. S. H. Chung, C. H. Chang, and A. Manthiram, “Progress on the Critical Parameters for Lithium–Sulfur Batteries to be Practically Viable”, *Advanced Functional Materials*, Vol. 28, No. 28, p. 1801188, 2018.

67. C. Luo, E. Hu, K.J. Gaskell, X. Fan, T. Gao, C. Cui, S. Ghose, X.Q. Yang, C. Wang, “A Chemically Stabilized Sulfur Cathode for Lean Electrolyte Lithium Sulfur Batteries”, *Proceedings of the National Academy of Sciences of the United States of America*, Vol. 117, No. 26, pp. 14712–14720, 2020.

68. J. Chen, W.A. Henderson, H. Pan, B.R. Perdue, R. Cao, J.Z. Hu, C. Wan, K.S. Han, K.T. Mueller, J.G. Zhang, Y. Shao, J. Liu, “Improving Lithium-Sulfur Battery Performance under Lean Electrolyte through Nanoscale Confinement in Soft Swellable Gels”, *Nano Letters*, Vol. 17, No. 5, pp. 3061–3067, 2017.

69. C. Shen, J. Xie, M. Zhang, P. Andrei, J.P. Zheng, M. Hendrickson, E.J. Plichta, “A Li-Li_2S_4 Battery with Improved Discharge Capacity and Cycle Life at Low Electrolyte/Sulfur Ratios”, *Journal of Power Sources*, Vol. 414, No. January, pp. 412–419, 2019.

70. R. Fang, S. Zhao, Z. Sun, D. W. Wang, H. M. Cheng, and F. Li, “More Reliable Lithium-Sulfur Batteries: Status, Solutions and Prospects”, *Advanced Materials*, Vol. 29, No. 48. pp. 1–25, 2017.

71. M. Hagen, S. Dörfler, P. Fanz, T. Berger, R. Speck, J. Tübke, H. Althues, M.J. Hoffmann, C. Scherr, S. Kaskel, “Development and Costs Calculation of Lithium–

Sulfur Cells with High Sulfur Load and Binder Free Electrodes", *Journal of Power Sources*, Vol. 224, pp. 260–268, 2013.

72. S. Urbonaite, T. Poux, and P. Novák, "Progress Towards Commercially Viable Li-S Battery Cells", *Advanced Energy Materials*, Vol. 5, No. 16, p. 1500118, 2015.

73. D. A. Dornbusch, R. Hilton, M. J. Gordon, and G. J. Suppes, "Effects of Carbon Surface Area On Performance Of Lithium Sulfur Battery Cathodes", *Journal of Industrial and Engineering Chemistry,* Vol. 19, No. 6, pp. 1968–1972, 2013.

74. Y.-J. Choi, Y.-D. Chung, C.-Y. Baek, K.-W. Kim, H.-J. Ahn, and J.-H. Ahn, "Effects of Carbon Coating on the Electrochemical Properties of Sulfur Cathode for Lithium/Sulfur Cell", *Journal of Power Sources*, Vol. 184, No. 2, pp. 548–552, 2008.

75. G. Zheng, Y. Yang, J. J. Cha, S. S. Hong, and Y. Cui, "Hollow Carbon Nanofiber-Encapsulated Sulfur Cathodes for High Specific Capacity Rechargeable Lithium Batteries", *Nano Letters*, Vol. 11, No. 10, pp. 4462–4467, 2011.

76. M. Hagen, D. Hanselmann, K. Ahlbrecht, R. Maça, D. Gerber, and J. Tübke, "Lithium-Sulfur Cells: The Gap between the State-of-the-Art and the Requirements for High Energy Battery Cells", *Advanced Energy Materials*, Vol. 5, No. 16, p. 1401986, 2015.

77. D. Lv, J. Zheng, Q. Li, X. Xie, S. Ferrara, Z. Nie, L.B. Mehdi, N.D. Browning, J.-G. Zhang, G.L. Graff, J. Liu, J. Xiao, "High Energy Density Lithium-Sulfur Batteries: Challenges of Thick Sulfur Cathodes", *Advanced Energy Materials*, Vol. 5, No. 16, p. 1402290, 2015.

78. S.-E. Cheon, K.-S. Ko, J.-H. Cho, S.-W. Kim, E.-Y. Chin, and H.-T. Kim, "Rechargeable Lithium Sulfur Battery", *Journal of the Electrochemical Society*, Vol. 150, No. 6, p. A800-A805, 2003.

79. S.-C. Han, M.-S. Song, H. Lee, H.-S. Kim, H.-J. Ahn, and J.-Y. Lee, “Effect of Multiwalled Carbon Nanotubes on Electrochemical Properties of Lithium/Sulfur Rechargeable Batteries”, *Journal of the Electrochemical Society*, Vol. 150, No. 7, p. A889, 2003.

80. L. Su, J. Zhang, Y. Chen, W. Yang, J. Wang, Z. Ma, G. Shao, G. Wang, “Cobalt-Embedded Hierarchically-Porous Hollow Carbon Microspheres as Multifunctional Confined Reactors for High-Loading Li-S Batteries”, *Nano Energy*, Vol. 85, p. 105981, 2021.

81. S. Zhang, Z. Xu, Z. Jiang, Z. Xiao, A. Tang, and H. Yang, “The Unique Interconnected Structure of Hollow Carbon Skeleton Doped by F and N Facilitating Rapid Li Ions Diffusion In Lithium-Sulfur Batteries”, *Carbon*, Vol. 195, pp. 207–218, 2022.

82. R. Saroha and J. S. Cho, “Nanofibers Comprising Interconnected Chain-Like Hollow N-Doped C Nanocages as 3D Free-Standing Cathodes for Li–S Batteries with Super-High Sulfur Content and Lean Electrolyte/Sulfur Ratio”, *Small Methods*, p. 2200049, 2022.

83. J. Liu, Y. Zhu, J. Cai, Y. Zhong, T. Han, Z. Chen, J. Li, “Encapsulating Metal-Organic-Framework Derived Nanocages into a Microcapsule for Shuttle Effect-Suppressive Lithium-Sulfur Batteries”, *Nanomaterials,* Vol. 12, No. 2, p. 236, 2022.

84. M. Marinescu, T. Zhang, and G. J. Offer, “A Zero Dimensional Model of Lithium-Sulfur Batteries During Charge and Discharge”, *Physical Chemistry Chemical Physics*, Vol. 18, No. 1, pp. 584–593, 2016.

85. Y. V. Mikhaylik and J. R. Akridge, “Polysulfide Shuttle Study in the Li/S Battery System”, *Journal of the Electrochemical Society*, Vol. 151, No. 11, p. A1969, 2004.

86. K. Kumaresan, Y. Mikhaylik, and R. E. White, “A Mathematical Model for a Lithium–Sulfur Cell”, *Journal of the Electrochemical Society*, Vol. 155, No. 8, p. A576, 2008.

87. N. Erisen and D. Eroglu, “Modeling the Discharge Behavior of a Lithium-Sulfur Battery”, *International Journal of Energy Research*, Vol. 44, No. 13, pp. 10599–10611, 2020.

88. H. M. Bilal and D. Eroglu, “Assessment of Li-S Battery Performance as a Function of Electrolyte-to-Sulfur Ratio”, *Journal of the Electrochemical Society*, Vol. 168, No. 3, p. 030502, 2021.

89. D. Li, F. Han, S. Wang, F. Cheng, Q. Sun, and W. C. Li, “High Sulfur Loading Cathodes Fabricated Using Peapodlike, Large Pore Volume Mesoporous Carbon for Lithium-Sulfur Battery”, *ACS Applied Materials and Interfaces*, Vol. 5, No. 6, pp. 2208–2213, 2013.

90. C.W. Park, H.S. Ryu, K.W. Kim, B.Y. Hur, K.K. Cho, J.H. Ahn, J.Y. Lee, H.J. Ahn, “Effect of Sulfur Electrode Composition on the Electrochemical Property of Lithium/PEO/Sulfur Battery”, *Metals and Materials International*, Vol. 10, No. 4, pp. 375–379, 2004.

91. J.W. Park, C. Kim, H.S. Ryu, G.B. Cho, K.K. Cho, K.W. Kim, J.H. Ahn, G. Wang, J.P. Ahn, H.J. Ahn,, “Effect of Sulfur Content in a Sulfur-Activated Carbon Composite on the Electrochemical Properties of a Lithium/Sulfur Battery”, *Materials Research Bulletin*, Vol. 69, pp. 24–28, 2015.

92. S. Chen, Y. Gao, Z. Yu, M. L. Gordin, J. Song, and D. Wang, “High Capacity of Lithium-Sulfur Batteries at Low Electrolyte/Sulfur Ratio Enabled by an Organosulfide Containing Electrolyte”, *Nano Energy*, Vol. 31, pp. 418–423, 2017.

93. S. Urbonaite and P. Novák, “Importance of ‘Unimportant’ Experimental Parameters in Li-S Battery Development”, *Journal of Power Sources*, Vol. 249, pp. 497–502, 2014.

94. F. Y. Fan and Y.-M. Chiang, “Electrodeposition Kinetics in Li-S Batteries: Effects of Low Electrolyte/Sulfur Ratios and Deposition Surface Composition”, *Journal of the Electrochemical Society*, Vol. 164, No. 4, pp. A917–A922, 2017.

95. J. Yan, X. Liu, and B. Li, “Capacity Fade Analysis of Sulfur Cathodes in Lithium–Sulfur Batteries”, *Advanced Science*, Vol. 3, No. 12, 2016.

96. S. Thieme, J. Brückner, A. Meier, I. Bauer, K. Gruber, J. Kaspar, A. Helmer, H. Althues, M. Schmuck, S. Kaskel, “A Lithium-Sulfur Full Cell with Ultralong Cycle Life: Influence of Cathode Structure and Polysulfide Additive”, *Journal of Materials Chemistry A,* Vol. 3, No. 7, pp. 3808–3820, 2015.

97. Schneider, C. Suchomski, H. Sommer, J. Janek, and T. Brezesinski, “Free-Standing And Binder-Free Highly N-Doped Carbon/Sulfur Cathodes with Tailorable Loading for High-Areal-Capacity Lithium-Sulfur Batteries”, *Journal of Materials Chemistry A*, Vol. 3, No. 41, pp. 20482–20486, 2015.

98. T. N. L. Doan, D. Gosselink, T. K. A. Hoang, and P. Chen, “The Effect of Sulfur Loading on the Electrochemical Performance of a Sulfur-Polymer Composite Cathode Coated on Aluminium Foil”, *Physical Chemistry Chemical Physics*, Vol. 16, No. 27, pp. 13843–13848, 2014.

99. S.-H. Kang, X. Zhao, J. Manuel, H.-J. Ahn, K.-W. Kim, K.-K. Cho, J.-H. Ahn, “Effect of Sulfur Loading on Energy Density of Lithium Sulfur Batteries: Energy Density of Lithium Sulfur Batteries”, *Physica Status Solidi A.,* Vol. 211, No. 8, pp. 1895–1899, 2014.

100. Song, M.-K., Zhang, Y., & Cairns, E. J. “Effects of Cell Construction Parameters on the Performance of Lithium/Sulfur Cells”, *AIChE Journal*, Vol. 61, No. 9, pp. 2749–2756, 2015.

101. K. Sun, H. Liu, and H. Gan, “Cathode Loading Effect on Sulfur Utilization in Lithium–Sulfur Battery”, *Journal of Electrochemical Energy Conversion and Storage*, Vol. 13, No. 2, p. 021002, 2016.

102. K. Sun, C.A. Cama, J. Huang, Q. Zhang, S. Hwang, D. Su, A.C. Marschilok, K.J. Takeuchi, E.S. Takeuchi, H. Gan, “Effect of Carbon and Binder on High Sulfur Loading Electrode for Li-S Battery Technology”, *Electrochimica Acta*, Vol. 235, pp. 399–408, 2017.

103. Barchasz, F. Mesguich, J. Dijon, J.-C. Leprêtre, S. Patoux, and F. Alloin, “Novel Positive Electrode Architecture for Rechargeable Lithium/Sulfur Batteries”, *Journal of Power Sources*, Vol. 211, pp. 19–26, 2012.

104. J.-W. Park, I. Kim, K.-W. Kim, T.-H. Nam, K.-K. Cho, J.-H. Ahn, H.-S. Ryu, H.-J. Ahn, “Effect Of Commercial Activated Carbons In Sulfur Cathodes On The Electrochemical Properties Of Lithium/Sulfur Batteries”, *Materials Research Bulletin*, Vol. 82, pp. 109–114, 2016.

105. J. Zheng, M. Gu, M.J. Wagner, K.A. Hays, X. Li, P. Zuo, C. Wang, J.-G. Zhang, J. Liu, J. Xiao, “Revisit Carbon/Sulfur Composite for Li-S Batteries”, *Journal of the Electrochemical Society*, Vol. 160, No. 10, pp. A1624–A1628, 2013.

106. Jozwiuk, H. Sommer, J. Janek, and T. Brezesinski, “Fair Performance Comparison of Different Carbon Blacks in Lithium–Sulfur Batteries with Practical Mass Loadings – Simple Design Competes with Complex Cathode Architecture”, *Journal of Power Sources*, Vol. 296, pp. 454–461, 2015.

107. X. Ji, K. T. Lee, and L. F. Nazar, “A Highly Ordered Nanostructured Carbon–Sulphur Cathode For Lithium–Sulphur Batteries”, *Nature Materials*, Vol. 8, No. 6, pp. 500–506, 2009.

108. Kilic, Ç. Odabaşı, R. Yildirim, and D. Eroglu, “Assessment of Critical Materials and Cell Design Factors for High Performance Lithium-Sulfur Batteries Using Machine Learning”, *Chemical Engineering Journal*, Vol. 390, p. 124117, 2020.

109. M.-S. Song, S.-C. Han, H.-S. Kim, J.-H. Kim, K.-T. Kim, Y.-M. Kang, H.-J. Ahn, S.X. Dou, J.-Y. Lee, “Effects of Nanosized Adsorbing Material on Electrochemical Properties of Sulfur Cathodes for Li/S Secondary Batteries”, *Journal of the Electrochemical Society*, Vol. 151, No. 6, p. A791, 2004.

110. S. Zeng, G.M. Arumugam, X. Liu, Y. Yang, X. Li, H. Zhong, F. Guo, Y. Mai, “Encapsulation of Sulfur into N-Doped Porous Carbon Cages by a Facile, Template-Free Method for Stable Lithium-Sulfur Cathode”, *Small*, Vol. 16, No. 39, p. 2001027, 2020.

111. X. Gao, Y. Huang, Z. Guang, and X. Li, “Constructing a Multifunctional Globular Polypyrrole Slurry Cladding Carbon Aerogel/Sulfur Cathode for High-Performance Lithium–Sulfur Batteries”, *Energy Fuels*, Vol. 34, No. 3, pp. 3931–3940, 2020.

112. Y. Yan, M. Shi, Y. Wei, C. Zhao, M. Carnie, R. Yang, Y. Xu, “Process Optimization for Producing Hierarchical Porous Bamboo-Derived Carbon Materials with Ultrahigh Specific Surface Area For Lithium-Sulfur Batteries”, *Journal of Alloys and Compounds,* Vol. 738, pp. 16–24, 2018.

113. Capková, T. Kazda, A. Straková Fedorková, P. Čudek, and R. Oriňaková, “Carbon Materials as the Matrices for Sulfur in Li-S Batteries”, *ECS Transactions*, Vol. 95, No. 1, pp. 19–26, 2019.

114. T. Cleaver, P. Kovacik, M. Marinescu, T. Zhang, and G. Offer, “Perspective—Commercializing Lithium Sulfur Batteries: Are We Doing the Right Research?”, *Journal of the Electrochemical Society*, Vol. 165, No. 1, pp. A6029–A6033, 2018.

115. S. Osella, A. Minoia, C. Quarti, J. Cornil, R. Lazzaroni, A.-L. Goffin, M. Guillaume, D. Beljonne, “Modelling Coupled Ion Motion in Electrolyte Solutions for Lithium-Sulfur Batteries”, *Batteries & Supercaps*, Vol. 2, No. 5, pp. 473–481, 2019.

116. V. Knap, D.-I. Stroe, M. Swierczynski, R. Purkayastha, K. Propp, R. Teodorescu, E. Schaltz, “A Self-Discharge Model of Lithium-Sulfur Batteries Based on Direct Shuttle Current Measurement”, *Journal of Power Sources*, Vol. 336, pp. 325–331, 2016.

117. F. Hofmann, D. N. Fronczek, and W. G. Bessler, “Mechanistic Modeling of Polysulfide Shuttle and Capacity Loss in Lithium-Sulfur Batteries”, *Journal of Power Sources*, Vol. 259, pp. 300–310, 2014.

118. P. Nelson, K. Gallagher, I. Bloom, and D. Dees, “Modeling the Performance and Cost of Lithium-Ion Batteries for Electric-Drive Vehicles”, *Argonne National Laboratory,* USA, 2012.

119. Eroglu, S. Ha, and K. G. Gallagher, “Fraction of the Theoretical Specific Energy Achieved on Pack Level for Hypothetical Battery Chemistries”, *Journal of Power Sources*, Vol. 267, pp. 14–19, 2014.

120. Rosenman, R. Elazari, G. Salitra, E. Markevich, D. Aurbach, and A. Garsuch, “The Effect of Interactions and Reduction Products of $LiNO_3$, the Anti-Shuttle Agent, in Li-S Battery Systems”, *Journal of the Electrochemical Society*, Vol. 162, No. 3, pp. A470–A473, 2015.

121. J. Liao and Z. Ye, “Nontrivial Effects of ‘Trivial’ Parameters on the Performance of Lithium–Sulfur Batteries”, *Batteries*, Vol. 4, No. 2, 2018.

122. S. S. Zhang, “Effect of Discharge Cutoff Voltage on Reversibility of Lithium/Sulfur Batteries with $LiNO_3$-Contained Electrolyte”, *Journal of the Electrochemical Society*, Vol. 159, No. 7, pp. A920–A923, 2012.

123. Jozwiuk, H. Sommer, J. Janek, and T. Brezesinski, “Fair Performance Comparison of Different Carbon Blacks in Lithium–Sulfur Batteries with Practical Mass Loadings – Simple Design Competes with Complex Cathode Architecture”, *Journal of Power Sources*, Vol. 296, pp. 454–461, 2015.

124. P. Novák, K. Müller, K. S. V. Santhanam, and O. Haas, “Electrochemically Active Polymers for Rechargeable Batteries”, *Chemical Reviews*, Vol. 97, No. 1, pp. 207–282, 1997.

125. C. Shen, J. Xie, M. Zhang, P. Andrei, M. Hendrickson, E.J. Plichta, J.P. Zheng, “Understanding the Role of Lithium Polysulfide Solubility in Limiting Lithium-Sulfur Cell Capacity”, *Electrochimica Acta*, Vol. 248, pp. 90–97, 2017.

126. D. Li, F. Han, S. Wang, F. Cheng, Q. Sun, and W.-C. Li, “High Sulfur Loading Cathodes Fabricated Using Peapodlike, Large Pore Volume Mesoporous Carbon for Lithium–Sulfur Battery”, *ACS Applied Materials Interfaces*, Vol. 5, No. 6, pp. 2208–2213, 2013.

127. S. S. Zhang, “Role of $LiNO_3$ in Rechargeable Lithium/Sulfur Battery”, *Electrochimica Acta*, Vol. 70, pp. 344–348, 2012.

128. S. Drvarič Talian, J. Moškon, R. Dominko, and M. Gaberšček, “Impedance Response of Porous Carbon Cathodes in Polysulfide Redox System”, *Electrochimica Acta*, Vol. 302, pp. 169–179, 2019.

129. S. Dörfler, H. Althues, P. Härtel, T. Abendroth, B. Schumm, and S. Kaskel, “Challenges and Key Parameters of Lithium-Sulfur Batteries on Pouch Cell Level”, *Joule*, Vol. 4, No. 3, pp. 539–554, 2020.

130. S. Evers and L. F. Nazar, “New Approaches for High Energy Density Lithium–Sulfur Battery Cathodes”, *Accounts of Chemical Research*, Vol. 46, No. 5, pp. 1135–1143, 2013.

131. Jin, Z. Mingang, Y. Shijian, Y. Xiaoyan, and W. Shiwei, “Electrochemical Properties of Modified Acetylene Black/Sulfur Composite Cathode Material for Lithium/Sulfur Batteries”, *Ionics*, Vol. 24, No. 8, pp. 2219–2225, 2018.

132. L. Huang, J. Li, B. Liu, Y. Li, S. Shen, S. Deng, C. Lu, W. Zhang, Y. Xia, G. Pan, X. Wang, Q. Xiong, X. Xia, J. Tu, “Electrode Design for Lithium-Sulfur Batteries:Problems and Solutions”, *Advanced Functional Materials,* Vol. 30, No. 22, p. 1910375, 2020.

APPENDIX A: SUPPLEMENTARY INFORMATION 1

A.1. Electrochemical Model

Newman and Tobias developed an electrochemical model applicable for the porous cathode. In the model, the following assumptions were made:

- Constant concentrations
- Single electrochemical reaction
- Zero fluid velocity
- Time independent
- Symmetrical discharge-charge reactions

Current-voltage relation and overpotential of the cathode is achieved with Tafel or Linear kinetics according to defined condition and can be described as

$$i_1 = -\sigma_{eff}\frac{d\phi_1}{dx} \tag{A.1}$$

$$i_1 = -\kappa_{eff}\frac{d\phi_2}{dx} \tag{A.2}$$

$$\frac{di_1}{dx} + \frac{di_2}{dx} = 0 \tag{A.3}$$

$$\nabla i_2 = a i_{0,pe}\begin{bmatrix} \exp\left(\frac{\alpha_a F}{RT}(\phi_1 - \phi_2)\right) \\ -\exp\left(\frac{\alpha_a F}{RT}(\phi_1 - \phi_2)\right) \end{bmatrix} \tag{A.4}$$

$$At\ x = 0, i_2 = I\ and\ \phi_2 = 0 \tag{A.5}$$

$$At\ x = L\ and\ i_1 = I. \tag{A.6}$$

where Equation (A.1) and Equation (A.2) represents the matrix and electrolyte currents based on the Ohm's law.

Overpotential can be calculated for Tafel kinetics: $|I| > ai_{0,pe}L_{pe}$ as

$$\frac{di_2}{dx} = -ai_{pe,a} + exp\left[\frac{ai_{0,pe}F}{RT}(\phi_1 - \phi_2)\right] \tag{A.7}$$

$$\frac{d^2j}{dy^2} = \frac{dj}{dy}(\delta j - \epsilon) \tag{A.8}$$

$$At\ y = 0\ and\ j = 0 \tag{A.9}$$

$$At\ y = 1\ and\ j = 1 \tag{A.10}$$

$$\phi_1(L) - \phi_2(0) = \frac{1}{\beta}\left\{\begin{matrix}(\delta - \epsilon)\left[\frac{\epsilon}{\delta} + \frac{2}{\delta} lnsec(\theta - \psi)\right] \\ + \frac{2\epsilon}{\delta} lnsec\psi + \ln\left(\frac{2|I|\theta^2}{ai_{0,pe}L_{pe}\delta}\right)\end{matrix}\right\} \tag{A.11}$$

where $y = \frac{x}{L_{pe}}$,$j = \frac{i_1}{-I}$, $\beta = \frac{\alpha_{pe,c}F}{RT}$, $\delta = L_{pe}|I|\beta\left(\frac{1}{\kappa_{eff}} + \frac{1}{\sigma_{eff}}\right)$, $\epsilon = \frac{L_{pe}|I|\beta}{\kappa_{eff}}$, $\theta = arctan\frac{2\delta\theta}{4\theta^2 - \epsilon(\delta - \epsilon)}$ and $\psi = arctan\frac{\epsilon}{2\theta}$.

Overpotential can be calculated for Linear kinetics: $|I| < ai_{0,pe}L_{pe}$ as

$$\frac{di_2}{dx} = (\alpha_{pe,a} + \alpha_{pe,c})\frac{ai_{0,pe}F}{RT}(\phi_1 - \phi_2) \tag{A.12}$$

$$\frac{d^2j}{dy^2} = \frac{dj}{dy}(\delta j - \epsilon) \tag{A.13}$$

$$At\ y = 0\ and\ j = 0 \tag{A.14}$$

$$At\ y = 1\ and\ j = 1 \tag{A.15}$$

$$\phi_1(L) - \phi_2(0) = \frac{I \times L_{pe}}{\kappa_{eff} + \sigma_{eff}}\left[1 + \frac{2 + \left(\frac{\sigma_{eff}}{\kappa_{eff}} + \frac{\kappa_{eff}}{\sigma_{eff}}\right)coshv}{vsinhv}\right] \tag{A.16}$$

where $y = \frac{x}{L_{pe}}, j = \frac{i_1}{-I}, \beta \frac{\alpha_{pe,c} F}{RT}, \delta = L_{pe}|I|\beta\left(\frac{1}{\kappa_{eff}} + \frac{1}{\sigma_{eff}}\right)$ and $\epsilon = \frac{L_{pe}|I|\beta}{\kappa_{eff}}$.

A.2. Cell design in the system-level performance model

Cell design in the system-level performance was developed by modifying the publicly available model as stated [118]. Main equations used in the cell design through the calculation of system-level performance can be written as

$$Width\ of\ positive\ electrode\ (mm) = \sqrt{A_{layer}/[\frac{L}{W}]_{pos.elect.}} \tag{A.17}$$

$$Length\ of\ positive\ electrode\ (mm) = A_{layer}/W_{pos.elect.} \tag{A.18}$$

$$Width\ of\ cell\ (mm) = W_{pos.elect.} + 2t_{cell\ edge\ from\ pos.elect.to\ outside\ of\ fold} \tag{A.19}$$

$$Length\ of\ cell\ (mm) = L_{pos.elect.} + 2L_{\text{top of pos.elect.to top of term}} \tag{A.20}$$

$$\begin{aligned} &Thickness\ of\ cell\ (mm) \\ &= (number\ of\ bicell\ layers + 1) \times t_{neg.foil} \\ &+ (Number\ of\ bicell\ layers) \times t_{pos.foil} \\ &+ (2Number\ of\ bicell\ layers) \times t_{pos.elect.at\ adj.OCV} \\ &+ t_{neg.elect.at\ adj.OCV} + t_{sep}) + 2t_{pouch} \end{aligned} \tag{A.21}$$

$$\begin{aligned} &Volume\ of\ cell\ (cm^3) \\ &= width\ of\ cell \times length\ of\ cell \times thickness\ of\ cell \end{aligned} \tag{A.22}$$

$$\begin{aligned} &Separator\ area\ (m^2) \\ &= 2Number\ of\ bicell\ layers \times ((w_{pos.elect.} \\ &+ 4) \times (L_{pos.elect.} + 6) \end{aligned} \tag{A.23}$$

$$Electrolyte\ volume\ (L) = \frac{m_{ne}}{\rho_{ne,total}} \times v_e + \frac{m_{pe}}{\rho_{pe,total}} + sep.area \times sep.length \times void\ vol + t_{cell} \times L_{pos.elect.} \times w_{pos.elect} \times (\frac{0.02}{1000}) \quad (A.24)$$

$$Active\ material\ mass\ in\ pos.elect.\ (g) = \frac{cell\ capacity}{positive\ active\ material\ capacity} \quad (A.25)$$

$$Total\ mass\ of\ positive\ electrode\ (g) = \frac{active\ material\ mass}{w_{pe,act}} \quad (A.26)$$

$$S\ loading\ in\ the\ electrode\ (g) = \frac{active\ material\ mass}{A_{cell}} \quad (A.27)$$

$$Electrolyte\ in\ pos.elect.\ (g) = \frac{total\ mass}{\rho_{total}} \times V_e \times \rho_{electrolyte} \quad (A.28)$$

$$Active\ mat.in\ neg.elect.\ (g) = \frac{cell\ capacity}{negative\ active\ material\ capacity} \times \frac{N}{P} \quad (A.29)$$

$$Total\ mass\ of\ pos.elect.\ (g) = \frac{active\ material\ mass}{w_{ne,act}} \quad (A.30)$$

$$Cell\ mass\ (g) = m_{pe} + m_{ne} + \left(A_{neg.foil} \times L_{neg.foil} \times \rho_{neg.foil}\right) + \left(A_{pos.foil} \times L_{pos.foil} \times \rho_{pos.foil}\right) + \left(A_{sep} \times L_{sep} \times \rho_{sep}\right) + V_e \times \rho_e + m_{pos.term.assy} + m_{neg.term.assy} + m_{cell\ holder} \quad (A.31)$$

$$\frac{E}{S} ratio(\mu L\ mg^{-1}) = \frac{V_{electrolyte}}{m_{active\ material\ in\ pos.electrode}}. \quad (A.32)$$

$$electrolyte\ mass\%\ in\ the\ cell = \frac{V_{electrolyte} \times \rho_e}{cell\ mass}. \quad (A.33)$$

A.3. Module design in the system-level performance model

The volume and mass of the module are achieved with the following equations. Electrolyte losses and for the module design 0.5 mm thick aluminum is used and the entrance of water vapor and electrolyte losses from the cell are prevented with the sealing of the module. Main equations used in the module design through the calculation of system-level performance can be written as

$$Terminal\ resistance\ factor\ \left(A - \frac{ohms}{cm}\right) = \left(\frac{terminal\ heating\ factor \times \rho_{Cu}}{\sigma_{Cu}}\right)^{0.5} \tag{A.34}$$

$$\begin{aligned} &Module\ terminal\ resistance\ (ohms) \\ &= if\ number\ of\ modules\ per\ battery\ pack \\ &= 1;\ 0 \\ &\times \frac{2}{\max current\ at\ full\ power} xterminal\ resistance\ factor\ if\ not; 0 \\ &\times \frac{2}{\max current\ at\ full\ power} xterminal\ resistance\ factor \end{aligned} \tag{A.35}$$

$$\begin{aligned} &Mass\ of\ each\ cell\ group\ interconnect\ (g) \\ &= if\ number\ of\ cells\ in\ parallel = 1\ ; 0 \\ &if\ not\ ; = number\ of\ cells\ in\ parallel \times t_{cell} \times \frac{t_{term}}{2} \times \\ &W_{term} \times 1.5 \times \rho_{Cu}. \end{aligned} \tag{A.36}$$

$$Module\ SOC\ regulator\ assembly\ (g) = \frac{8 \times number\ of\ cells\ per\ module}{number\ of\ cells\ in\ parallel} \tag{A.37}$$

$$Module\ width\ (mm) = (t_{cell} + t_{cooling\ fin}/2) \times number\ of\ cells\ per\ module + 1 + 2t_{module\ wall} \quad (A.38)$$

$$Module\ height\ (mm) = w_{cell} + 2t_{module\ wall} + 2t_{cooling\ fin} \quad (A.39)$$

$$Module\ volume\ (L) = module\ (height \times length \times width) \quad (A.40)$$

A.4. Battery Design in the system-level performance model

In the battery system, the interconnection between the negative and positive terminals of the modules is provided with the help of copper connectors. Also, compression force is exerted on the modules via steel bands. In order to ensure the flow capability of heat transfer fluid ethylene glycol-water solution, a tray on the top and bottom of the battery jacket is used. All size and mass calculations of the battery system are given as

$$Total\ number\ of\ cells\ in\ a\ battery\ system = number\ of\ cells\ in\ battery\ system \times number\ of\ battery\ system\ in\ vehicle \quad (A.41)$$

$$Total\ number\ of\ modules\ in\ a\ battery\ system = number\ of\ rows\ of\ modules\ in\ battery\ system \times number\ of\ modules\ in\ row \quad (A.42)$$

$$Battery\ system\ capacity\ (Ah) = module\ capacity \times number\ of\ modules\ in\ parallel \quad (A.43)$$

$$
\begin{aligned}
&Total\ battery\ system\ energy\ storage\ (kWh) \\
&\quad = cell\ group\ capacity \\
&\quad \times number\ of\ modules\ in\ parallel \\
&\quad \times (nominal\ battery\ voltage \\
&\quad - cells\ per\ battery\ system) \times \left(cell\ \frac{capacity}{5}\right) \\
&\quad \times \left(\frac{ASI_{total\ cell\ energy}}{A_{cell}} \times number\ of\ cells\ in\ parallel\right. \\
&\quad \left. \times number\ of\ modules\ in\ parallel\right)
\end{aligned}
\tag{A.44}
$$

$$
\begin{aligned}
&Volume\ of\ battery\ system\ and\ integration\ unit\ (L) \\
&\quad = \left(L_{batt.syst.} \times H_{batt.syst.} \times W_{batt.syst.}\right) \\
&\quad + V_{syst.integration\ unit}
\end{aligned}
\tag{A.45}
$$

$$
\begin{aligned}
&Mass\ of\ battery\ system\ and\ integration\ unit\ (kg) \\
&\quad = m_{batt.coolant} + m_{batt\ jacket} + m_{syst.integration\ unit} \\
&\quad + number\ of\ modules\ per\ battery\ system \\
&\quad \times module\ mass
\end{aligned}
\tag{A.46}
$$

$$
\begin{aligned}
&Nominal\ battery\ voltage\ (V) \\
&\quad = \frac{cells\ per\ battery\ pack}{number\ of\ cells\ in\ parallel} \\
&\quad \times \frac{\text{OCV average for discharge (OCV at 50\% SOC)}}{\text{number of modules in parallel}}
\end{aligned}
\tag{A.47}
$$

$$
\begin{aligned}
&OCV\ at\ full\ power\ battery\ (V) \\
&\quad = \frac{cells\ per\ battery\ pack}{number\ of\ cells\ in\ parallel} \\
&\quad \times \frac{\text{OCV at full power cell}}{\text{number of modules in parallel}}
\end{aligned}
\tag{A.48}
$$

$$
Max.current\ at\ full\ power\ (A) = \frac{total\ system\ power}{\frac{V_p}{U} \times OCV\ at\ full\ power\ battery}. \tag{A.49}
$$

A.5. ASI Calculation

ASI for the battery system is calculated using following relations

$$Electrode\ system\ ASI\ for\ power\ at\ SOC\ for\ vehicle\ type\ (ohm - cm^2) = ASI_p - cell\ hardware\ and\ battery\ ASI \tag{A.50}$$

$$Current\ collector\ (CC)\ ASI\ (ohms - cm^2) = CC_{resistance\ par.} \times \frac{L_{pos.elect.}^{\ 2}}{3} \times L_{cc\ tabs.} \tag{A.51}$$

$$Cell\ terminal\ and\ connection\ ASI\ (ohms - cm^2) = \frac{\frac{10}{\sigma_{Al}} + \frac{10}{\sigma_{Cu}}}{t_{term}} \times \frac{L_{term.}}{W_{term.}} \times A_{cell} + cell\ terminal\ contact\ voltage\ loss \times \frac{OCV\ at\ full\ power}{\max current\ at\ full\ power} \times A_{cell} \tag{A.52}$$

$$Resistance\ of\ module\ interconnects\ (ohms) = (Number\ of\ modules\ per\ battery\ system - 1) \times 2((3 \times terminal\ resistance\ factor / \max current\ at\ full\ power)) \tag{A.53}$$

$$Resistance\ of\ module\ and\ system\ (ohms) = Module\ terminal\ resistance + resistance\ of\ module\ interconnects + (resistance\ of\ battery\ system\ terminals /(number\ of\ modules\ per\ battery\ system \times number\ of\ modules\ in\ parallel^2)) \tag{A.54}$$

$$Total\ cell\ hardware\ and\ battery\ ASI\ (ohm - cm^2) = CC_{ASI} + Cell\ terminal\ and\ connection\ ASI + resistance\ of\ module\ and\ system\ hardware\ per\ cell \times A_{cell} \tag{A.55}$$

$$Total\ cell\ ASI\ for\ energy\ (ohm - cm^2) = Total\ cell\ hardware\ and\ battery\ ASI + ASI_e \quad \text{(A.56)}$$

$$Sustained\ power\ (W) = \frac{Total\ cell\ ASI\ for\ energy\ (\frac{C}{5} rate)}{A_{cell}} \times \frac{cells\ per\ battery\ system}{number\ of\ cells\ in\ parallel^2 \times number\ of\ modules\ in\ parallel^2} \quad \text{(A.57)}$$

$$Heat\ generation\ rate\ for\ battery\ system\ (W) = Sustained\ power\ (W) \times \left(\frac{Battery\ system\ capacity}{5}\right)^2. \quad \text{(A.58)}$$

APPENDIX B: PERMISSIONS FOR FIGURES USED IN THIS DOCUMENT

The figures that existed within the scope of this document and whose copyrights were transferred to the publisher were used in the thesis in accordance with the "publishing policy suitable to the reuse of the text and graphics produced by the author" on the website of the publishing house.'